NOTICE

The quality of this microform is heavily dependent upon the quality of the original thesis submitted for microfilming. Every effort has been made to ensure the highest quality of reproduction possible.

If pages are missing, contact the university which granted the degree.

Some pages may have indistinct print especially if the original pages were typed with a poor typewriter ribbon or if the university sent us an inferior photocopy.

Reproduction in full or in part of this microform is governed by the Canadian Copyright Act, R.S.C. 1970, c. C-30, and subsequent amendments.

AVIS

La qualité de cette microforme dépend grandement de la qualité de la thèse soumise au microfilmage. Nous avons tout fait pour assurer une qualité supérieure de reproduction.

S'il manque des pages, veuillez communiquer avec l'université qui a conféré le grade.

La qualité d'impression de certaines pages peut laisser à désirer, surtout si les pages originales ont été dactylographiées à l'aide d'un ruban usé ou si l'université nous a fait parvenir une photocopie de qualité inférieure.

La reproduction, même partielle, de cette microforme est soumise à la Loi canadienne sur le droit d'auteur, SRC 1970, c. C-30, et ses amendements subséquents.

A MOLECULAR MODELLING, NOED, AND SPIN-LATTICE RELAXATION STUDY OF THE STEREOCHEMISTRY OF SOME ORGANIC COMPOUNDS

Qing Ning

A Thesis

in

The Department

of

Chemistry and Biochemistry

Presented in Partial Fulfillment of the Requirements
for the Degree of Doctor of Philosophy at
Concordia University
Montreal, Quebec, Canada

May, 1991

ISBN 0-315-68722-3

ABSTRACT

A MOLECULAR MODELLING, NOED, AND SPIN-LATTICE RELAXATION STUDY OF THE STEREOCHEMISTRY OF SOME ORGANIC COMPOUNDS

Qing Ning, Ph.D.

Concordia University, 1991

The theory and experimental methods for using the ^{1}H and ^{13}C spin-lattice relaxation phenomenon, in conjunction with molecular mechanics calculations, are described. Rotational barriers of methyl groups subject to varying steric interactions have been calculated using the MM2 force field for fifteen steroids, ten aromatic compounds and seven terpenes. Correlations between the computed methyl rotational barriers and ^{1}H and ^{13}C spin-lattice relaxation rates have been investigated. In most cases, the relaxation rates are consistent with the predicted rotational barriers, but exceptions were noted for some steroids which are highly substituted with polar groups. Such compounds must be investigated in polar solvents. This observation is attributed to limitations in the computational model employed, which does not account for the effects of specific solvation or molecular association. Some strained terpenes, where the MM2 force field is believed to be inadequate, also showed poor consistency.

The complete assignments of the ^{1}H and ^{13}C spectra of a newly synthesized compound and some terpenes have been made, using nuclear Overhauser enhancement difference spectroscopy (NOED), spin-lattice relaxation rate (R_1) and

two-dimensional (2D) nuclear magnetic resonance (NMR) techniques. The stereochemistry of these compounds has been studied by molecular mechanics calculations and NMR data. The computed conformational preferences of molecules examined in this thesis are in good agreement with their NOE data, indicating the value of molecular modelling in stereochemical studies of this type.

A correlation between calculated and experimental spin-lattice relaxation rates of five organic compounds have been investigated. The stereochemistry and chemical shift assignments of these molecules have been examined. The ^1H-R_1 values calculated from molecular mechanics showed general consistency with the experimental R_1 data. Off-diagonal points in a correlation chart indicated local conformational exchanges or proton-solvent exchanges, which have been reported previously. The effects of water molecules coordinated to heteroatoms, such as nitrogen and oxygen, to the relaxation rates of surrounding protons, have been discussed. This method can be used as a test for abilities of molecular mechanics and associated calculations in predicting R_1 values of molecules.

ACKNOWLEDGEMENTS

The author highly appreciates and gratefully acknowledges the aid and advice of the following, who helped in making this thesis possible.

Dr. L. D. Colebrook, for his great encouragement and patient supervision throughout these research projects and the preparation of this thesis.

Dr. T. J. Adley and Dr. J. A. Capobianco, Concordia University, for their friendly and supportive discussions in Committee meetings.

Dr. R. Glaser, University of the Negev, Israel, for helpful communications and collaborations about the compound nefopam.

Dr. J. T. Edward, A. Kon, and F. L. Chubb, McGill University, for the synthesis of the compound 5,7-diisopropyl-8,8-dimethyl-2-oxo-3-phenylimidino-[1,2-c]-tetrahydro-[1,3]-oxazine (DDPTO).

Dr. F. Commodari, Neurological Institute, for his collaboration in running 2D NMR spectra of methyl O-methylpodocarpate.

Dr. Phan Viet Minh Tan, University de Montreal, for instruction in use of the Bruker WH-400 NMR spectrometer.

Finally, special thanks to Mr. Qixiu Cheng, my husband and all my family members, for their encouragement and understanding during the course of the Ph.D. program.

ACKNOWLEDGEMENTS

The author highly appreciates and gratefully acknowledges the aid and advice of the following, who helped in making this thesis possible.

Dr. L. D. Colebrook, for his great encouragement and patient supervision throughout these research projects and the preparation of this thesis.

Dr. T. J. Adley and Dr. J. A. Capobianco, Concordia University, for their friendly and supportive discussions in Committee meetings.

Dr. R. Glaser, University of the Negev, Israel, for helpful communications and collaborations about the compound nefopam.

Dr. J. T. Edward, A. Kon, and F. L. Chubb, McGill University, for the synthesis of the compound 5,7-diisopropyl-8,8-dimethyl-2-oxo-3-phenylimidino-[1,2-c]-tetrahydro-[1,3]-oxazine (DDPTO).

Dr. F. Commodari, Neurological Institute, for his collaboration in running 2D NMR spectra of methyl O-methylpodocarpate.

Dr. Phan Viet Minh Tan, University de Montreal, for instruction in use of the Bruker WH-400 NMR spectrometer.

Finally, special thanks to Mr. Qixiu Cheng, my husband and all my family members, for their encouragement and understanding during the course of the Ph.D. program.

To my husband

TABLE OF CONTENTS

LIST OF FIGURES

Chapter 1

Chapter 2

Chapter 3

Chapter 4

Chapter 5

LIST OF TABLES

Chapter 2

Chapter 3

Chapter 4

Chapter 5

LIST OF ABBREVIATIONS

$\mathbf{B_0}$	Static magnetic field
CHORTLE	1D heteronuclear chemical shift correlation experiment
COSY	2D chemical shift correlation experiment
DEPT	Distotionless enhancement by polarization transfer experiment
FID	Free induction decay
HD	Homonuclear decoupling experiment
HETCOR	2D heteronuclear chemical shift correlation experiment
$\mathbf{M_0}$	Magnetization at equilibrium
NOE	Nuclear Overhauser enhancement
NOED	Nuclear Overhauser enhancement difference experiment
NOESY	2D NOE experiment
η	NOE factor
R_1	Spin-lattice relaxation rate
γ	Magnetogyric ratio
S	Nuclear spin
SCF	Self-consistent field
S/N	Signal to noise ratio
T_1	Spin-lattice relaxation time, = $1/R_1$
$T_{1\rho}$	Spin-lattice relaxation time in the rotating frame
τ_c	Motional correlation time of the vector between nuclei (s/rad)
υ	Larmor frequency (Hz)
ω	Larmor frequency ($\omega = 2\pi\upsilon$, rad/s)

Chapter 1

INTRODUCTION

In the past 25 years, nuclear magnetic resonance spectroscopy (NMR) has become one of the most powerful techniques available to experimental chemists for structural analysis of molecules. Within the same period, molecular mechanics calculations have been extensively developed in parallel with the development of computers which have become available to chemists. Today, both techniques are widely applied to the analysis of molecular geometry. However, there remain some questions of importance to practical and theoretical chemists: is the geometry of a molecule predicted from calculation the same as is observed from experiment? Can a theoretical model interpret the conformational information which has been obtained from NMR spectra? What are the limitations of molecular mechanics calculations in predicting molecular geometry? This study addresses these questions by applying both techniques (NMR and molecular mechanics calculations) to a series of molecules, making a critical comparison between experimental and calculated results, then identifying and trying to explain the good and the bad correlations. This is the main objective of this thesis. The principal NMR techniques used were spin-lattice relaxation and the nuclear Overhauser effect (NOE), both of which are very sensitive to molecular geometry.

1.1 Spin-lattice relaxation

The best experimental technique for investigating molecular geometry in solution is nuclear magnetic resonance spectroscopy. Particularly important for obtaining stereochemical information are techniques based on nuclear spin cross-relaxation, namely, spin-lattice relaxation and the nuclear Overhauser effect. The theory of spin-lattice relaxation and the nuclear Overhauser effect will be briefly presented in Chapter 2, and a thorough and illustrative explanation may be found in ref. 1-3.

In 1968, Vold and coworkers (4) reported on the development of a convenient method to measure spin-lattice relaxation rates (R_1 values) using a pulse Fourier transform method, but it was not until some years later that the utility of proton R_1 measurements became apparent. In 1970, Freeman, Wittekoek, and Ernst (5) proposed and demonstrated that by using an "initial-slope" approximation, it was possible to define an effective R_1 for each proton in a loosely coupled spin system. The first real experimental use of ^1H dipolar relaxation for structural analysis came at about the same time, when Burton, Grant, and Hall (6) found that ^1H-R_1 values of a number of cis- and trans-alkenes could be correlated to their structures. By 1976 it became apparent that ^1H-R_1 values could be utilized for the determination of structure and stereochemistry in organic molecules.

The potential of ^1H-R_1 values for providing structural information has been investigated on a wide variety of molecules. A systematic survey of ^1H-R_1 values of steroids was first reported by Colebrook and Hall (7) and the investigation of ^1H spin-lattice relaxation of alkaloids has been carried out by Chazin and Colebrook

(8).

The sensitivity of methyl group relaxation in steroids to steric factors was first studied by ApSimon et al (9). They measured the ^{13}C relaxation times of the 18- and 19-methyl groups for a number of compounds, and proposed a model for methyl group rotation and relaxation in steroids based on the number and type of steric interactions experienced by each methyl group. The model assumes that a decrease in steric hindrance from a neighbouring group will stabilize the ground state more than the transition state thereby increasing the activation energy for rotation of the methyl group with respect to the rest of the molecule. The net effect of the resultant decrease in rotation rate will be an increase in the observed R_1 value. The relative rates of rotation of the 18- and 19-methyl groups of the trans-anti-trans androstane/cholestane system were rationalized in terms of the number of syn-clinal interactions with axial hydrogen atoms of rings A, B, and C, plus smaller interactions with hydrogen atoms of ring D. Following this analysis, the rate of rotation of the 18-methyl group of androstane should be lower and, hence its R_1 value should be greater than that of the 19-methyl group. The experimental data for the 18- and 19-methyl groups reported by Colebrook and Hall (7) were consistent with this model.

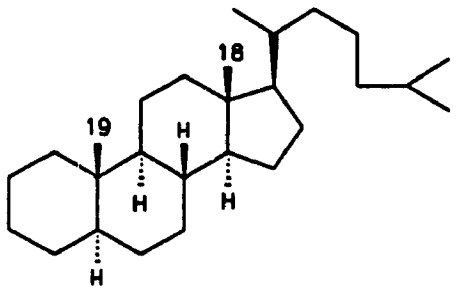

Cholestane

A severe limitation of this qualitative model is the difficulty in predicting the magnitude of the steric interactions affecting a methyl group. As has been noted (7), the predictions become much more difficult when other interactions are involved. The net steric influence on the rotational barrier of a methyl group will be the sum of a number of interactions of varying magnitude, which may affect both ground and transition states for rotation. What is needed is a quantitative, non-subjective method for estimating methyl group rotational barriers. This thesis reports an investigation of the application of molecular mechanics (force field) calculations to this problem.

The influence of methyl group geometry on the methyl rotational barriers for the C-19 methyl group of some Δ^5 steroids was estimated from ^{13}C NMR relaxation

data by Blount and Stothers (10). A molecular dynamics study of methyl group rotation in some podocarpanes, using force field calculations and ^{13}C relaxation times, has been reported by Bernassau et al (11). Agreement was found between methyl group rotational barriers computed from NMR relaxation measurements and from force field calculations.

Proton spin-lattice relaxation rates are affected by intra-molecular motions, such as ring flapping, methyl rotation, and proton-solvent exchange. These motions have been comprehensively studied by several NMR techniques. The most commonly used method is line shape analysis under different temperatures (12). Based on measurement of ^{13}C-R_1 values, the rotational barriers of methyl groups could be determined through diffusion factors (13, 14). Deverell et al. (15) have shown how measurement of $T_{1\rho}$ (spin-lattice relaxation time in the rotating frame) can be used to give exchange rates, or rates of rotation about C-N bonds. Usually, intra-molecular motions and exchange processes influence proton relaxation rates. Therefore, by comparing the ^1H-R_1 values from a normal inversion-recovery experiment with calculated R_1 values based on inter-proton distances derived from molecular mechanics calculations, information on intra-molecular motions should be obtainable. Studies of this type have not so far been reported.

^1H methyl group relaxation is complicated by the presence of cross-correlation (16). In the triply degenerate methyl spin system, there are two components of magnetization, a quartet and a doublet state, which have separate spectral parameters, including R_1 values (17). This can result in bi-exponential decay in the relaxation recovery curve used to determine R_1 values (18). However, for

molecules tumbling in the extreme narrowing limit ($\omega_0\tau_c << 1$, where ω_0 is the Larmor frequency, and τ_c is the correlation time for molecular tumbling, s/rad), the second, narrower, component of magnetization is usually fairly weak; the total spectral intensity and measured R_1 values are dominated by the broader primary component (17). By working with data in the initial slope region of the recovery curve (5), where the effects of dipolar cross-correlation have been shown to be negligible (16), the R_1 data can be accurately characterized by a single exponential.

1.2 Molecular mechanics (19)

Over the last 20 years, molecular mechanics has developed into a standard powerful method for studying molecular structure and related properties. Molecular mechanics or force field calculations are based on a simple classical-mechanical model of molecular structure. They employ the fundamental formulations of vibrational spectroscopy, and some of the basic ideas can be traced back to 1930 (20). However, serious attempts to use the method were not forthcoming until 1946. In that year three important papers appeared. T. L. Hill (21) proposed that van der Waals interactions, together with stretching and bending deformations, should be used to minimize steric energies, and that this would lead to information regarding structure and energy in crowded systems. Dostrovsky, Hughes, and Ingold (22, 23) simultaneously and independently utilized the same basic idea in an effort to better understand the rates at which various halides underwent the S_N2 reaction. Although the results were not very convincing at the time, they certainly did indicate events to come. The third and most important paper, by Westheimer and Mayer (24), was

successful in studying the problem concerned the relative rates of racemization of some optically active halo-substituted biphenyls. The methods and results were quite impressive. All of these papers together provided the basis for the subsequent development of the molecular mechanics method.

With the advent of computers during the 1950s and thereafter, interest in this approach to the determination and understanding of molecular structure rapidly increased. It can now be said that molecular mechanics is one of the standard methods of structural chemistry. The two force fields most widely used in the early 1970's were Allinger's MM1, introduced in 1973 (25), and the so-called EAS force field, developed by Engler, Andose and Schleyer in 1973 (26). Schleyer et al. (26) also surveyed the predictions and reliabilities of the two force fields. The predictions were usually in good agreement with each other, with some notable exceptions. The MM2 force field which was developed in 1977 (27) produced great improvements in the torsion term, and uses smaller and softer hydrogens than the previous version (MM1).

Structure and energy

Molecular mechanics calculations apply an empirically derived set of equations for the Born-Oppenheimer surface whose mathematical form is familiar from classical mechanics (28). This set of potential functions, called the force field, contains adjustable parameters that are optimized to obtain the best fit of calculated and experimental properties of the molecules, such as geometries, conformational energies, heats of formation, or other properties. Simple molecular mechanics force

fields include bond stretching, angle bending, torsion, and van der Waals interactions in the equation. More elaborate force fields may also include either 1,3-nonbonded interactions or cross-interaction terms, electrostatic terms and so on. The sum of all these terms is called the **steric energy** of a molecule.

Because of the intimate connection between structure and energy, molecular mechanics calculations always involve both. To find the structure, one necessarily has to examine the energy to find where energy minima occur. The force field defines the mechanical model used to represent the molecule. The purpose of the molecular mechanics program is to determine the optimum structure and energy based on this mechanical model. The input to the program must therefore define a starting structure for the molecule. This involves giving Cartesian (x,y,z) coordinates for the individual atoms and defining the bonds joining them. In practice often only the heavy (non hydrogen) atoms are so defined. The program then adds the hydrogens as necessary. The model nature of molecular mechanics calculations requires that bonds be defined in the input. The model corresponds strictly to the classical valence bond picture of chemical bonding. Carbon atoms may be either sp^3, sp^2, or sp, and there are three completely different force fields for the three different types. This is in contrast to MO calculations, in which the electronic state determines the bonding pattern, which is therefore not defined in the input.

Calculations (29)

The first step in the molecular mechanics calculation is determination of the interatomic distances, bond angles, and torsion angles in the starting geometry. The

values obtained are then used in the different potential function expressions to calculate an initial steric energy, which is simply the sum of the various potential energies calculated for all the bonds, bond angles, torsion angles, nonbonded pairs of atoms in the molecule. Once the energy and structure remain constant from iteration to iteration and the first derivatives are all close to zero, the program prints the final steric energy and the optimized geometry. This geometry may then be used to calculate such properties as the moment of inertia and the dipole moment (from the vector sum of the bond moments). The heat of formation can be calculated from the steric energy by a group or bond increment method.

The next step in the calculation, the determination of the strain energy, is not specific to molecular mechanics programs, but is also performed using experimental heats of formation. The definition of strain energy is, however, not simple, because the heat of formation of a strain-free reference molecule must be defined. The conventional definition states that the strain energy is the difference in heat of formation between the molecule itself and a totally strain-free molecule of the same constitution (i.e. one that consists of the same numbers of each different type of group). The total process used by a molecular mechanics program to calculate heats of formation and strain energies is shown diagrammatically in Fig. 1.1. The steric energy calculated from the force field is converted to a heat of formation by adding the group and bond increments from the parameterization.

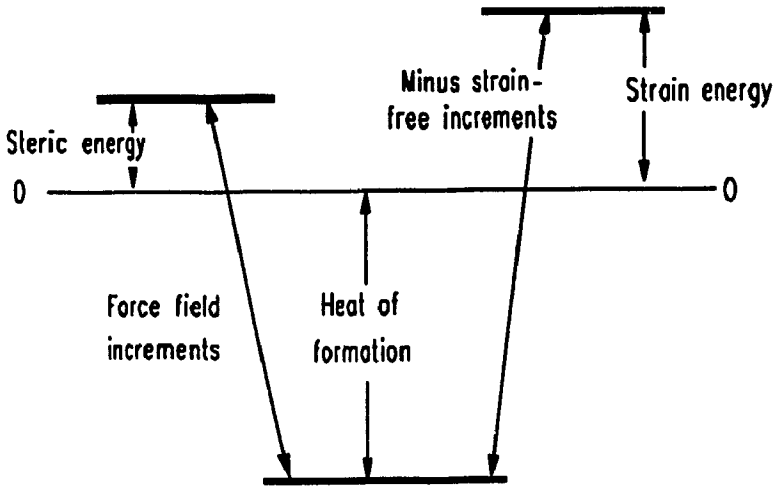

Fig. 1.1. Schematic energy diagram for determination of the strain energy in a molecular mechanics calculation.

The calculation can, therefore, give a structure, some spectroscopic d[illegible] dipole moment, and the heat of formation, from which the strain energy can be evaluated. One problem for the force fields is how to treat conjugated trienes or aromatic molecules. Allinger and Sprague (25, 30) have used a simple, but very effective, combination of quantum and classical mechanics to solve this problem. A

simple π-only MO section is built into the molecular mechanics program. The first step of a calculation is then to perform a MO calculation on the conjugated system only at the input geometry. This calculation gives a set of bond orders and a total electronic energy. The bond orders are then used to modify the force field for the conjugated system. The equilibrium bond length, the stretching force constant and the rotation barrier are all assumed to depend on the calculated bond orders. The program then uses the normal force field for those parts of the molecule that are not involved in the conjugated system and the modified force field for the delocalized bonds. An ordinary geometry optimization is then performed with this force field.

The molecule is considered to be optimized when the energy and structure remain constant. The total delocalization energy given by the SCF (self-consistent field) calculation must be included in the calculation of the heat of formation because it will automatically correct for the energetic effects of conjugation or aromaticity.

To date, the MM2 force field deals well with most hydrocarbons and many kinds of functionally substituted molecules. Recently, a new force field, which is called MM3, has been published (31-33). It differs from MM2 in several ways. e.g. in congested molecules, the C-C rotational barriers of MM2 are too low because of the poor assumption that the entropy term, $\Delta S^{\neq} = 0$ ($\Delta G^{\neq} = \Delta H^{\neq} - T\Delta S^{\neq}$). The MM3 force field calculates $\Delta S^{\neq}$, and it is definitely not zero. It becomes increasingly negative with increasing congestion. The MM3 for field also gives different parameters for five-, four-, and three-membered rings that makes

predictions for these ring systems more accurate.

Advantages and limitations of molecular mechanics

Advantages:

1. **Understanding**. A calculational method that gives good results contains a potential for understanding that is not easily obtained from experimental data.

2. **Practical matters**. To determine the structure of a molecule by x-ray or other methods may involve a few weeks of work. It requires that a suitable crystal be available and the compound is stable during the measurements. Also a sizable amount of pure material is required for any measurements which will yield thermodynamic parameters. In contrast, molecular mechanics needs only few minutes of computer time plus one or two hours of analysis. Most or all of the information that could or could not be determined from experiments will be obtained without needing any sample provided that the molecular mechanics calculations are valid.

3. **Efficiency**. The efficiency of molecular mechanics is much higher than MO methods. For the same kind of calculation, the time consumed in molecular mechanics calculations may be more than an order of magnitude less than that needed for MO calculations.

Limitations:

Since molecular mechanic calculations is an "empirical" method, studies must be confined to a previously examined class. Therefore, many parameters for the

calculations need to be known from previous experiments on similar kinds of molecules. The other limit which has been proved significant in this thesis (Chapter 3) is that molecular mechanics calculations (MM2) do not take solvent effects into account. They treat a molecule as an isolated gas phase model. For non-polar hydrocarbons, the results from molecular mechanics calculations are in good agreement with the experimental data. However, if several polar functional groups replace hydrogens in the molecule, the calculated results will deviate from the experimental data.

1.3 Organization of this thesis

The relevant theory required for the relaxation analysis and molecular mechanics calculations is summarized in Chapter 2. The basic phenomena of NMR and spin-lattice relaxation are described in an illustrative manner. A description of the inversion-recovery pulse sequence is presented along with a vector diagram. The nuclear Overhauser effect is interpreted in a understandable way, and the 2D-NOESY technique is also mentioned. The MM2 force field from molecular mechanics is described in detail. The potential terms in the MM2 force field are expressed with defined parameters. Energy minimization and the calculation strategy are illustrated.

In Chapter 3, the spin-lattice relaxation rates and computed rotational barriers of methyl groups in fifteen steroids, ten aromatic compounds, and seven terpenoids are investigated. A general consistency between R_1 values and rotational barriers have been found. The exceptions due to solvation and force field limitations are

discussed.

Chapter 4 is concentrated on complete ^1H spectral assignments of a newly synthesized compound, 5,7-diisopropyl-8,8-dimethyl-2-oxo-3-phenylimidino-[1,2-c]tetrahydro-[1,3]-oxazine (DDPTO), and four terpenoids. The NOED (nuclear Overhauser enhancement difference spectrum) technique, together with 2D COSY, HETCOR and 1D CHORTLE are used to assign ^1H and ^{13}C spectra. The stereochemistry of these compounds is studied from R_1, NOE data and molecular mechanics.

Comparison of computed R_1 values (except methyl R_1's) from molecular mechanics with experimental spin-lattice relaxation rates is discussed in Chapter 5, which is concerned with the study of intra-molecular motion in certain organic compounds. Correlation charts based on this approach have demonstrated different flexibilities within a series of molecules, from the most rigid (gibberellic acid), to the most mobile (nefopam). A reasonably clear idea of the location in the structure where local motion is occurring, and which protons are more mobile than others, can be obtained from the R_1 correlation charts.

Experimental conditions and procedures of molecular mechanics calculations are described in Chapter 6. Chapter 7 is the summary of the research for this thesis.

Chapter 2

BASIC THEORY

This Chapter will be divided into two parts. Part one is the theory of nuclear magnetic resonance, including the behaviour of a nucleus in a magnetic field, relaxation mechanisms and NOE effects. The second part contains the basic theory of molecular mechanics, force fields, and energy minimization.

2.1 Basic concepts of NMR (34-37)

Nuclear magnetic resonance deals with the interactions between the magnetic moments of atomic nuclei and magnetic fields. The magnetic moment of the nucleus is associated with the nuclear spin, **S**. Only those nuclei for which $S \neq 0$ have a magnetic moment and can be detected by NMR. In the presence of a static magnetic field, $\mathbf{B}_0$, the nuclear magnetic moment precesses about the direction of $\mathbf{B}_0$. The frequency of this precession is known as the Larmor frequency, ω_0, and is proportional to the strength of $\mathbf{B}_0$:

$$\omega_0 = \gamma_n B_0 \qquad [2.1]$$

where γ_n, the magnetogyric ratio, is the factor which characterizes the efficiency of the interaction between a nucleus and a magnetic field. For a spin 1/2 nucleus, e.g. a proton, the energy difference, ΔE, between the two allowed spin states is given by:

$$\Delta E = \gamma_n (h/2\pi) B_0 \qquad [2.2]$$

where h is Planck's constant. The effect of the magnitude of B_0 on ΔE is shown in Fig. 2.1. The two energy states for the nuclei are unequally populated, the ratio of the populations at equilibrium being given by the Boltzmann equation:

$$N_\beta/N_\alpha = \exp(\Delta E/kT) \qquad [2.3]$$

where N_α and N_β are the number of spins in the lower state α and upper state β, respectively. The population difference is dependent both on the field and also the nuclear species under observation.

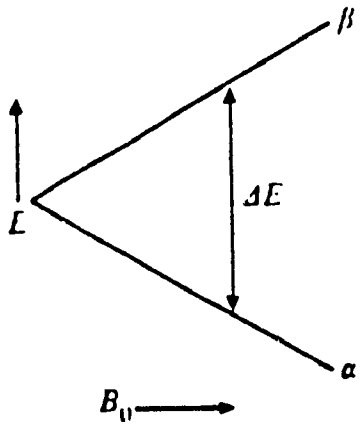

Fig. 2.1. Energy separation in a magnetic field.

Consider a sample containing nuclei with spin 1/2 placed in the magnetic field, $\mathbf{B}_0$. The nuclei will precess around the direction of the field with the frequency ω_0 (Larmor frequency). The nuclei are either aligned with, or opposed to, the direction of $\mathbf{B}_0$, as shown in Fig. 2.2. Since there is, at equilibrium, a slight Boltzmann excess of nuclei aligned with the magnetic field, these will give rise to a resultant bulk magnetization, $\mathbf{M}_0$, the sum of the magnetization of the individual spins, aligning with the direction of $\mathbf{B}_0$. Usually, the direction of $\mathbf{B}_0$ is defined as the z direction.

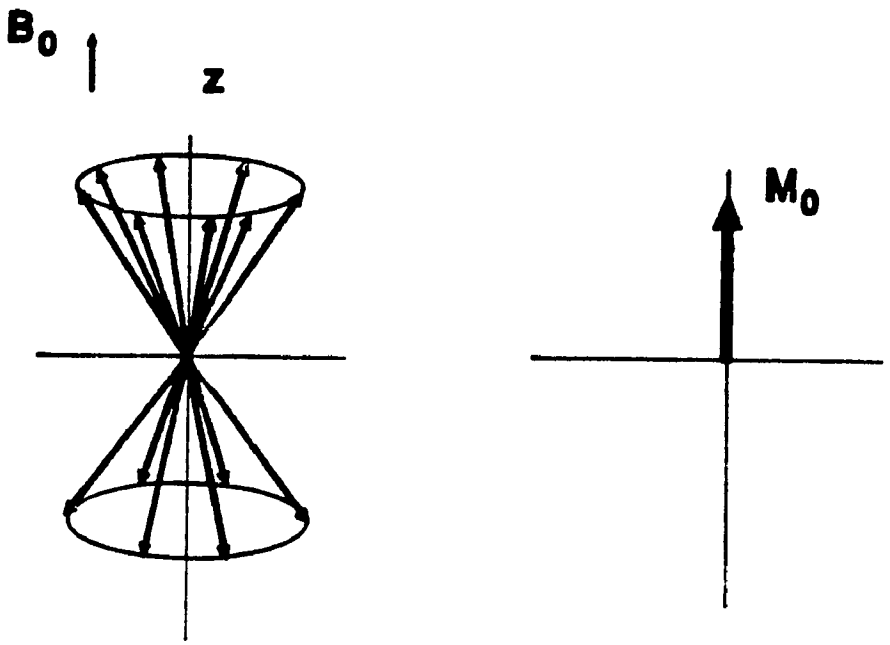

Fig. 2.2. Nuclear spins in a magnetic field.

It is a very useful simplification to consider NMR experiments in a rotating frame rather than a fixed laboratory frame. The rotating frame is one in which the z' axis is the same as the z axis in the laboratory frame, but the x' and y' axes rotate about the z' axis in synchronization with a radio frequency field, $\mathbf{B}_1$. Hence, the effect of a pulse (from the $\mathbf{B}_1$ field) is much easier to describe in the rotating frame than in a fixed frame. The $\vec{\mathbf{B}}_1$ vector is considered as the reference for the rotating frame, and is defined as the x' axis. The magnetization is initially aligned along z' and perpendicular to x', and consequently, the precession about $\mathbf{B}_1$ is simply a rotation of the magnetization in the y'z' plane. The magnetization will remain perpendicular to the $\mathbf{B}_1$ field and a $\pi/2$ pulse would put the magnetization along the y' axis (Fig. 2.3).

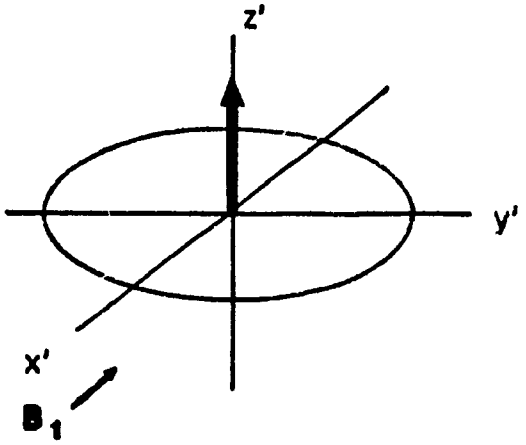

Fig. 2.3. Rotating frame

Once the $\mathbf{B}_1$ pulse is removed, the perturbed magnetization will begin to relax back towards its equilibrium condition by means of two separate processes.

Firstly, the component of the magnetization remaining along the z axis, $\mathbf{M}_z$, returns to its original value, $\mathbf{M}_0$, by an exponential decay process characterized by a relaxation time constant, T_1, or the rate constant, R_1 ($R_1 = 1/T_1$). This process is known as spin-lattice relaxation, and will be discussed in the following section.

In the second process, the nuclear spins interchange with one another so that some spins now precess faster than **M**, while others process more slowly, with the result that the spins begin to lose phase coherence in the x'y' plane. The process is known as the spin-spin relaxation process, defined by the spin-spin (or transverse) relaxation time constant, T_2, or the rate constant, R_2 ($R_2 = 1/T_2$).

For a normal NMR experiment, a 90° pulse of radio frequency along the x' axis is applied to tip the bulk vector, $\mathbf{M}_0$, from the z' axis to the y' axis, then the response of the system to the disturbance will be monitored. The whole procedure can be expressed as equilibrium--perturbation--detection, and is shown in Fig. 2.4.

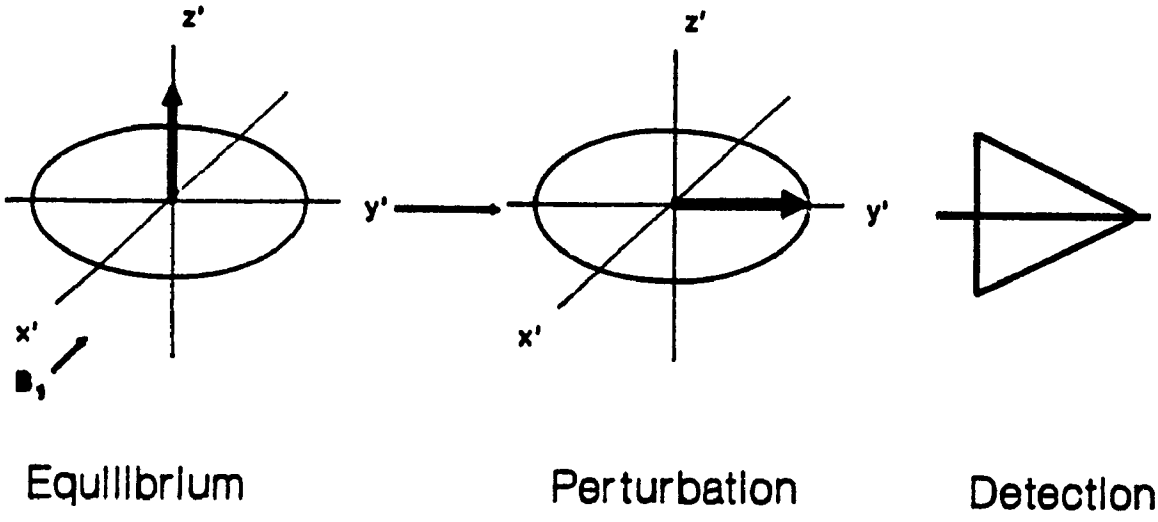

Fig. 2.4. Diagram of magnetization in NMR experiment.

2.1.1 Spin-lattice relaxation

Spin-lattice relaxation is the process of energy exchange between nuclear spins and the surrounding environment. Relaxation to an equilibrium position usually occurs exponentially, following a law of the form:

$$(n - n^e)_t = (n - n^e)_0 \exp(-t/T_1) \qquad [2.4]$$

where $(n - n^e)_t$ is the displacement from the equilibrium value, n^e, at time t, and $(n - n^e)_0$ that at time zero. The spin-lattice relaxation rate constant, R_1, is given by $1/T_1$,

where T_1 is the time constant for the relaxation process.

Fig. 2.5 shows the energy level diagram for two protons, i and s, which are relaxing each other but are not J-coupled. The diagram also shows an approximation to the equilibrium population distribution. The transition probability of nucleus i relaxation between states 1,3 and states 2,4 is the single-quantum process W_{1i}, while the s transition probability between 1,2 and 3,4 is W_{1s}. W_2 is a double-quantum process which corresponds to the simultaneous relaxation of both spins, while W_0 is a zero-quantum process corresponding to a mutual spin flip. The latter process gives no net relaxation, but leads to the excess energy being moved from one spin to another. The zero- and double-quantum processes are not observed directly, but they can be detected through their effects on relaxation.

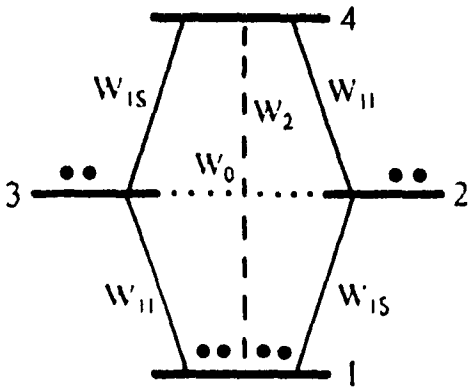

Fig. 2.5. Energy level diagram for two protons, i and s, which are relaxing each other.

Relaxation through W_1 requires magnetic field fluctuations at a frequency of the order of the Larmor precession frequency, ω_0, i.e. 10^8 to 10^9 Hz, while W_2 requires 2ω. Because the necessary field fluctuations are produced by molecular tumbling at a rate $(\tau_c)^{-1}$, it follows that W_1 and W_2 are most efficient when $\omega_0\tau_c \approx 1$.

Since ω_0 depends on the field strength, the relaxation rate of spins in a molecule is also field dependent (Fig. 2.6).

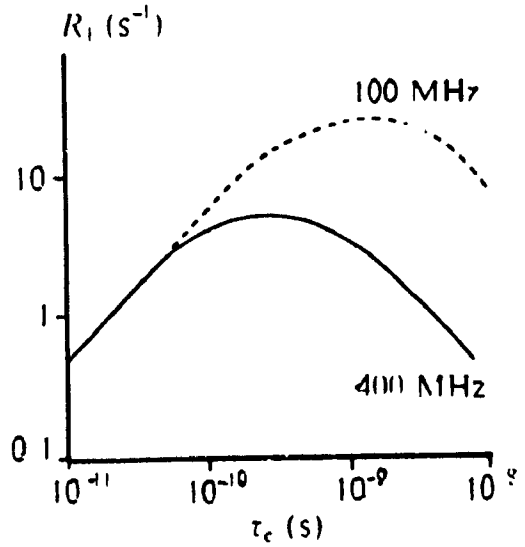

Fig. 2.6. The effect of τ_c on proton R_1 at 100 and 400 MHz.

There may be several relaxation mechanisms existing during an NMR measurement. The overall R_1 is the sum of the contributions from these mechanisms:

$$R_{1tot} = R_{1dd} + R_{1sr} + R_{1ca} + R_{1eq} + ... \qquad [2.5]$$

where R_{1dd}: dipole-dipole relaxation mechanism.

R_{1sr}: spin-rotation relaxation mechanism.

R_{1ca}: chemical shift anisotropy relaxation mechanism.

R_{1eq}: electric quadrupole relaxation mechanism.

Of these mechanisms, dipole-dipole relaxation is the most important mechanism for **S** = 1/2 nuclei, usually dominating the overall relaxation rate. In this Chapter, only R_{1dd} and R_{1sr} will be discussed in detail, since the R_{1ca} mechanism becomes important only for large molecules and R_{1eq} for I > 1/2 nuclei. Those situations are not involved in the studies described in this thesis.

Dipole-dipole relaxation

The dipole-dipole relaxation is caused by the fluctuating magnetic fields of nearby nuclear dipoles through space. It may be modulated by molecular tumbling or by translational diffusion. For nuclei tumbling isotropically in a non-viscous solution,

$$R_{idd} = K\gamma_i^2\gamma_s^2\ \tau_c(r_{is})^{-6} \qquad [2.6]$$

where γ_i, γ_s: magnetogyric ratios of nuclei which relax to each other.

r_{is}: distance between nuclei i and s.

τ_c: motional correlation time of the vector between nuclei i and s (s/rad).

K: the proportionality constant, depends on the spins involved and units used for γ and r.

Because of the r^{-6} term in Eq. [2.6], the influence of a relaxation pathway is attenuated very rapidly with increasing distance between nuclei, so that it is the near neighbours of a nucleus which dominate its relaxation. For example, a methyl proton relaxes largely to its neighbouring protons on the same carbon atom. The carbon atom of a methyl group is relaxed almost exclusively by the protons it carries. Therefore, differences between the ^1H relaxation rates of methyl groups (R_{1a}, R_{1b}) in the same molecule arise mainly from differences in the correlation times for local motion of the methyl groups. Also, differences between the ^{13}C relaxation rates of methyl groups in the same molecules arise almost entirely from this origin.

$$\frac{R_{1a}}{R_{1b}} = \frac{(\tau_c)_a}{(\tau_c)_b} \qquad [2.7]$$

Spin-rotation relaxation

For small molecules which rotate rapidly, or for rapidly rotating groups, such as a methyl group, the spin-rotation relaxation mechanism becomes important. Since increasing the tumbling rate (or rotation rate) results in an increase of the contribution of the spin-rotation mechanism to the overall R_1 ($R_{1sr} \propto 1/\tau_c$), the relative contribution from dipole-dipole mechanism is decreased significantly. Therefore, the spin-lattice relaxation rate is, eventually, decreased.

Measurement of spin-lattice relaxation rate

The most common method of measuring the spin-lattice relaxation rate is known as the "inversion-recovery sequence". We invert the magnetization from its equilibrium value, M_0, to $-M_0$ by a non-selective π pulse, allow it to evolve (relax) after the perturbation, and then detect what happened during the evolution (relaxation) period. The recovery procedure can be detected by another $\pi/2$ pulse which converts $-M_0$ to $-M_y$ for detection purposes. The pulse sequence of inversion-recovery is shown as follows:

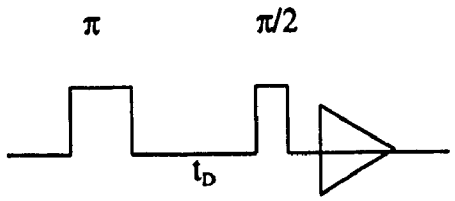

where π is a π pulse, which rotates M_0 to $-M_0$.

$\pi/2$ is a $\pi/2$ pulse, which rotates any $\mathbf{M}_z$ into the xy plane.

t_D is a delay which is under the control of the operator.

Fig. 2.7 represents the inversion-recovery sequence in terms of a vector diagram. The magnetization is initially aligned along the z axis and is inverted to -z by the π pulse. After a short delay, the magnetization will not have recovered to any significant extent and the $\pi/2$ pulse will rotate it to the -y axis. The signal is inverted compared with the signal generated by a $\pi/2$ pulse on the equilibrium magnetization. If, in a separate experiment, we wait a little longer (insert a delay t_D) before applying the $\pi/2$ pulse, the magnetization would recover to a point just below the origin. Now a $\pi/2$ pulse will move the magnetization to the -y axis, producing a smaller but inverted signal. If the t_D inserted between the two pulses is longer, the magnetization will pass through the origin so the $\pi/2$ pulse will generate +y magnetization and a positive signal. If the t_D is long enough (e.g. 5 * T_1), the magnetization will have recovered to its equilibrium value of $\mathbf{M}_0$. The experiment is repeated several times with different delays. The intensity of the magnetization $\mathbf{M}_t$ will grow, exponentially, from the most negative, $-\mathbf{M}_0$, through the null point ($\mathbf{M}_t$ = 0), to the positive value, and eventually return to its original position, $\mathbf{M}_0$ (Fig. 2.8). The spin-lattice relaxation rate R_1 will be calculated from Eq. [2.8].

$$M_t = M_0[1 - 2\exp(-R_1/t)] \qquad [2.8]$$

where M_t is the intensity of the magnetization at a time t after the π pulse.

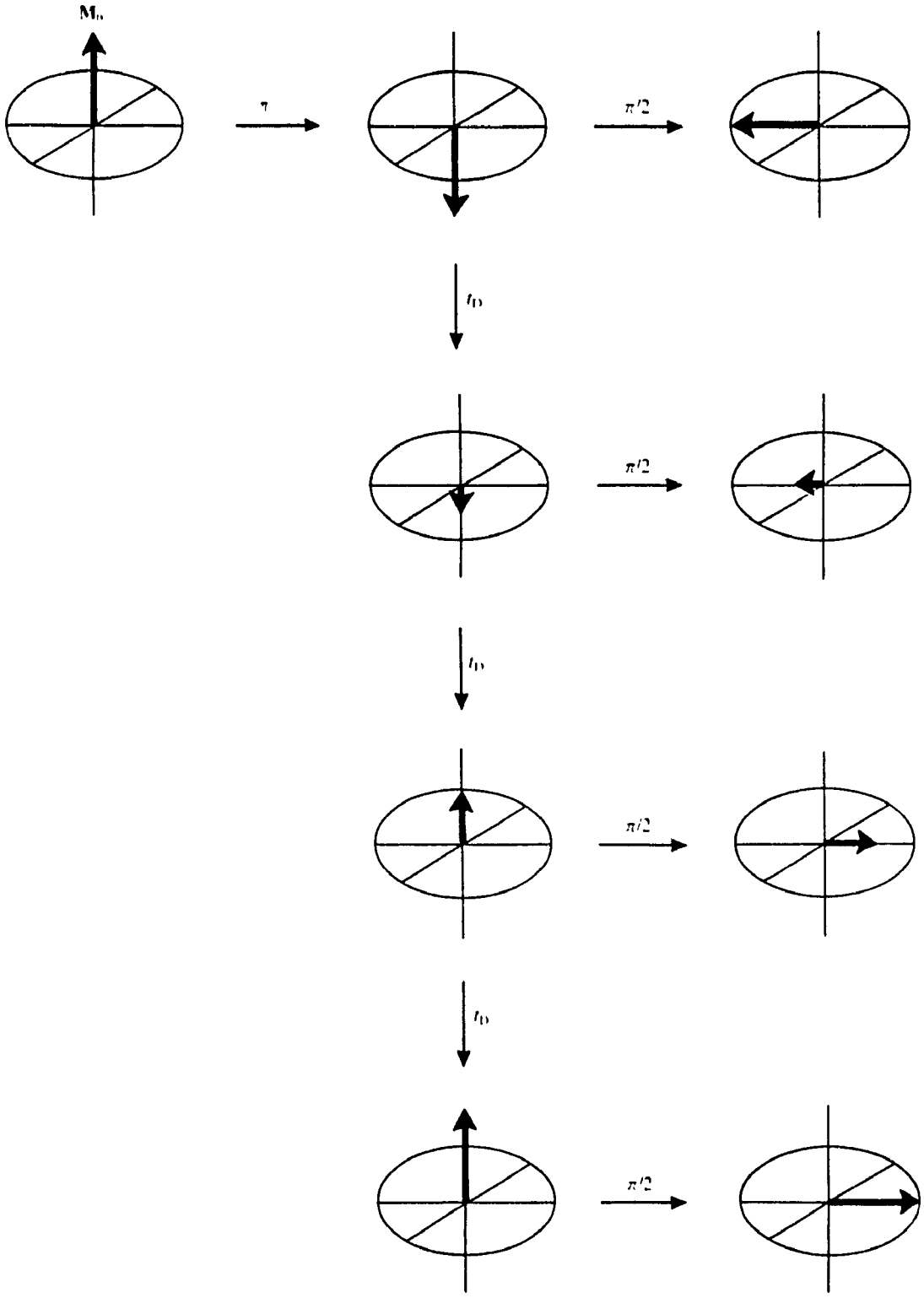

Fig. 2.7. Inversion recovery sequence vector diagram.

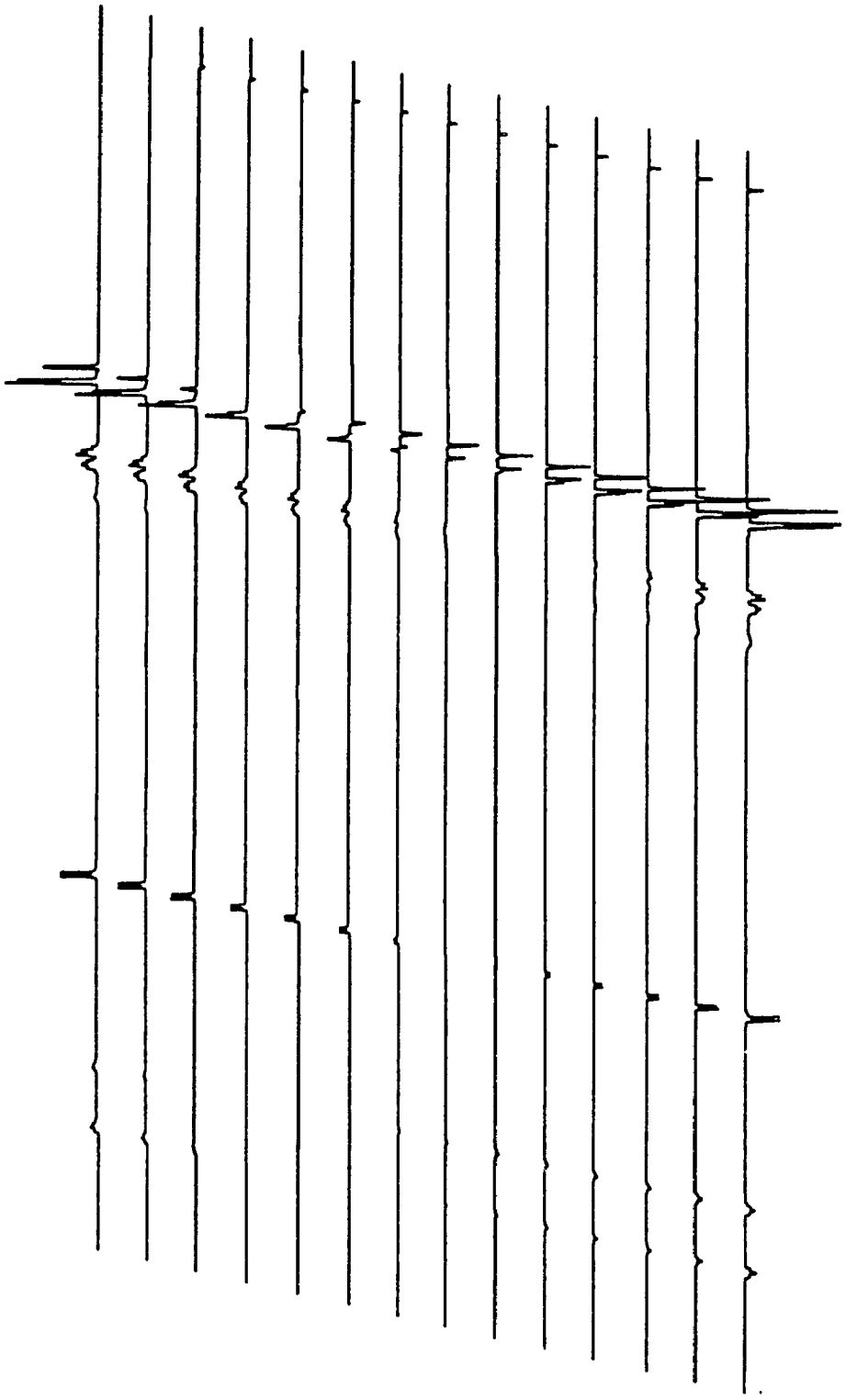

Fig. 2.8. Stack plot of R_1 determination (geraniol).

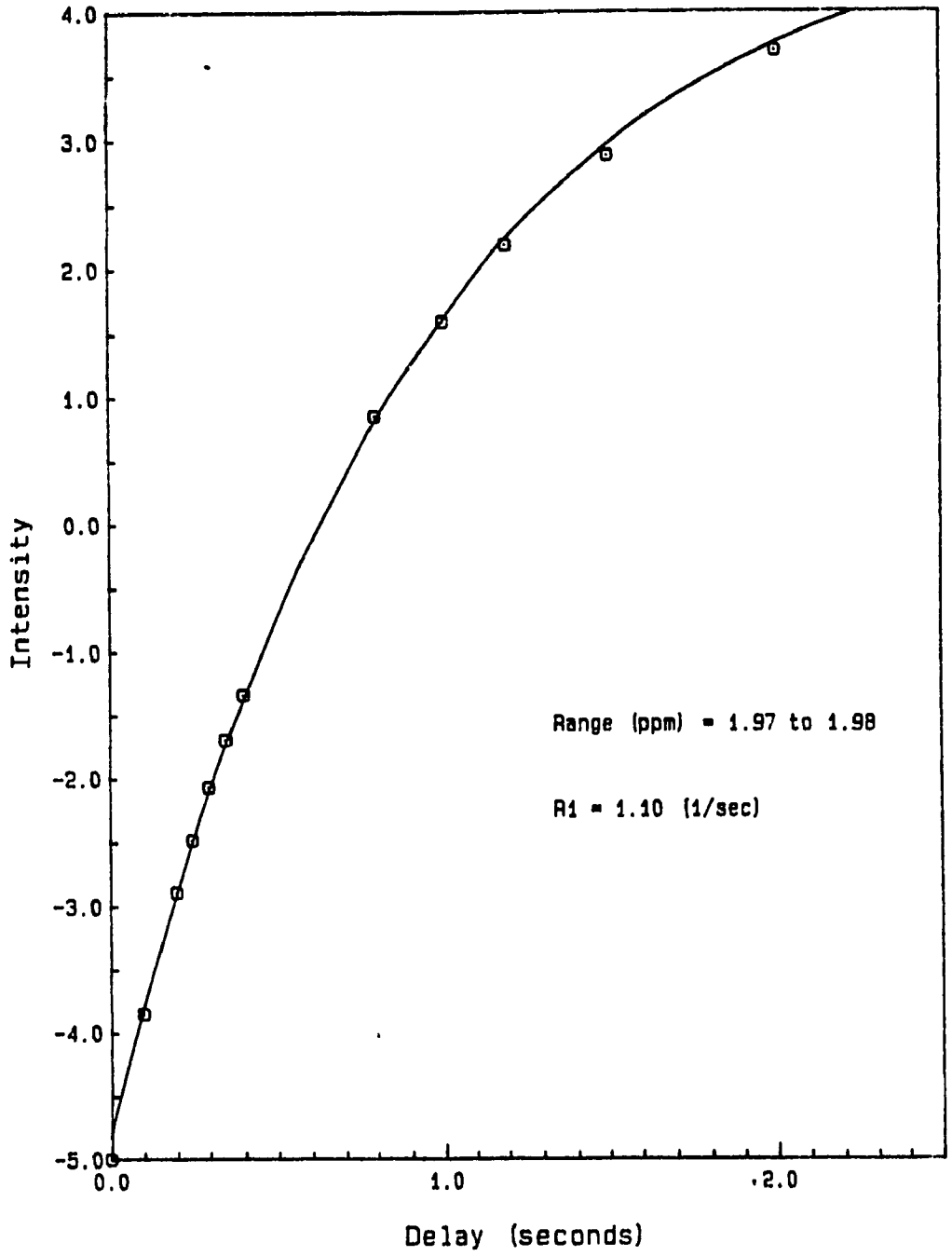

Fig. 2.9. Plot of spin-lattice relaxation rate (intensity vs time) for gelsemine.

R_1 data analysis

There are two methods used in this laboratory for analyzing R_1 data, non-linear regression (38) and the null point method (39). The former uses a computer to fit equation [2.8] to the intensity data of nuclear resonances from NMR measurement, finding R_1 values for each proton resonance. The summed intensities of the components of multiplets are processed using software written in this laboratory, then R_1 values are calculated using a SIMPLEX algorithm (40) based on two parameters, $\mathbf{M_0}$ and $\mathbf{R_1}$, in equation [2.8]. The reasons for using the two parameter method instead of three parameters ($\mathbf{M_0}$, R_1, and a parameter replacing the factor 2 in Eq. [2.8]) have been discussed in ref. 3. This method has been widely used in R_1 data analysis due to its efficiency and accuracy. The null point method involves an explicit evaluation of Eq. [2.8] at the time when $\mathbf{M_t} = 0$, giving R_1 directly:

$$R_1 = \frac{0.69}{t_{null}} \qquad [2.9]$$

The term, t_{null}, is the time when $\mathbf{M_t} = 0$, and is obtained from a stacked plot of a series of inversion-recovery experiments (Fig. 2.8). The reliability of the null point method has been evaluated thoroughly in this laboratory (3). The results from the null point method and from non-linear regression showed excellent agreement. In practice, non-linear regression is always the first choice when the resolution of resonances in a spectrum is reasonably good. However, the null point method presents obvious advantages when a proton resonance shows a high degree of

multiplicity or partial overlap with other resonances. In this thesis, most ^{1}H and ^{13}C R_1 values were measured by a two parameter non-linear regression computational method. The null point method was used when necessary.

Normalization

When R_1 values of protons measured in different experiments are to be compared, allowance must be made for changes in operating conditions and differences in molecular size and shape which will affect the motional correlation time, τ_c . Consequently, the R_1 values will be affected by the experimental conditions. This problem is overcome by normalizing the observed rates internally to that of a proton which is remote from the site of structural variation. For the molecules studied in this thesis, normaiization was used when comparisons (in Chapter 3) and correlations (in Chapter 5) were made, so that the differences resulting from experimental conditions and from the computational method will be eliminated.

Isotropic and anisotropic motions

For a rigid isotropically tumbling molecule, all of the τ_c values of nuclei in the molecule will be equivalent, and the rate equation can be written as:

$$R_{1j} = K_j \sum (1/r_{ij})^6 \qquad [2.10]$$

The ratio of R_1 values of any two protons in the same molecule will, therefore, depend on inter nuclear distances:

$$\frac{R_{1i}}{R_{1j}} = \frac{K_i \sum (1/r_{ij})^6}{K_j \sum (1/r_{ij})^6} \qquad [2.11]$$

If molecular tumbling is anisotropic, the spin-lattice relaxation rate of nuclei in the molecule will be influenced by the rotational diffusion tensor, D, the cosines λ, μ, and ν of the angles assumed by the bonds relative to the principal axis of this tensor:

$$R_{1dd} = f(D_1, D_2, D_3, \lambda, \mu, \nu) \qquad [2.12]$$

where the subscripts of D are motional axes.

For example, the C-H nuclei in the para position of monosubstituted benzene derivatives relax faster than those in the ortho or meta position (41) (Fig. 2.10).

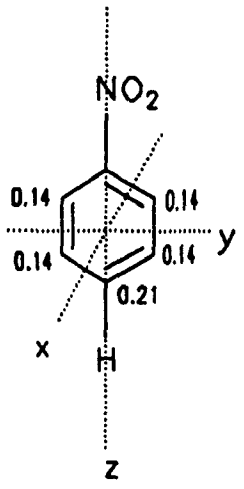

Fig. 2.10. Motional axes and ^{13}C R_1 values of nitrobenzene.

The reason for this behaviour lies in a preferred rotation about the molecular axis passing through the substituent NO_2 and the para-carbon. As has been mentioned, any additional motion will affect the τ_c term in equation [2.6], since the para C-H bond does not change its direction relative to the field $\mathbf{B}_0$ during this motion (fluctuating local fields can only arise at the para-C nucleus by rotation of the molecule perpendicular to the preferred axis). the relaxation rate R_1 at C-4 is not affected by the molecular rotation about the z axis. Generally speaking, for ^{13}C spin-lattice relaxation measurements, carbon relaxation is efficient when the C-H bond aligns with the principal axis of molecular tumbling, and a less efficient when the C-H bond has a somewhat different angle with the principal rotational axis.

Therefore, in R_1 measurements, it is always wise to check for anisotropic motion through ^{13}C-R_1 data before trying to explain the proton R_1 values.

2.1.2 NOE effect

If selected irradiation of a nucleus, s, is continued long enough, a new population distribution gradually develops as relaxation occurs through W_2 and W_0 (see Fig. 2.3). W_2 increases the intensity of the i transitions by attempting to establish a Boltzmann distribution between levels 1 and 4, while W_0 decreases the i intensity by equilibrating levels 2 and 3. The resulting net change in the intensity of i as a result of the competition between W_2 and W_0 is called the **nuclear Overhauser enhancement,** since it was first found by A. W. Overhauser in a cross-relaxation experiment (42). This is the basis of the one-dimensional (1D) nuclear Overhauser effect experiment.

Quantitatively, if we define the initial intensity of the i transitions before irradiation as I_0, and the intensity of i when s is saturated as I, then,

$$\eta_i\{s\} = \frac{(I - I_0)}{I_0} \frac{\gamma_s}{\gamma_i} \qquad [2.13]$$

$\eta_i\{s\}$: NOE factor. NOE at nucleus i when nucleus s is saturated.

I_0: intensity of i at equilibrium.

I: intensity of i when s is saturated.

γ_s,γ_i: magnetogyric ratios of i and s.

i and s are not J coupled and are close in space (< 5 Å).

If: i and s are ^1H's, $\eta_i\{s\}_{max} = 0.5$

i and s are ^{13}C and ^1H, respectively, $\eta_i\{s\}_{max} = 1.98$

If nucleus i relaxes to s via a pure dipole-dipole mechanism, and if the steady-state is reached by long irradiation, the NOE factor can be expressed by the relaxation process:

$$\eta_i\{s\} = \frac{W_2 - W_0}{2W_1 + W_2 + W_0} \frac{\gamma_s}{\gamma_i} \qquad [2.14]$$

i and s must be relaxing to each other by the spin-lattice mechanism. There must be appreciable "cross-relaxation". W_2, W_0 are cross relaxation terms. They are only important in the dipole-dipole relaxation mechanism.

If there is an I-S-R three spin system and r_{sr} is known, then the inter-proton distance r_{is} can be measured as follows:

$$\frac{\eta_s\{i\}}{\eta_s\{r\}} = \left\{\frac{r_{sr}}{r_{is}}\right\}^6 \qquad [2.15]$$

Since:
$$W_2 - W_0 = \frac{\gamma_i^2 \gamma_s^2}{2\,(h/2\pi)^2} \tau_c\, (r_{is})^{-6} \qquad [2.16]$$

1D NOE difference spectroscopy (NOED)

For a small or medium sized molecule, 1D NOE measurement is an efficient and reliable technique for the study of stereochemistry. Usually, we saturate one resonance and then compare the intensities of others with their equilibrium values. This could, in principle, be done simply by integrating resonances with and without a period of pre-saturation. However, in practice, this is not accurate enough to detect small NOE's. The superior method, NOE difference spectroscopy, which can improve the sensitivity of measurements significantly, was used in this study. The basic scheme used for the difference experiment is the acquisition of a few scans with saturation of a resonance, followed by the acquisition of an equal number of scans with the irradiation frequency set to the end of the spectrum (control spectrum) under identical experimental conditions. Then the FID (free induction decay) of the control spectrum is subtracted from the FID which contains NOE information. Thus, unperturbed peaks from the NOE experiment will be cancelled, leaving the "pure" NOE enhancements for those resonances which are affected by the pre-saturation. The sensitivity of this technique is dependent on the strength of the magnetic field, and the amount of signal averaging. Usually, a 1% enhancement can be detected reliably by the NOED experiment.

2D NOE (NOESY)

The two-dimensional experiment, NOESY, uses a non-selective pulse sequence to disturb the populations of the nuclei which are close in space to the other protons. Unlike the 1D NOE experiment, NOESY does not have a long

irradiation period and a long recovery time for the disturbed nuclei to relax to equilibrium. Correlations for the entire molecule are achieved at the same time. Usually, if a measurement is made at the extreme narrowing limit ($\omega_0\tau_c << 1$), 1D NOE measurement shows advantages in sensitivity, efficiency, and data analysis. NOESY is used when a molecule to be determined is relatively large, and tumbling slowly (beyond the extreme narrowing limit), so that spin diffusion may be a problem.

In the studies described in this thesis, the 1D NOE difference technique was chosen for stereochemistry determinations, since relatively small molecules were investigated and non-viscous solutions were used.

2.2 Molecular mechanics (19, 27)

Molecular mechanics is a widely used calculation method which is designed to give accurate structures and energies for molecules. It treats the molecule as an array of atoms governed by a set of classical-mechanical potential functions. The method is a natural outgrowth from older ideas of bonds between atoms in molecules and van der Waals forces between nonbonded atoms. The basic idea of molecular mechanics is that all bonds have "natural" lengths and angles, and molecules will adjust their geometries so as to take up these values in the most reasonable case.

2.2.1 Force field

The "force field" is a set of potential functions which contains adjustable parameters that are optimized to obtain the best fit of calculated and experimental properties of molecules, such as geometries, steric energies, heat of formation, etc. A simple force field includes bond stretching, angle bending, torsion and van der Waals interactions, as follows:

$$V_{pot} = \Sigma V_{stretch} + \Sigma V_{bend} + \Sigma V_{torsion} + \Sigma V_{VDW} \qquad [2.17]$$

where the sums extend over all bonds, bond angles, torsion angles and nonbonded interactions between all atoms not bound to each other or to a common atom.

Bond stretching and angle bending

In the molecular mechanics model, the atoms of a molecule can be thought of as being joined together by mutually independent springs, restoring "natural" values of bond lengths and angles. Assume a harmonic potential with Hooke's law functions as follows:

$$V_{stretch} = 1/2\ k_r(r - r_0)^2 \qquad [2.18]$$

$$V_{bend} = 1/2\ k_\theta(\theta - \theta_0)^2 \qquad [2.19]$$

where r is the distance between nuclei, θ is the bond angle, and k is the constant.

At very large deformations, a Morse function may be used, but it requires excessive amounts of computer time. An optional method is simply to add a cubic term in the Hooke's law function, as follows:

$$V_{stretch} = 1/2\ k_r\ (r - r_0)^2 + k'\ (r - r_0)^3 \qquad [2.20]$$

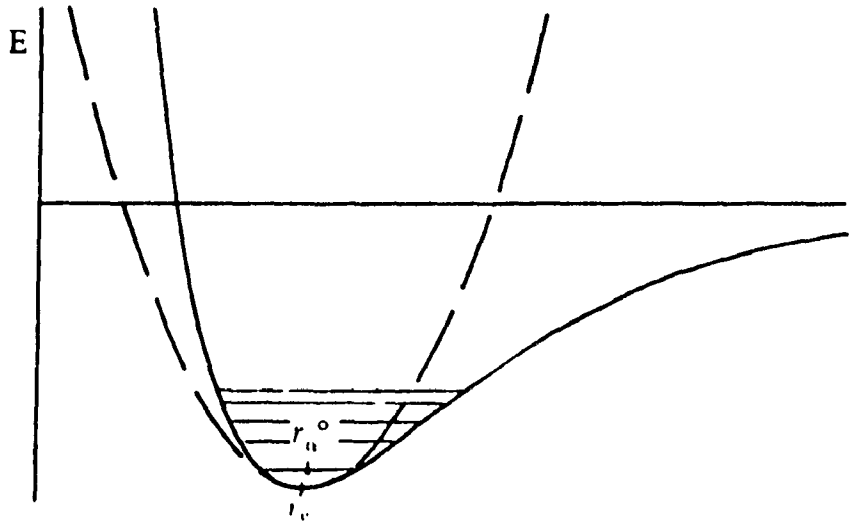

Fig. 2.11 The energy-distance relationship between two atoms bonded together. Solid curve, Morse function; dashed curve, harmonic approximation.

Torsional energy

· Modern force fields contain many more types of potential functions designed to find a good fit to the experimental data. The most important of these are the torsional potentials. This energy term has usually been thought of as resulting from a repulsion between the bonds not covered by van der Waals interactions.

$$V_{tor} = k_{\phi}(1 - \cos 3\phi) \qquad [2.21]$$

where ϕ is the dihedral angle of four atoms.

Without this term the rotational barrier of ethane (Fig. 2.12), for example, cannot be expressed successfully by the force field.

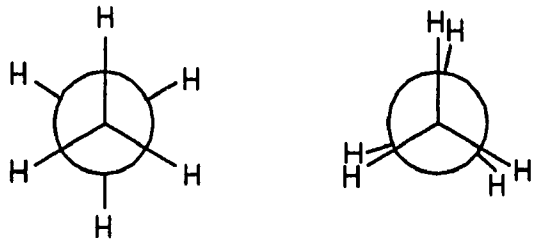

Fig. 2.12. Two conformations of ethane.

The combination of stretching, bending and torsional potential functions is often known as a "valence force field", because it accounts for the properties normally attributed to chemical bonds.

Nonbonded interactions

For high quality calculations, valence force fields are, however, not completely adequate. Molecular mechanics uses another potential, van der Waals functions, to account for steric interactions (1,3-, 1,4-interactions and higher). Usually these potentials take the form of a "6/12" function as in Eq. 2.21:

$$V_{VDW} = \varepsilon \left[(r_0/r)^{12} - 2(r_0/r)^6\right] \qquad [2.21]$$

where ε defines the depth of the potential well, r_0 the minimum energy distance. The MM2 force field, however, uses an "exponential minus 6" expression, in which the 12th power term is replaced by an exponential as follows:

$$V_{VDW} = \frac{\varepsilon}{1-6/\alpha}\left[\frac{6}{\alpha} e^{\alpha(1-r/r0)} - (r_0/r)^6\right] \qquad [2.22]$$

The constant, α is between 14 and 15.

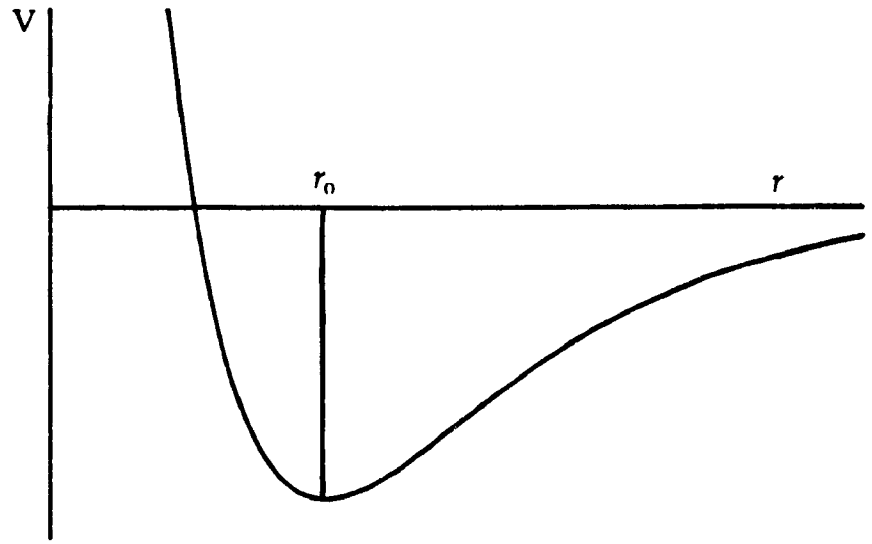

Fig. 2.13. Van der Waals potential function.

Fig. 2.13 shows the form of such a function with a shallow minimum at an ideal interatomic distance.

The steric interaction in molecular mechanics force fields is, however, not without problems. One particular problem arises from the fact that steric repulsions between atoms bonded to a common centre (1,3-interactions) are not the same for an open chain, and six-, five-, four-, and three-membered ring systems. In all rings with more than four members, there is the same number of 1,3-interactions as there

are atoms in the ring. For a four-membered ring, however, there are only two sets of atoms 1,3 to each other, and in a three-membered ring there is no 1,3 pair at all (Fig. 2.14).

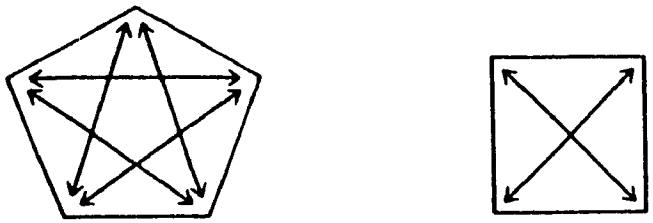

Fig. 2.14. 1,3-interactions of ring system

This means that three- and four-membered rings cannot be treated successfully using the same potential functions as acyclic molecules or larger rings. Also the bending parameters for these small rings should not be the same.

Allinger and co-workers have designed a new force field, MM3, to solve some practical problems, including the four- and three-membered ring calculations. Totally different parameters for each five-, four-, and three-membered ring system are introduced in the new force field that considerably increase the reliability of

molecular mechanics calculations on these kinds of ring systems.

Beside the four main potential functions in Eq. [2.17], modern elaborate force fields (42) may also include cross-interaction terms and electrostatic terms to reach the best fit with experimental data.

$$E_{pot} = \Sigma D_b [1-e^{a(b-b_0)^2}] + \frac{1}{2} \Sigma H_\theta (\theta-\theta_0)^2 + \frac{1}{2} \Sigma H_\phi [1+s\cos(n\phi)] +$$

$$\frac{1}{2} \Sigma H_\chi \chi^2 + \Sigma\Sigma F_{bb'} (b-b_0) (b'-b_0') + \Sigma\Sigma F_{\theta\theta'} (\theta-\theta_0) (\theta'-\theta_0') +$$

$$\Sigma\Sigma F_{b\theta} (b-b_0) (\theta-\theta_0) + \Sigma F_{\phi\theta\theta'} \cos(\theta-\theta_0) (\theta'-\theta_0') + \Sigma\Sigma F_\chi \chi\chi' +$$

$$\Sigma\epsilon [(r^*/r)^{12} - 2(r^*/r)^6] + \Sigma \frac{q_i q_j}{\epsilon r_{ij}} + \Sigma \left[\frac{C_{ij}}{r_{ij}^{12}} - \frac{D_{ij}}{r_{ij}^{10}} \right] \qquad [2.23]$$

Eq. 2.23 gives a representation that has been used successfully to describe such a force field. The terms 1 to 4 are stretching, bending, torsion and out of plane potentials which are called "diagonal interactions", while terms 5 to 9 are cross terms which account for "off-diagonal interactions". The final three summation

represents the nonbonded interactions by a sum of repulsions, electrostatics, and attractive dispersion forces as a function of the distance between atoms pairs r_{ij}.

Note that a Morse potential is used for the bond stretching term. If a molecule is relatively small and not very crowded, a Hooke's potential can be used in Eq. [2.23] instead. The potentials used in the MM2 force field are shown in Table 2.1:

Table 2.1. MM2 force field potentials (27)

Term	Expression
Stretching	$E_s = 71.94K_s(l - l_0)^2[1 - 200(l - l_0)]$
Bending	$E_\theta = 0.0219K_\theta(\theta - \theta_0)[(1 + 7.0(10)^{-8}(\theta - \theta_0)^4]$
Stretch-bend	$E_{s\theta} = 2.51124K_{s\theta}(\theta - \theta_0)[(l - l_0)_a + (l - l_0)_b]$
Van der Waals	$E_v = \varepsilon\,[2.90(10)^5\exp(-12.50/P) - 2.25P^6]$
Torsion	$E_\omega = V_1/2(1 + \cos\omega) + V_2/2(1 - \cos 2\omega) + V_3/2(1 + \cos 3\omega)$

where l: bond length.

θ: bond angle.

ε: depth of the potential well.

P: Sum of van der Waals radii (Σr^*) divided by the distance (r)

between interaction centres.

ω: dihedral angle of four atoms.

k_s, k_θ, $k_{s\theta}$: constants.

2.2.2 Energy minimization (44)

Most minimization algorithms assume that the energy surface is approximately harmonic (Fig. 2.15). Given a target function that defines the energy surface and an initial starting point (x_0, y_0), a line search is usually used to a one dimensional minimization along a direction which was given by the derivative of the target function. e.g., if the target function is

$$E(x,y) = x^2 + 5y^2 \qquad [2.24]$$

a good initial direction is simply the derivative of the function at the current point:

$$\nabla E = (\partial E/\partial x, \partial E/\partial y) = (2x, 10y) \qquad [2.25]$$

the minimization along this line will be performed until the lowest value obtained (point c in Fig. 2.15), then another direction, which is usually perpendicular to the previous one, is chosen to be searched again. The line search procedure is like stairs pointing to the energy minimum. There are several algorithms such as Steepest descents, Conjugate gradients, Newton-Raphson, commonly used in molecular mechanics minimization, and they all follow the basic idea of line search but use different ways to define a new direction.

The target function used in a calculation depends on the force fields to be used, and the algorithm chosen is based on the requirement of accuracy and efficiency of the calculation.

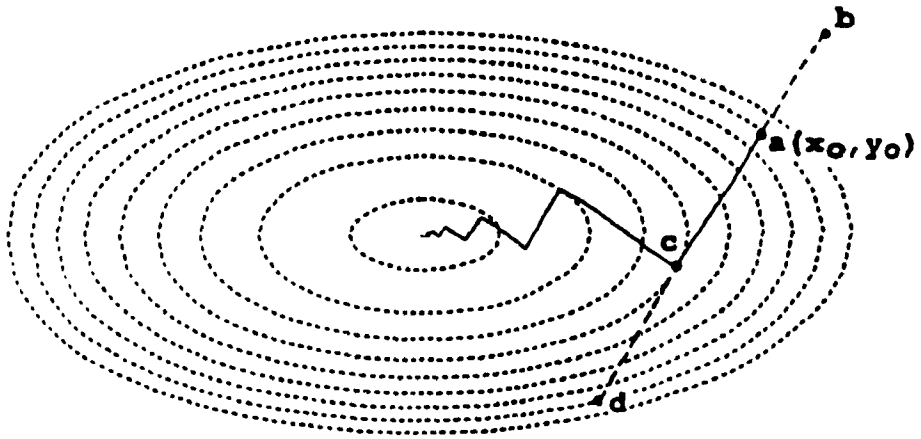

Fig. 2.15. An energy surface for Eq. [2.24] with the gradient from the initial point a (x_0, y_0) defining the line search direction.

Chapter 3

A STUDY OF COMPUTED ROTATIONAL BARRIERS OF METHYL GROUPS AND ^{1}H AND ^{13}C SPIN-LATTICE RELAXATION RATES

Nuclear magnetic resonance measurement of spin-lattice relaxation rates (R_1 values) is a valuable technique for obtaining information on the structure and dynamics of organic molecules in solution. Most ^{1}H relaxation studies have involved the analysis of R_1 values of methine or methylene groups, because of complications associated with the relaxation behaviour of methyl groups, in part associated with the internal rotation of the methyl group which is superimposed on the overall tumbling of the molecule. Methyl group ^{1}H R_1 values have proved difficult to analyze because there is no simple way to model explicitly the motion of the methyl relaxation vectors. Most experimental studies of the effects of internal rotation on methyl relaxation have concentrated on the determination of methyl rotational barriers from ^{13}C R_1 measurements (45).

^{13}C R_1 values of methyl groups in aromatic compounds and alkenes have been qualitatively interpreted in terms of steric influences on methyl group rotation (41). This Chapter reports a study of ^{1}H and ^{13}C methyl relaxation rates of some steroids, aromatic compounds and terpenes in conjunction with a molecular mechanics investigation of methyl group rotational barriers.

3.1 Some theoretical and practical considerations

3.1.1 Dipole-dipole relaxation

In dilute solution (0.1 M in a deuteriated solvent) the spin-lattice relaxation of most ^1H and ^{13}C nuclei is dominated by the intramolecular dipole-dipole mechanism. For a molecule tumbling isotropically in the extreme narrowing region ($\omega_0\tau_c << 1$), the dipole-dipole contribution, $R_1(dd)$, to the overall relaxation rate is given by Eq. [3.1], in terms of the relaxation contribution between two non-equivalent nuclei i, j:

$$R_1(dd) \propto \sum_i \frac{\gamma_i^2\gamma_j^2}{r_{ij}^6}\,\tau_c(i,j) \qquad [3.1]$$

where γ_i and γ_j are the magnetogyric ratios of the i and j nuclei, r_{ij} is their internuclear separation, and $\tau_c(i,j)$ is the motional correlation time of the vector between them. The net R_1 value for a nucleus is dependent on the overall tumbling rate of the molecule as a unit, plus the contribution from any additional motion of a substituent group which carries that particular nucleus. Because of the $1/r^6$ term in Eq. [3.1], the influence of a relaxation pathway is attenuated very rapidly with increasing distance between nuclei, so that it is the near neighbours of a nucleus which dominate its relaxation. As has been mentioned in Chapter 2, a methyl proton relaxes largely to its neighbouring protons on the same carbon atom (8, 46). The carbon atom of a methyl group is relaxed almost exclusively by the protons it carries. The ^1H and ^{13}C R_1 values of methyl groups are known to be sensitive to steric factors which influence the rate of methyl group rotation (8-11). We note that an <u>increase</u> in the rate of methyl group rotation <u>reduces</u> the efficiency of the

dipole-dipole relaxation mechanism.

3.1.2 Spin-rotation relaxation

Relaxation rates of nuclei in methyl groups may also be influenced by the spin-rotation mechanism. There is an inverse dependence of the two mechanisms on the rotational rate of the methyl group (47), i.e. an increase in the rate of methyl group rotation results in an decrease in the efficiency of relaxation by the dipole-dipole mechanism and that will reduce the sensitivity of the overall relaxation rate, R_1.

The presence of spin-rotation contributions to the relaxation of methyl groups may be conveniently detected by measuring the nuclear Overhauser effect enhancements of ^{13}C nuclei under conditions of broad-band proton decoupling. Since the NOE effect is determined by dipole-dipole interactions, its magnitude will be reduced if spin-rotation contributions are significant. Spin-rotation contributions to the ^{13}C relaxation of "freely rotating" methyl groups of aryl methyl compounds have previously been identified by ^{13}C-{^1H} NOE difference experiments (45). These groups showed reduced NOE enhancements compared to those of hindered methyl groups.

^{13}C-{^1H} heteronuclear Overhauser effect difference experiments have been carried out for a number of monoterpenes. None of the methyl groups showed any detectable reduction in their ^{13}C NOE enhancements, indicating that ^{13}C spin rotation relaxation is insignificant in these compounds (Fig. 3.1). The calculated rotational barriers are, in most cases, several kcal/mol higher than those of the aryl methyl

compounds which exhibited spin rotation relaxation. These aryl methyl groups (e.g. in toluene) are effectively free rotators, with rotational barriers close to zero (48). Steroids, which have higher molecular weights and more efficient dipole-dipole relaxation than the terpenes which were examined, are unlikely to exhibit significant relaxation contributions from the spin-rotation mechanism. Bernassau et al (11) established that the dipole-dipole mechanism is the sole ^{13}C relaxation mechanism in their podocarpanes, which are similar in molecular weight and geometry to steroids. ^{13}C-{^{1}H} heteronuclear NOED measurements on 11α-hydroxyprogesterone (**12** in Fig. 3.4), showed no significant changes in the intensities of the 18- and 19-methyl group signals, supporting this assumption (Fig. 3.2). It is assumed that contributions to ^{1}H relaxation mechanisms will parallel those of the ^{13}C nucleus of the same methyl group.

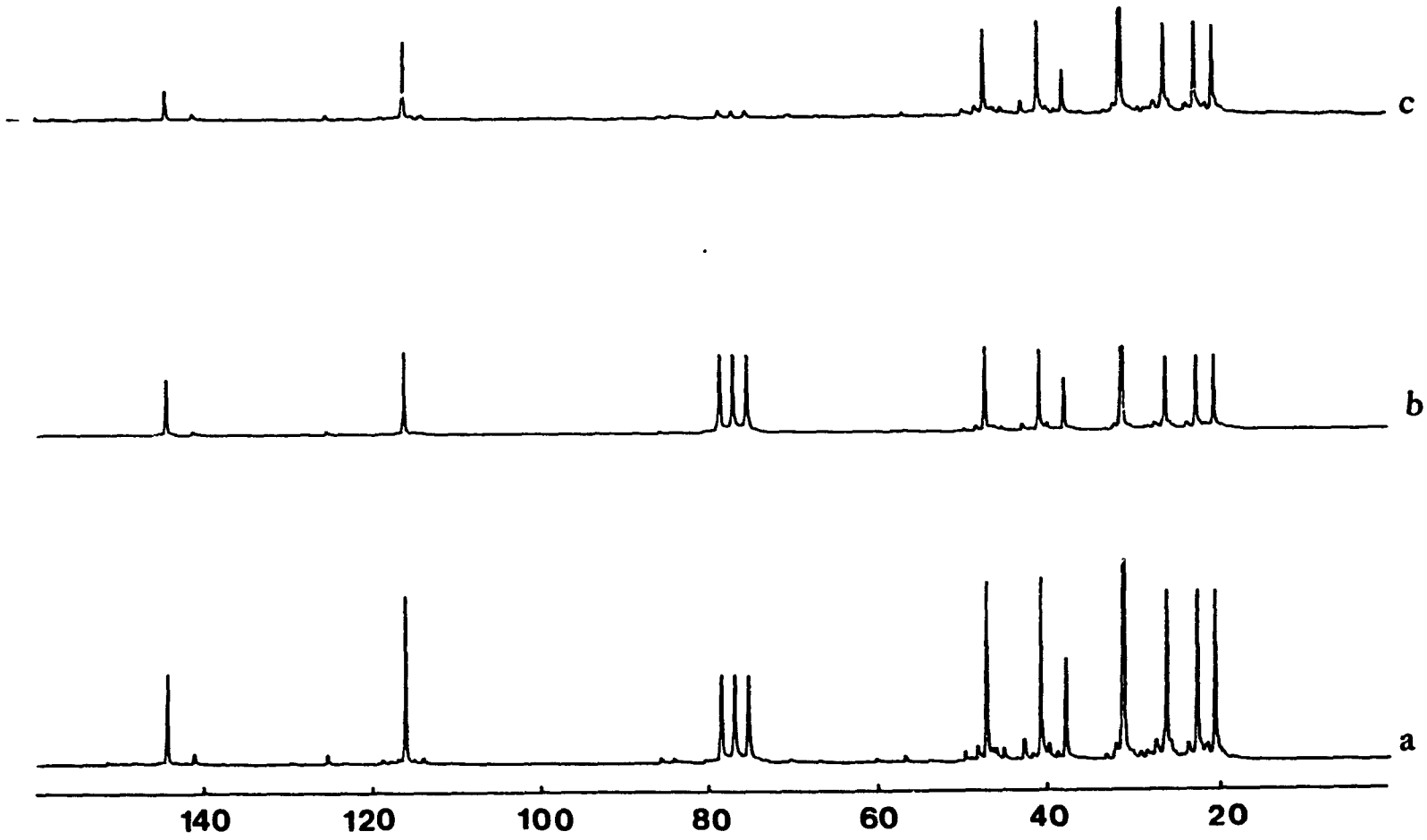

Fig. 3.1. ^{13}C-{^{1}H} NOE experiments of α-pinene. a) with NOE, b) without NOE, c) difference spectra (b-a).

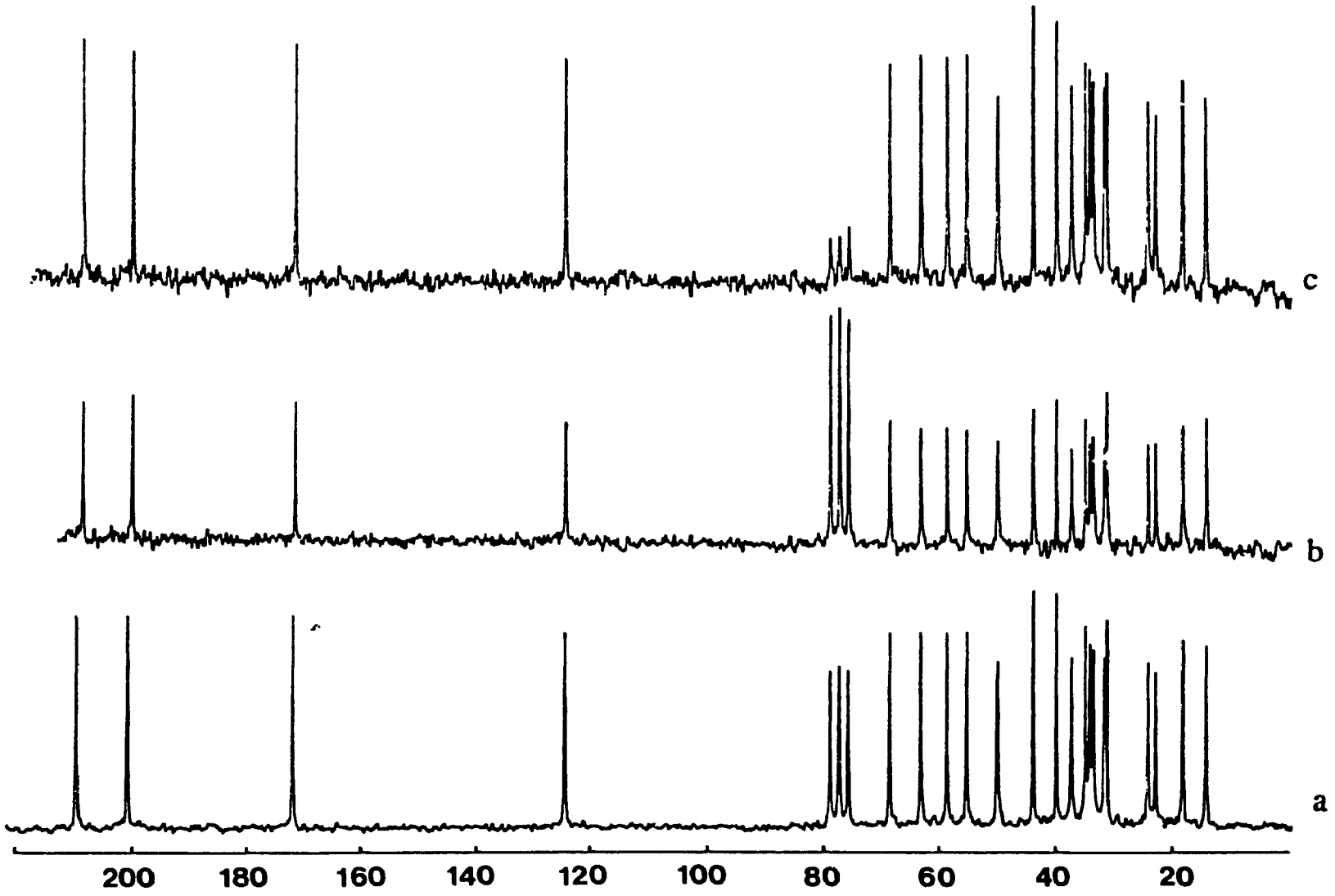

Fig. 3.2. ^{13}C-{^{1}H} NOE experiments of 11α-hydroxyprogesterone. a) with NOE, b) without NOE, c) difference spectra (b-a).

3.1.3 Rotational barriers

ApSimon et al proposed (9) a model for methyl group ^{13}C relaxation in steroids based upon the number and magnitude of 1,3 non-bonded interactions experienced by a methyl group and their effect on the rotational barrier. Similar models have been proposed (8) to explain the relaxation rates of methyl groups in aryl compounds.

These models rely on a qualitative assessment of the nature and number of steric interactions. In less predictable situations than in sparsely substituted steroids and simple methyl substituted aryl hydrocarbons it becomes very difficult to evaluate the effects of steric interactions in order to predict which of a pair of methyl groups will be the more hindered, and hence will relax faster. A certain, efficient method which can be used for estimation of methyl group rotational barriers is highly desired.

3.1.4 Molecular mechanics

The increasing accessibility and simplicity of operation of molecular mechanics calculations make computation of the barriers to rotation of methyl groups feasible. This offers the possibility of combining quantitative estimates of methyl group rotational barriers with experimentally determined R_1 values to evaluate steric influences on methyl group rotation. The calculations can readily be carried out using a suitably equipped personal computer, minicomputer, or workstation. This procedure has been evaluated for a number of types of compounds

containing two or more methyl groups.

Methyl group rotational barriers may be calculated using the "dihedral driver" option of the MM2 or MMP2 algorithms (19), following optimization of the molecular structure. In this procedure, a rotational energy profile is calculated, the energy of the structure being minimized for each chosen dihedral angle of the group being rotated, so that the energy calculated for the transition state of rotation allows conformational changes in the rest of the molecule to accommodate rotation (Fig.3.3).

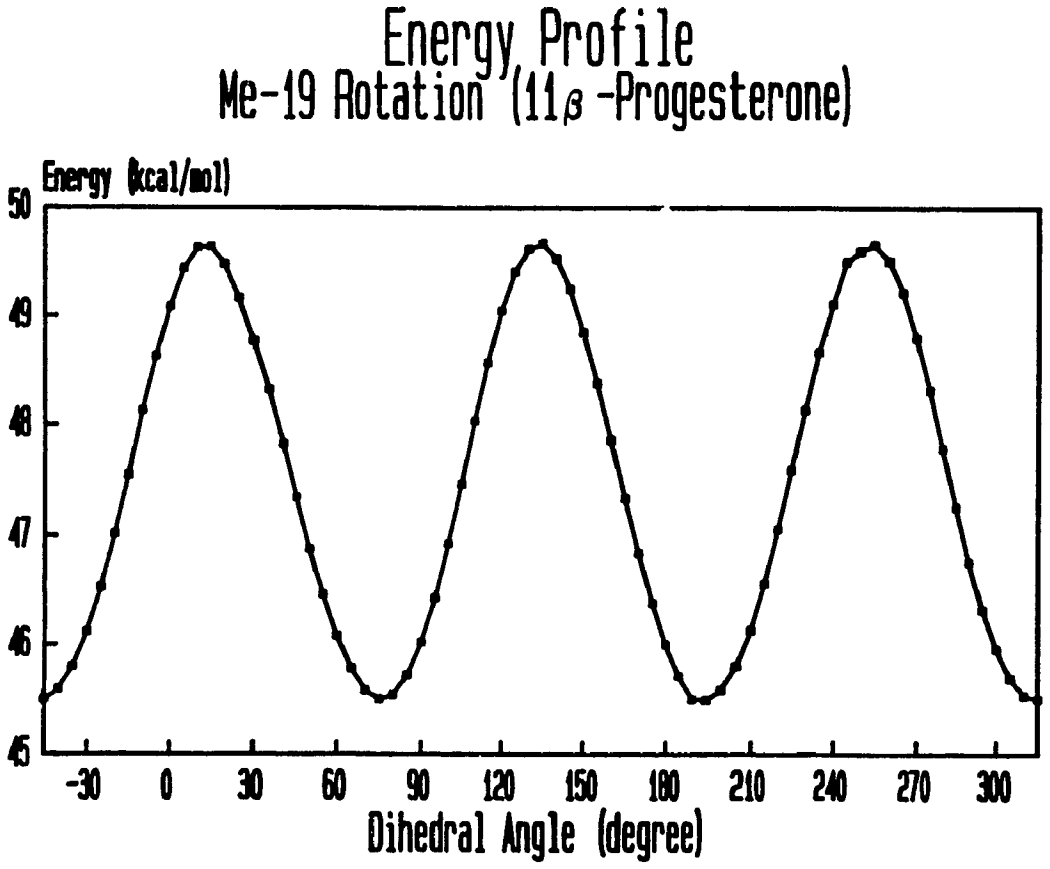

Fig. 3.3. Rotational barrier profile for 11β-progesterone

In the presence of dissolved oxygen, paramagnetic dipolar relaxation will contribute to the overall relaxation rate. In this study, samples for ^{1}H relaxation measurements were degassed by the freeze-pump-thaw cycle to remove any relaxation contribution from oxygen (49). Samples for ^{13}C relaxation studies were measured without degassing.

3.2 Results and Discussion

3.2.1 Chemical shift assignments

Reliable ^{1}H chemical shift assignments of steroids (**1-15**) (Fig. 3.4) based on NOED measurements have been reported for progesterone acetate (50) and 1-dehydrotesterone, **3** (51). The 18- and 19-methyl group chemical shifts in prednisone, **9** , were also assigned using this technique. The remaining steroids (**1, 2, 4-8,** and **10-15**, in the study were assigned (Table 3.1) by comparing their chemical shifts with those of the models, or by correlation with previously assigned ^{13}C spectra.

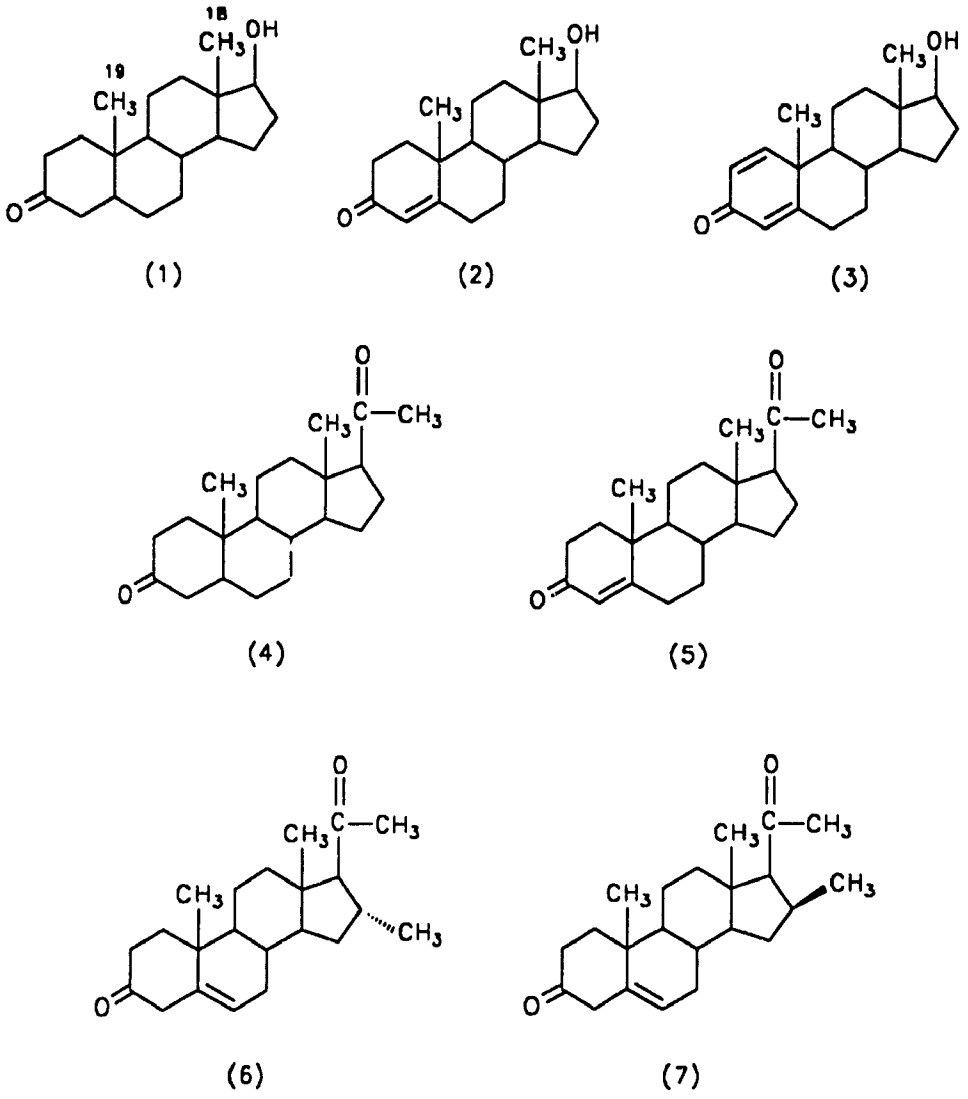

Fig. 3.4. Structures of steroids

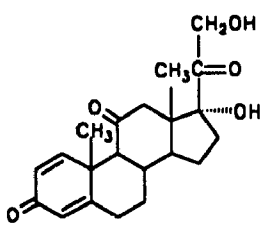

(8)

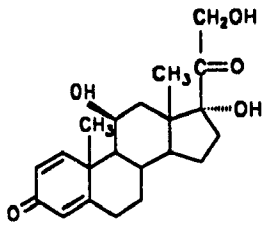

(9)

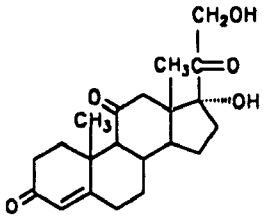

(10)

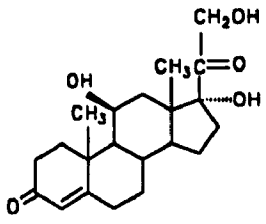

(11)

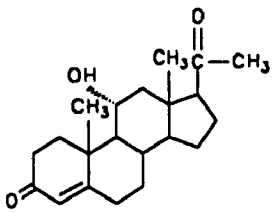

(12)

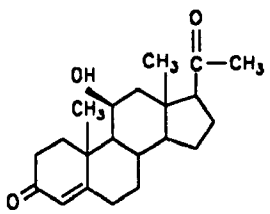

(13)

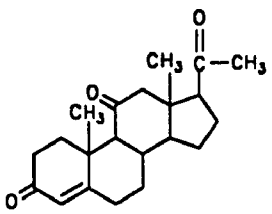

(14)

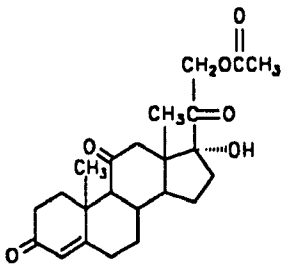

(15)

Fig. 3.4. Structures of steroids (continued)

^{1}H and ^{13}C chemical shifts of methyl groups in the aromatic compounds (**16-25**, Fig. 3.5) studied have been assigned previously (52).

^{1}H and ^{13}C methyl group assignments of terpenes (Fig.3.6) were based on standard methods where possible, or literature chemical shift values considered reliable. Nuclear Overhauser effect difference (NOED) methods were used when necessary and possible for ^{1}H spectra. ^{13}C chemical shifts were correlated with those of the previously assigned ^{1}H spectra when necessary, using the CHORTLE (53) and 2D-HETCOR techniques.

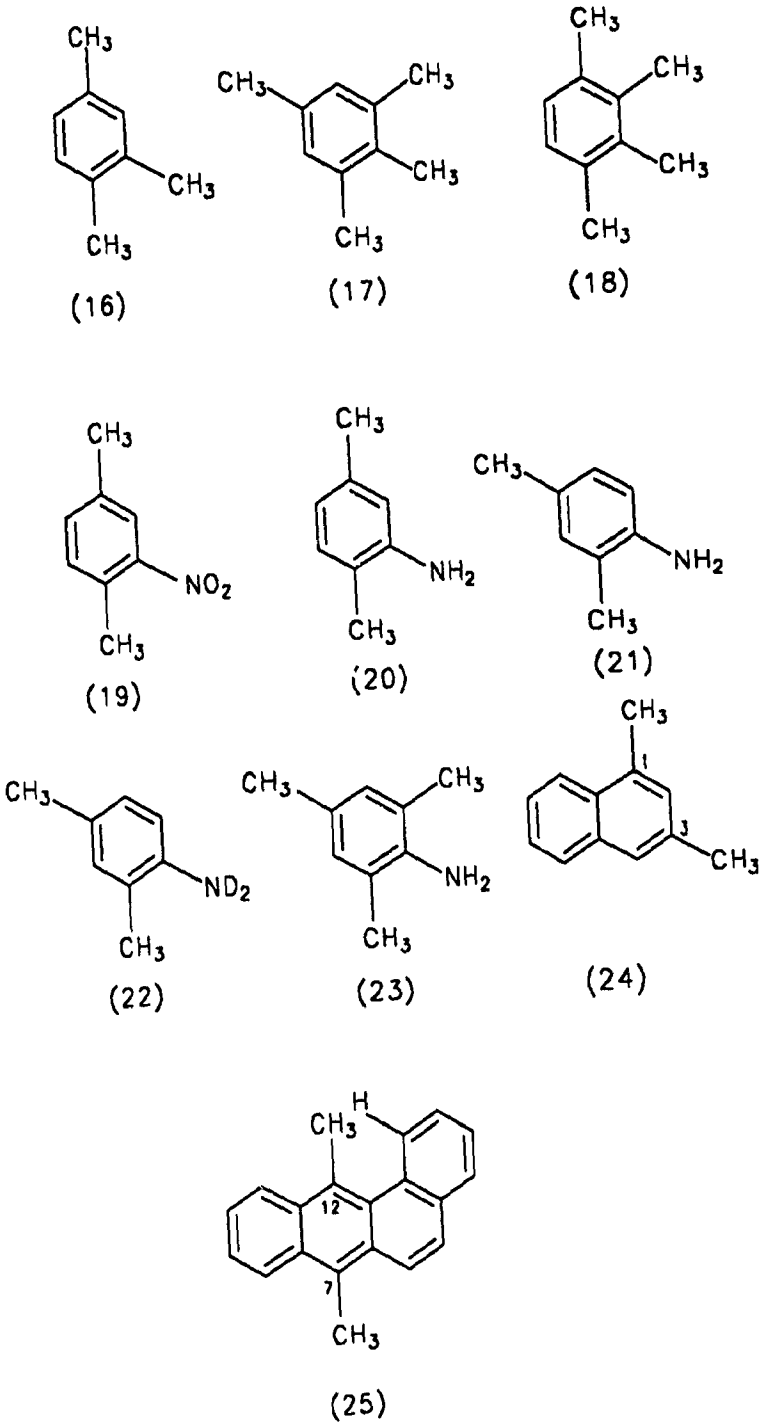

Fig. 3.5. Structures of aromatic compounds.

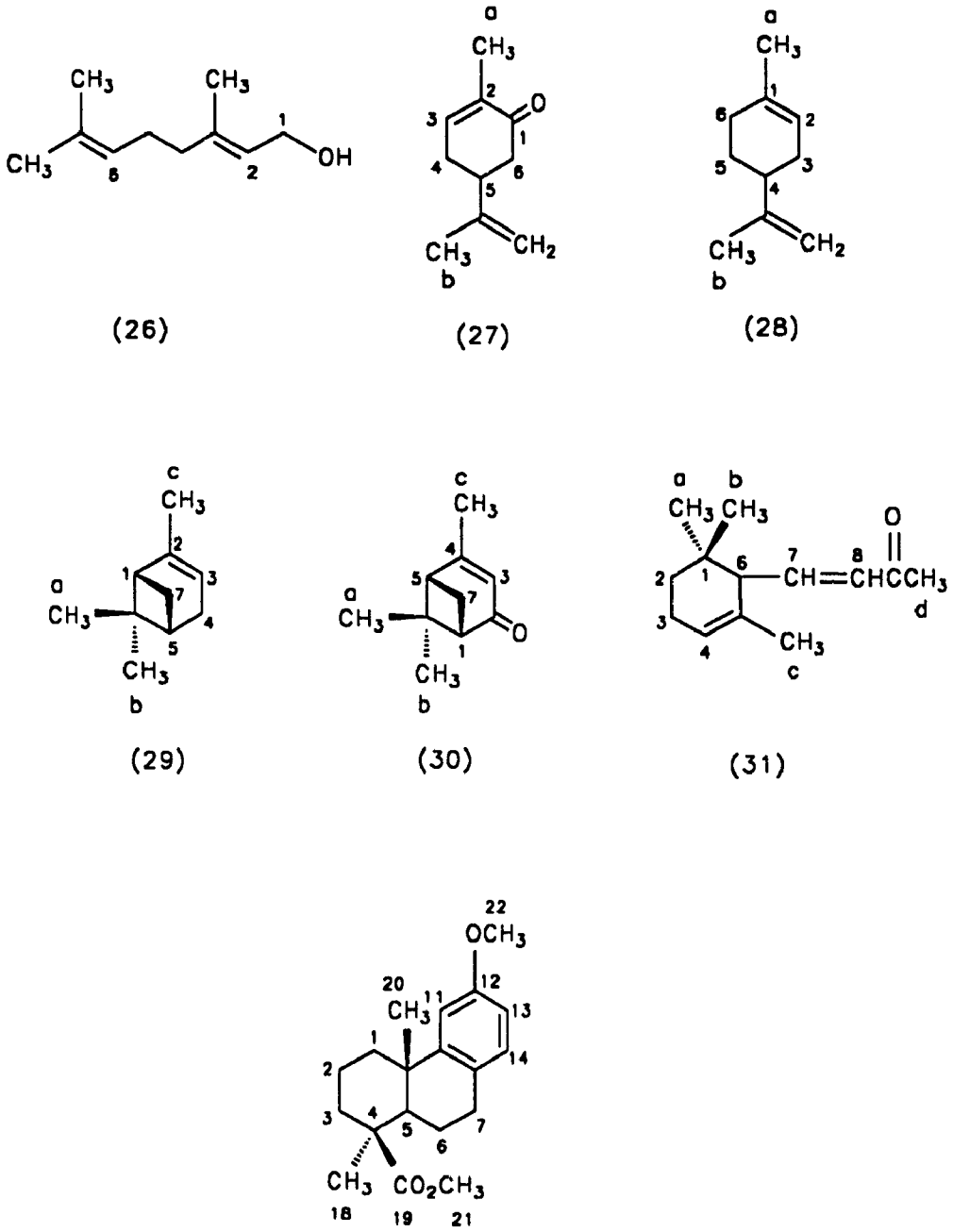

Fig. 3.6. Structures of terpenoids

Geraniol, (**26** in Table 3.2): Three fairly closely spaced methyl singlets, at δ1.60, 1.67, and 1.68, were assigned through NOED experiments (Fig. 3.7). Irradiation of the δ1.67 singlet produced a distinct enhancement of the H-1 signal (2H, δ4.13, doublet, assigned from its integral and chemical shift), so this signal was assigned to the C-3 methyl group (c). Irradiation of the lowest field methyl singlet (δ1.68) enhanced the H-6 signal (1H, δ5.08, vinylic), so this signal was assigned to methyl-b, cis to H-6. The remaining methyl signal (δ1.60) produced no significant enhancement of other signals on irradiation, and was assigned to methyl-a, trans to H-6. Irradiation of the H-1, H-2, and H-6 transitions confirmed the assignments.

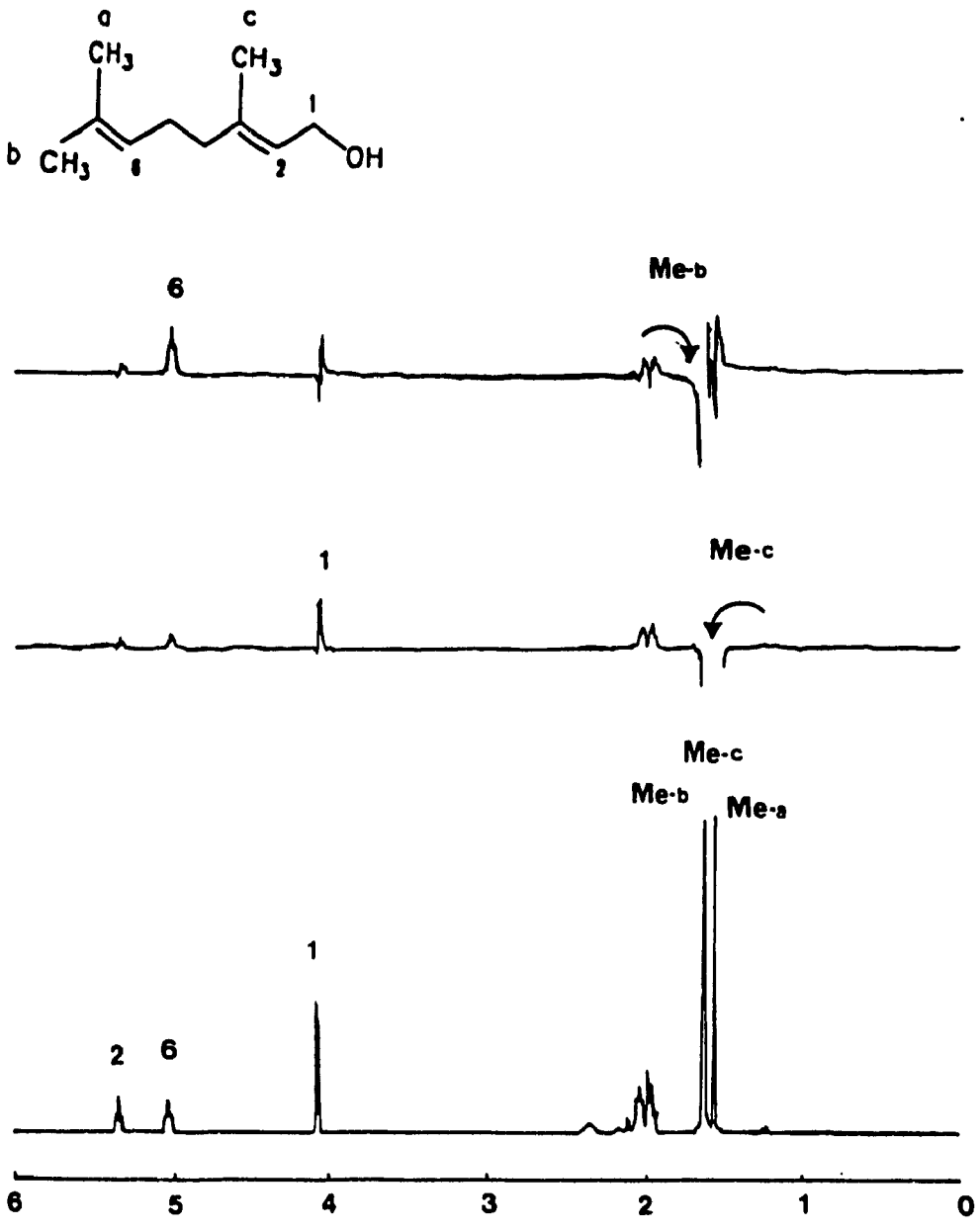

Fig. 3.7. NOED spectra of geraniol at 400 MHz in a 0.1 M $CDCl_3$ solution. Irradiating frequencies are indicated by arrows.

Carvone, **27**: Assignment of the two closely spaced methyl singlets at δ1.72 and 1.74 was based on NOED measurements (Fig. 3.8). Since irradiation of the lower field (δ1.74) methyl transitions enhanced the ring vinylic proton signal (1H, δ6.71), the δ1.74 signal was assigned to methyl-a. Irradiation of the δ1.72 signal produced a weak enhancement of a signal near δ4.8 (2H, terminal vinylic protons), confirming the assignment of the δ1.72 signal to methyl-b.

Limonene, **28**: Individual assignment of the three-proton singlets at δ1.58 and 1.64 to the two allylic methyl groups was achieved through observation of NOE enhancements of the vinyl protons (Fig. 3.9). Thus, irradiation of the δ1.64 methyl (methyl-b) transitions led to enhancement of the terminal vinylic (2H) proton signal (δ4.72), whereas irradiation of the δ1.58 methyl (methyl-a) transitions enhanced the signal of the ring vinylic proton (1H, δ5.34, H-2).

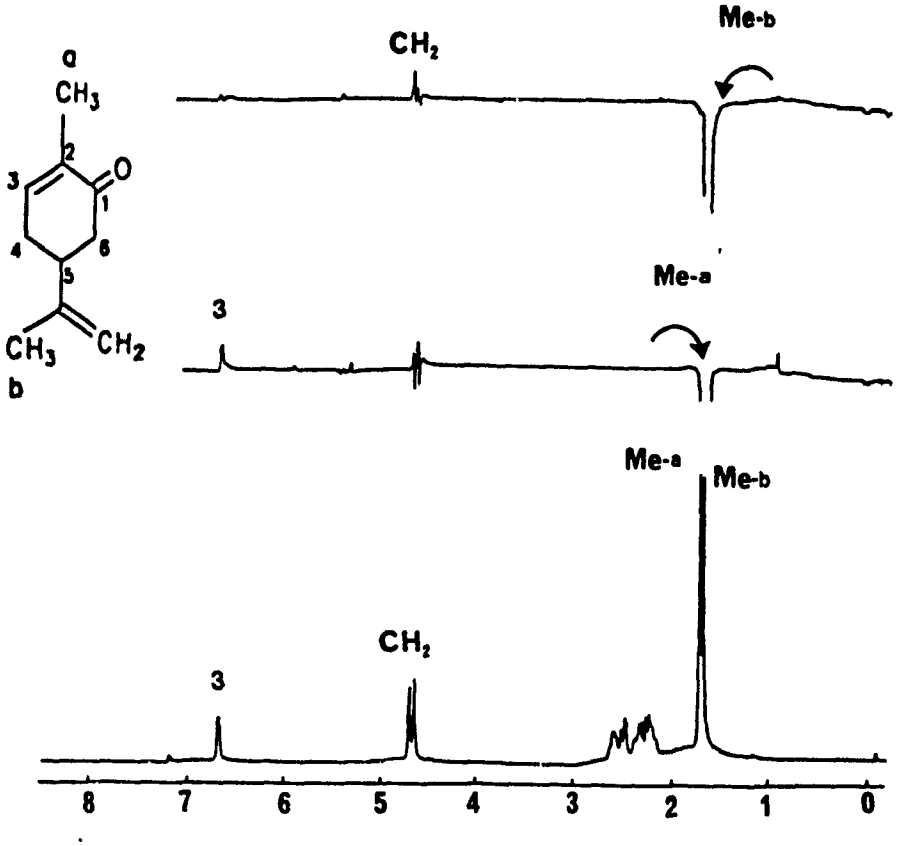

Fig. 3.8. NOED spectra of carvone at 400 MHz in a 0.1 M $CDCl_3$ solution.

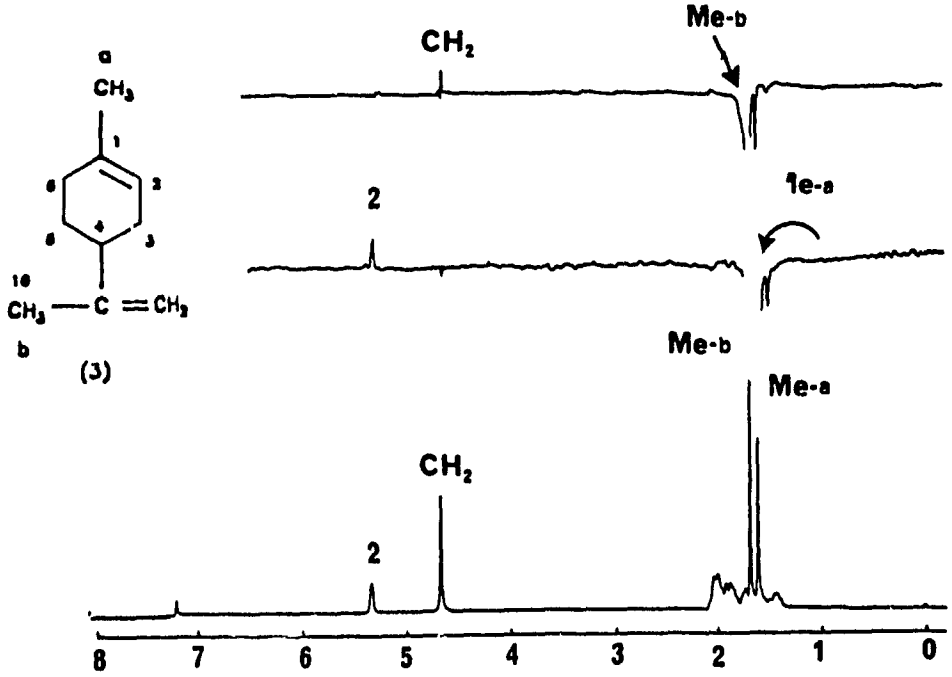

Fig. 3.9. NOED spectra of limonene at 400 MHz in a 0.1 M $CDCl_3$ solution.

α-Pinene, **29**: The δ1.65 methyl signal was assigned to the allylic methyl group (c), based on its chemical shift. The diastereotopic geminal methyl groups, with signals at δ0.84 and 1.26, were assigned through NOED experiments (Fig. 3.10). Irradiation of the higher field singlet (δ0.84) enhanced the intensity of a broad singlet (1H) at δ5.18, assigned to vinylic proton H-3 on the basis of chemical shift, indicating that the δ0.84 methyl group is directed towards C-3 (methyl-b). Irradiation of the lower field methyl signal (δ1.26) enhanced the signals of several ring protons (H-1, H-5, and one of the C-7 protons, assigned later), confirming that this methyl group is directed towards C-7 (methyl-a).

Irradiation of the allylic methyl (c) signal caused enhancements at 5.18 ppm (H-3), and 1.93 ppm, assigned to the allylic proton (H-1) at the bridgehead. Since irradiation of the 2.33 ppm signal caused strong enhancement of the 1.15 ppm signal, confirmed by the reverse experiment, these resonances were assigned to the geminal C-7 protons. Since the 2.33 ppm signal was enhanced when methyl-a was irradiated, it must arise from the C-7 proton (7b) directed towards methyl-a. The 1.15 ppm signal, which on irradiation caused enhancement only of the signal from its geminal neighbour, was assigned to the C-7 proton (7a) directed towards C-3. Irradiation of a multiplet at 2.21 ppm (2H) enhanced the H-3 signal, so this signal was assigned to the C-4 protons. The only unassigned signal, at 2.18 ppm (1H), must arise from H-5.

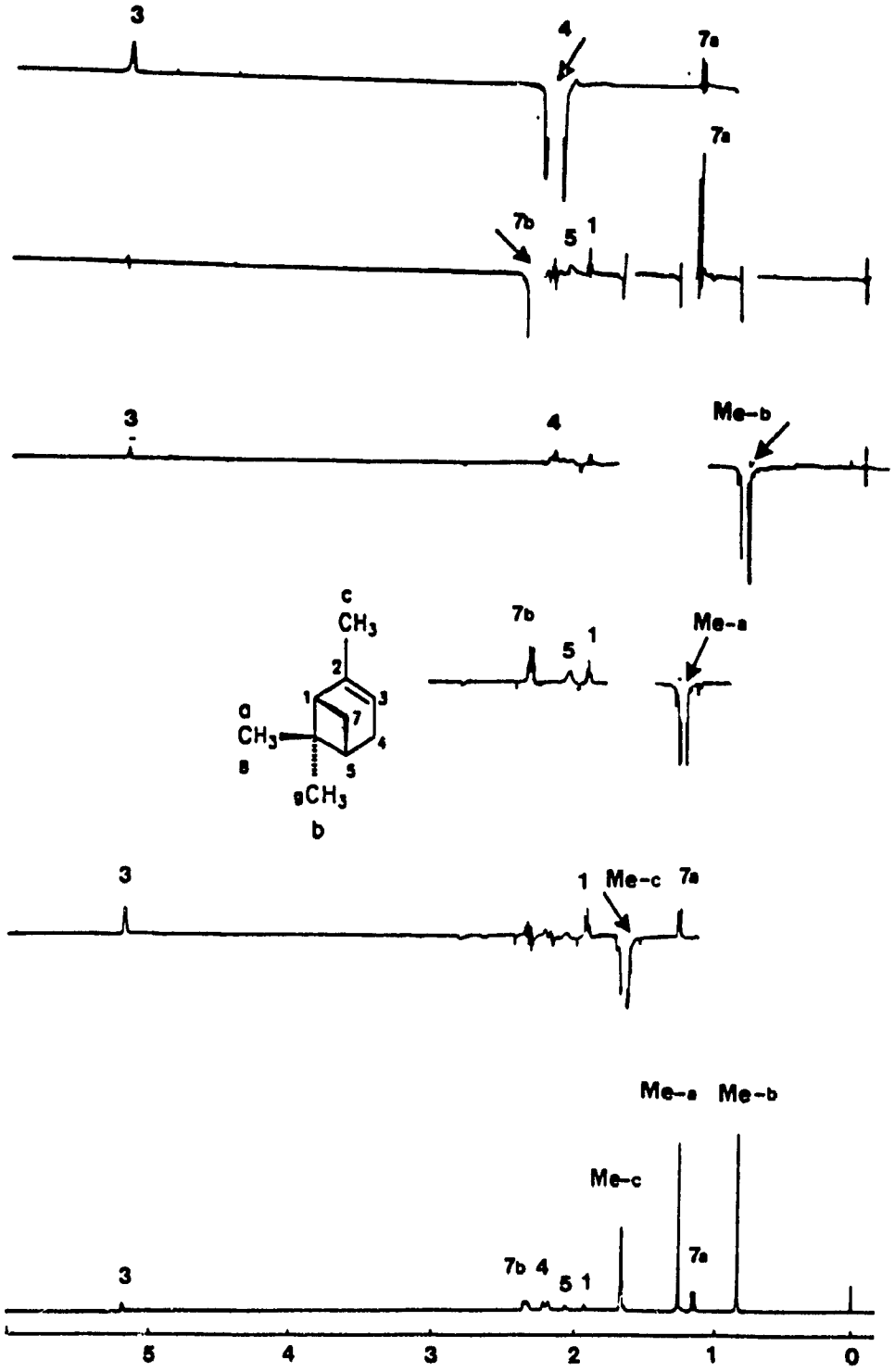

Fig. 3.10. NOED spectra of α-pinene at 400 MHz in a 0.1 M $CDCl_3$ solution.

Verbenone, **30**: The δ2.1 methyl singlet was assigned on the basis of chemical shift to the allylic methyl group (c). The diastereotopic geminal methyl groups give rise to sharp singlets at δ1.5 and 1.0, and were assigned by NOED measurements (Fig. 3.11). Irradiation of the high field, δ1.0, geminal methyl transitions caused enhancement of the δ1.5 methyl signal (confirming its assignment as a geminal methyl) and a weak enhancement of the H-3 signal. The existence of a relaxation pathway between this methyl group and H-3 indicates that the δ1.0 methyl group must be directed towards C-3 (methyl-b in the structure). Irradiation of the other geminal methyl signal (δ1.5) resulted in enhancement of the signal of its geminal neighbour (δ1.0), and the signals at δ2.9, 2.7, and 2.4, consistent with its being directed towards C-7 (methyl-a). Irradiation of the δ2.0 allylic methyl signal (methyl-c) enhanced the signals of H-3 (its cis vinylic neighbour) and the δ2.4 signal, which is, therefore, assigned as the vicinal neighbour, H-5.

Irradiation of the δ2.9 signal caused strong enhancement of the δ2.2 signal, verified by the reverse experiment. These two signals were, therefore, assigned to the diastereotopic geminal proton pair on the bridge at C-7. Since irradiation of the methyl-a transitions caused enhancement of the δ2.9, but not the δ2.2 signal, the δ2.9 signal is assigned to the C-7 proton (7b) which is directed towards, and in close proximity to, this methyl group. By elimination, the signal at δ2.7 must be assigned to H-1.

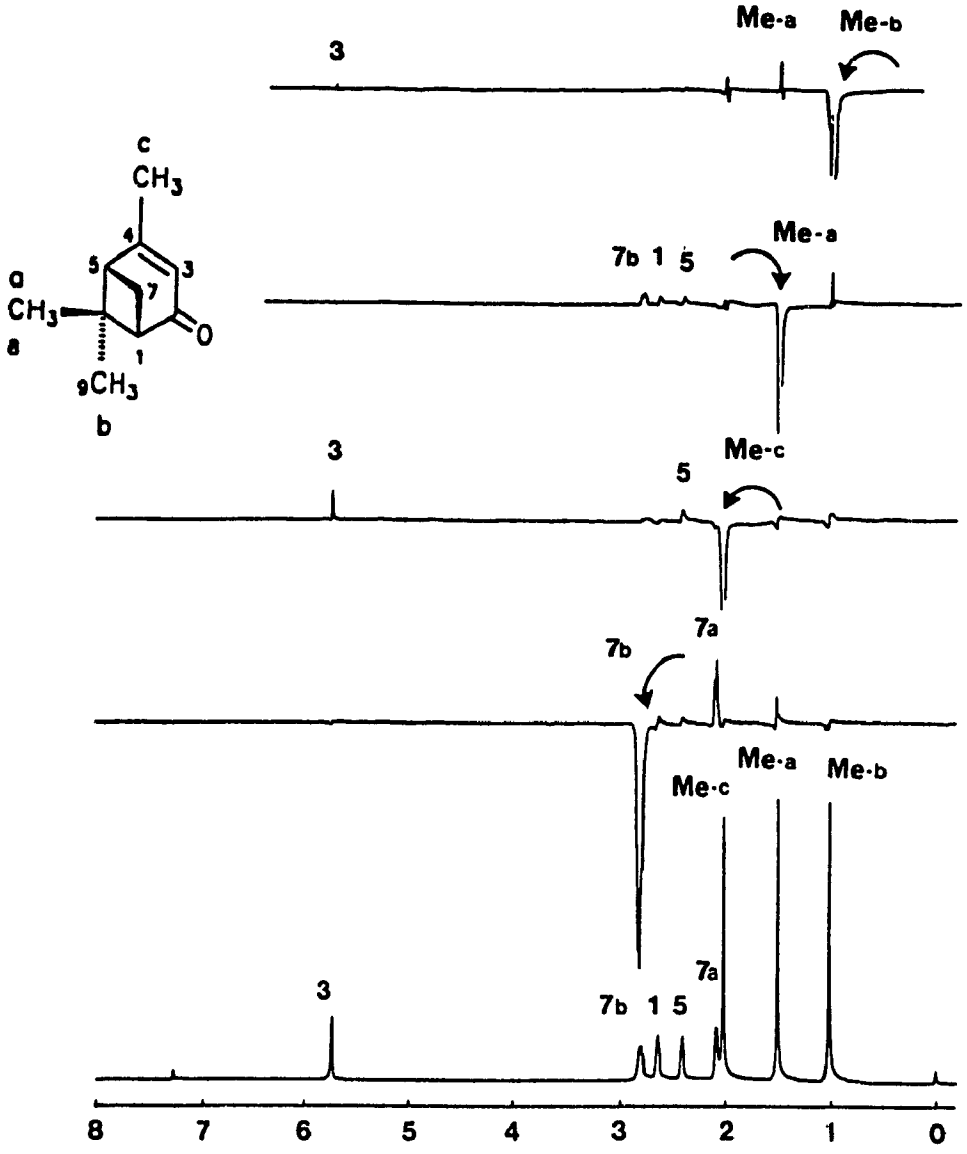

Fig. 3.11. NOED spectra of verbenone at 400 MHz in a 0.1 M $CDCl_3$ solution.

α-Ionone, **31**, and methyl O-methylpodocarpate, **32**: Chemical shift assignments were carried out using earlier ^{13}C assignments (40, 53), NOED, COSY, and HETCOR methods in conjunction with stereochemical and molecular modelling studies, which will be reported in Chapter 4 (54).

Table 3.1.

Chemical shifts[a] of the 18- and 19-methyl groups of steroids

Compound	^{1}H (ppm)		^{13}C (ppm)	
	18	19	18	19
1 Androstanolone	0.76	1.03	11.04[b]	11.37[b]
2 Testosterone	0.81	1.21	10.93	17.35
3 1-Dehydrotestosterone	0.82	1.25	11.04	18.59
4 Pregnanedione	0.60	1.00	11.63	13.57
5 Progesterone	0.65	1.18	13.44	17.63
6 16α-Methylpregnenolone	0.66	1.02		
7 16β-Methylpregnenolone	0.96	1.00		
8 Prednisone[c]	0.50	1.40	15.18	18.47
9 Prednisolone[c]	0.80	1.40	16.68	20.69
10 Cortisone[c]	0.46	1.30	15.25	16.78
11 Hydrocortisone[c]	0.74	1.36	16.81	20.37
12 11α-Hydroxyprogesterone	0.70	1.32	14.06	17.92
13 11β-Hydroxyprogesterone	0.92[d]	1.46[d]		
14 11-Ketoprogestone	0.62	1.40	13.74	16.79
15 Cortisone acetate	0.61	1.36		

[a] $CDCl_3$ solution, unless otherwise noted.

[b] Uncertain assignment.

[c] DMSO-d_6 solution.

[d] Assigned by comparison with progesterone, **5**.

Table 3.2. Chemical shifts of methyl groups[a] of terpenes

Compound	Methyl	^{1}H (ppm)	^{13}C (ppm)
Geraniol, **26**	a	1.60	17.42
	b	1.68	25.40
	c	1.67	16.01
Carvone, **27**	a	1.74	15.23
	b	1.72	20.10
Limonene, **28**[b]	a	1.60	23.61
	b	1.64	20.89
α-Pinene, **29**	a	1.26	26.33
	b	0.84	20.74
	c	1.65	22.86
Verbenone, **30**	a	1.50	26.57
	b	1.01	22.03
	c	2.02	23.44
α-Ionone, **31**	a	0.86	27.79
	b	0.93	26.91
	c	1.57	22.79
	d	2.24	26.91
Methyl O-methyl podocarpate, **32**[c]	18	1.26	
	20	1.02	
	21	3.64	
	22	3.75	

[a] Measurements were made on $CDCl_3$ solutions, 400.1 MHz for ^{1}H, 20.1 MHz for ^{13}C.

[b] 0.1M C_6D_6 solution.

[c] ^{13}C assignments for this compound have been reported (54).

3.2.2 Spin-lattice relaxation rates and rotational barriers

3.2.2.1 Steroids

The steroids examined in this study were classified into four groups according to the effects of structural changes on the 18- and 19-methyl groups (Fig. 3.4):

Series I: Compounds **1-5**. Double bonds were successively introduced into ring A, so that non-bonded interactions involving the 19-methyl group were affected, but the 18-methyl group remained essentially unaffected.

Series II: Compounds **6,7**. The configurations of substituents (H, CH_3) at C-16 were interchanged, with consequent changes in non-bonded interactions with the 18-methyl groups.

Series III: Compounds **8-11**. The configuration of a hydroxyl group at C-11 was inverted and it was replaced by an oxo group to study the influence on rotational barriers and relaxation rates of both the 18- and the 19-methyl groups.

Series IV: Compounds **12-14**. The configurations of hydroxyl groups and the oxidation state at C-11 were varied for another series of compounds with a different substitution pattern at C-17.

a. Two types of comparison

The influences of structural changes on the rotational barriers and relaxation rates of the 18- and 19-methyl groups were investigated using two types of comparisons. Internal comparison permitted direct study of ^1H and ^{13}C spin-lattice

relaxation rates of the 18- and 19-methyl groups and their computed rotational barriers within a molecule as structural changes were introduced (Series I and II). Since the relaxation rates of the 18- and 19-methyl groups are being compared within a single molecule both groups experience similar influences from overall molecular tumbling. Examination of the ^{13}C relaxation rates of the protonated ring carbon atoms of testosterone, **2**, showed no evidence for anisotropic motion of the ring backbone (56), and it is assumed that any effects of overall anisotropic motion on 18- and 19-methyl group relaxation are negligible in all of the compounds examined. External comparison was necessary when the effects of structural changes influence both the 18- and 19-methyl groups, requiring study of the relaxation rates and computed rotational barriers in different compounds (Series III and IV). Normalization of the relaxation rates to that of a nucleus remote from the site of structural change is essential when external comparisons are being made, since the effects of differing experimental conditions and molecular tumbling rates must be eliminated.

b. Spin-lattice relaxation rates and rotational barriers

^{1}H and ^{13}C 18- and 19-methyl group R_1 values are reported for fifteen steroids (Tables 3.3 - 3.5). In Series I, androstanolone, **1**, testosterone, **2**, and dehydrotestosterone, **3**, double bonds are successively introduced into the A ring, the rest of the molecule remaining unchanged. Similarly, the pair of compounds, 5α-pregnane-3,20-dione, **4**, and progesterone, **5**, differ by the introduction of a C4-C5 double bond into the latter (Table 3.3). It has been demonstrated previously that

removal of 1,3-nonbonded interactions between axial A-ring hydrogens and the 19-methyl group following the introduction of double bonds influences the ^{1}H and ^{13}C relaxation rates of this group (7, 8). Using qualitative arguments, this effect has been attributed to changes in the rate of rotation of the group resulting from changes in steric interference.

Removal of 1,3-nonbonded interactions is predicted to cause an increase in the rotational barrier of the 19-methyl group. In androstanolone, **1**, the compound with the maximum number of nonbonded interactions, the 19-methyl group has no energetically favorable conformation available--its rotational ground state energy is high. As nonbonded interactions are removed, available conformations become energetically more favorable, and the differences between rotational ground and transition state energies increase--the rotational barrier increases (4).

In Series I, the computed rotational barriers for the 18-methyl groups are essentially identical (Table 3.3), as expected. The computed barriers of the 19-methyl groups reflect the stabilization of the rotational ground state energies as double bonds are successively introduced (Table 3.3), increasing from 3.22 kcal/mol in androstanolone, **1**, to 5.07 kcal/mol in dehydrotestosterone, **3**. In androstanolone, the computed barrier for the 19-methyl group is smaller (89%) than that of the 18-methyl group - in the other compounds it is larger, 120% and 142% in testosterone and dehydrotestosterone, respectively. Thus, computation supports the qualitative model used previously (4, 5).

The ^{13}C R_1 values in this series correlate well with the computed rotational barriers. Thus, in androstanolone, **1**, the 19-methyl group is predicted to have a

lower barrier than the 18-methyl, and the observed ^{13}C relaxation rate is lower (85%). However, the ^{1}H relaxation rates of these groups are the same within experimental error in this compound. In the other two compounds, the 19-methyl group is predicted to have a higher barrier than the 18-methyl, and both the observed ^{1}H and ^{13}C R_1 rates are higher.

The dynamic range of ^{1}H R_1 values is much smaller than that of the ^{13}C R_1 values, and the correlation with predicted rotational barriers is not quite as good. In androstanolone, **1**, the 18- and 19-methyl relaxation rates are almost identical despite the predicted higher rate of the 18-methyl group. In the other two compounds, the 19-methyl group ^{1}H R_1 rates correlate well with prediction. Throughout the group, the changes in the 19-methyl group relaxation rates correlate well with the predicted changes in the rotational barriers.

Similarly, in the pregnanedione - progesterone pair, **4** and **5**, the predicted 18-methyl rotational barriers are identical, whereas the predicted 19-methyl group rotational barriers increase on the introduction of unsaturation to the A-ring. In both cases, the 19-methyl group is predicted to have a higher rotational barrier than the 18-methyl group. In both cases, the ^{13}C relaxation rates are significantly higher for the 19-methyl group, in accord with prediction. In pregnanedione, **4**, the ^{1}H R_1 values of the 18- and 19-methyl groups are almost identical, despite prediction, but the correlation is better in progesterone, with a higher predicted rotational barrier.

The 16α- (**6**) and 16β-methylpregnenolone (**7**) pair (Series II) differ through a configurational change at C-16, which should affect the 18- more than the 19-methyl group. Internal comparison shows a good correlation between rotational

barriers and relaxation rates for both compounds, e.g. the rotational barrier of the 19-methyl group of **6** is higher than that of the 18-methyl group. (3.78 vs 3.21 kcal/mol), and the ^1H R_1 value of the 19-methyl group is higher than that of the 18-methyl group (1.64 vs 1.35 s^{-1}). Steroid **7** showed as good a correlation as **6**. The ^1H R_1 data show that epimerization at C-16 does affect that relaxation rate of the 18-methyl group, as predicted, but there is no detectable influence at the 19-methyl group.

Table 3.3. Calculated methyl rotational barriers[a] and spin-lattice relaxation rates[b] of steroids (Series I & II)

Compound	--- 18-methyl --- R_1 (s^{-1}) ^1H	^{13}C	RB[c]	--- 19-Methyl --- R_1 (s^{-1}) ^1H	^{13}C	RB[c]	---- Ratios ---- R_1(19/18) ^1H	^{13}C	RB
Series I									
1	1.01 0.92[d]	0.27	3.61	1.04 0.96[d]	0.23	3.22	1.03 1.04[d]	0.85	0.89
2	0.94 1.04[d]	0.29	3.59	1.17 1.20[d]	0.38	4.32	1.24 1.15[d]	1.31	1.20
3	1.13	0.33	3.58	1.58	0.75	5.07	1.40	2.27	1.42
4	0.96	0.22	2.58	0.95	0.27	3.47	0.99	1.23	1.34
5	0.98	0.32	2.58	1.12	0.43	4.35	1.14	1.34	1.69
Series II									
6[d]	1.35		3.21	1.64		3.79	1.21		1.18
7[d]	1.22		2.51	1.64		3.10	1.34		1.24

[a] Calculated using the dihedral driver option of MMX.

[b] Measured at 400 MHz (^1H, degassed 0.1M $CDCl_3$ solutions) or 20.1 MHz (^{13}C, non-degassed $CDCl_3$ solutions), and calculated by non-linear regression, unless otherwise noted.

[c] Calculated rotational barrier, kcal/mol.

[d] Measured at 270 MHz (non-degassed 0.1 M $CDCl_3$ solutions), and calculated using the null point method (8).

The compounds in series III provide a somewhat different comparison. Since the changes in the molecules at C-11 should affect both the 18- and the 19-methyl groups, external comparison was applied in this series by normalizing the methyl group R_1 values to those of ^{1}H-4 and ^{13}C-4. The calculated rotational barriers of the 18- and 19-methyl groups in **8** are lower than those of **9** (18-: 2.78 vs 3.24 kcal/mol; 19-: 4.08 vs 4.82 kcal/mol, respectively), thus the normalized ^{1}H relaxation rates of both methyl groups in **8** showed lower values than in **9** (18-: 3.67 vs 4.30; 19-: 3.47 vs 3.69) (Table 3.4). The normalized ^{13}C R_1 values, which show a small range, did not give as good correlations as the ^{1}H R_1 values (18-: 0.48 vs 0.50; 19-: 0.46 vs 0.42). Similarly, the rotational barriers of **10** and **11** correlated well with the R_1 values except that the ^{13}C R_1 values of both compounds are again similar. Internal comparisons in this series show anomalies which are discussed later.

Comparison of **8** with **10**, and **9** with **11** shows that removal of 1,3 non-bonded interactions significantly increases the rotational barrier and the ^{1}H relaxation rates of the 19-methyl groups.

Series IV enables comparison of the effects of equatorial and axial hydroxyl and oxo groups in the 11-position of steroids. External comparison shows that both the 18- and the 19-methyl groups are affected by a change in stereochemistry or oxidation state at C-11. The 18-methyl group in 11β-hydroxyprogesterone, **13**, has the highest rotational barrier (3.95 kcal/mol) and the highest normalized (3.00) ^{1}H R_1 value in the series, while its epimer, 11α-hydroxyprogesterone, **12**, has the lowest rotational barrier (2.47 kcal/mol) and the lowest normalized relaxation rate (2.09).

The ketone, **14**, has an intermediate barrier (2.78 kcal/mol) and relative R_1 value (2.67). The 19-methyl groups in this series are less sensitive to the substituent at C-11. The rotational barrier of the 19-methyl group of **12** (4.35 kcal/mol) is slightly higher than that of **13** (4.32 kcal/mol), as is its normalized ^1H R_1 (2.45 vs 2.20), whereas the ketone, **14**, has the lowest rotational barrier (4.08 kcal/mol) and relative relaxation rates (2.09). Thus, external correlations between rotational barriers and relaxation rates in series IV are all in the expected sense.

Table 3.4. Calculated methyl rotational barriers[a] and spin-lattice relaxation rates[b] of steroids (Series III & IV)

Compound	--- 18-methyl --- $R_1(s^{-1})$ ^1H	^{13}C	RB[c]	--- 19-Methyl --- $R_1(s^{-1})$ ^1H	^{13}C	RB[c]	----- Ratios ----- R_1(19/18) ^1H	^{13}C	RB
Series III (DMSO-d_6 solution)									
8	3.67	0.48	2.78	3.47	0.46	4.08	0.95	0.96	1.47
9	4.30	0.50	3.24	3.69	0.42	4.82	0.86	0.84	1.49
10	2.36	0.54	2.72	1.90	0.42	3.19	0.80	0.78	1.17
11	3.86	0.53	3.23	3.12	0.48	4.01	0.81	0.91	1.24
Series IV ($CDCl_3$ solution)									
12	2.09	0.48	2.47	2.45	0.66	4.35	1.17	1.38	1.76
13[d]	3.00		3.95	2.20		4.32	0.74		1.09
14	2.67	0.81	2.78	2.09	0.51	4.08	0.78	0.63	1.47

[a] Calculated using the dihedral driver option of MMX.

[b] Determined at 400 (^1H, degassed) or 20.1 (^{13}C, non-degassed) MHz, and calculated by non-linear regression, unless otherwise noted. The R_1 values are normalized to the R_1 value of ^1H-4 or ^{13}C-4 (= 1.0).

[c] Calculated rotational barrier, kcal/mol.

[d] Determined at 270 MHz (0.1 M in $CDCl_3$, non-degassed), and calculated using the null point method (8).

In series III and IV all 19-methyl groups are predicted to have higher rotational barriers than the 18-methyl groups. However, internal comparison shows that both the ^{1}H and ^{13}C relaxation rates of all of the 18-methyl groups are higher than those of the 19-methyl groups, with the exception of compound **12.** Since these compounds contain several carbonyl and hydroxyl groups, it is suggested that the methyl group rotational barriers are affected by strong solvation or association in solution.

Limited solubility in non-polar solvents of steroids highly functionalized with polar groups restricted investigation of solvent effects on methyl group relaxation. However, ^{1}H relaxation rates in both $CDCl_3$ and DMSO-d_6 solutions of 11α-hydroxyprogesterone, **12**, and cortisone acetate, **15**, could be measured. Average relaxation rates were higher in the more viscous solvent, DMSO-d_6, than in $CDCl_3$ solution in both compounds, e.g. the ^{1}H R_1 of H-4 in **15** is 1.35 s^{-1} in DMSO-d_6 and 0.79 s^{-1} in $CDCl_3$.

For compound **12**, the normalized (with respect to H-4) R_1 values in DMSO-d_6 of both the 18- and the 19-methyl groups are higher than those in $CDCl_3$, indicating that solvation affects the local motion of both methyl groups (Table 3.5). Since the molecule has polar functional groups adjacent to both methyl groups (a hydroxyl group centrally located and carbonyl groups flanking the methyl groups), solvation affects both methyl groups. Therefore, experimental R_1 data for the two methyl groups are consistent with the prediction.

For compound **15**, the density of polar functional groups is higher near ring D and, in DMSO-d_6 solution, the spin-lattice relaxation rate of the 18-methyl group is higher than that of the 19-methyl group (2.76 vs 2.00, normalized), contrary to prediction (Table 3.5). The same discrepancy has been noted for compounds **8** - **13**. However, in $CDCl_3$ solution, the 18-methyl group of **15** relaxes more slowly than the 19-methyl group (1.96 vs 2.35, normalized), in accord with prediction. These results indicate that there are differential solvent effects on the spin-lattice relaxation rates of the 18- and 19-methyl groups of **15**, and that the discrepancies from predictions based on molecular modelling occur when the more polar solvent is used.

Table 3.5 Calculated methyl rotational barriers[a] and ^1H spin-lattice relaxation rates[b] (12 & 15)

Solvent	18-methyl		19-methyl		Ratio, 19/18	
	R_1[c]	RB[d]	R_1[c]	RB[d]	R_1	RB
12 DMSO-d_6	2.90	2.47	3.53	4.35	1.22	1.76
	(2.26)		(2.75)			
12 $CDCl_3$	2.72	2.47	3.21	4.35	1.17	1.76
	(2.09)		(2.47)			
15 DMSO-d_6	3.73	3.71	2.70	3.79	0.72	1.02
	(2.76)		(2.00)			
15 $CDCl_3$	2.48	3.71	2.97	3.79	1.20	1.02
	(1.96)		(2.35)			

[a] Molecular mechanics calculations were carried out on an Olivetti M24 computer, using PCMODEL and MMX.

[b] ^1H-R_1 values were determined at 400 MHz, 0.1 M solutions.

[c] R_1 values are normalized to that of H-4, except experimental values are in parentheses.

[d] Calculated rotational barrier, kcal/mol.

3.2.2.2 Aromatic compounds

The ^{13}C spin-lattice relaxation rates of methyl groups in certain aromatic compounds have become classic examples of the consequences of steric influences on the rate of methyl group rotation (41). Thus, the peri hydrogen atom in the 8-position of 1-methylnaphthalene restricts the methyl group to a preferred conformation and so hinders its rotation; in consequence it has a fast ^{13}C R_1, 0.17 s^{-1}. Computation predicts a three-fold rotational barrier of 1.69 kcal/mol. However, in 9-methylanthracene the methyl group experiences two equivalent peri interactions so that there is no preferred conformation and methyl rotation is less hindered. The ^{13}C R_1 is 0.07 s^{-1} (40). Computation shows a six-fold rotational barrier of only 0.16 kcal/mol.

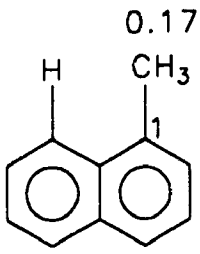

1-methylnaphthalene

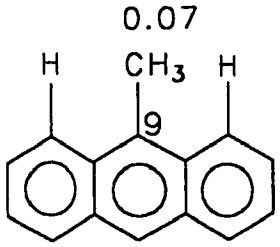

9-methylanthracene

^1H spin-lattice relaxation rates of a number of methyl-substituted aromatic compounds have been reported by Chazin and Colebrook, and qualitative correlations with inferred methyl group rotational barriers demonstrated (8) (Fig. 3.5). It was shown that "unhindered" aryl methyl groups, as in toluene, may have significant relaxation contributions from the spin-rotation mechanism. Methyl group rotational barriers have now been computed for a number of the aromatic compounds previously reported (8). Table 3.6 demonstrates that "hindered" methyl groups, with a single ortho substituent, normally have higher computed rotational barriers and faster spin-lattice relaxation rates than isolated methyl groups.

An isolated methyl group, as in toluene, has a two set of three-fold rotational symmetry axis, with no strongly preferred rotational ground state conformation, so that the energy difference between the ground states and the conformational transition state is small. The barrier to methyl group rotation is essentially insignificant (about 0.1 kcal/mol). For this reason, the spin-rotation mechanism makes an important contribution to the overall relaxation rate (8). When a single ortho substituent is present, the computed rotational energy profile shows three-fold symmetry about the rotational axis, and the methyl group has more strongly preferred ground state conformations, so that the rotational barrier is higher. Computed rotational barriers for methyl groups with one, unbuttressed, ortho methyl substituent range from 0.50 to 0.69 kcal/mol (compound **16** in Table 3.6). When the ortho methyl group is buttressed by further methyl group(s), as in **17** and **18**, the computed barrier increases to 0.99 - 1.41 kcal/mol. An ortho amino group (**20**,

21, **22**) is predicted to produce a higher barrier (0.65 - 1.27 kcal/mol) than a methyl group, while an ortho nitro group is predicted to produce a still higher barrier (1.95 kcal/mol). An amino group buttressed by a methyl group (**23**) is predicted to produce a higher barrier (0.92 kcal/mol) than an unbuttressed amino group (**21**), 0.78 kcal/mol.

Methyl groups flanked by two other methyl groups, as in **17** and **18**, show two set of three-fold symmetry in their computed rotational energy profiles, have no strongly preferred conformational ground state, and so have predicted rotational barriers (0.38 - 0.55 kcal/mol) which are relatively low, but higher than those of methyl groups flanked by hydrogen atoms.

A relatively high barrier (1.32 kcal/mol) is predicted for the 1-methyl group of the naphthalene derivative, **24**, resulting from steric interaction with the peri-hydrogen in the 8-position. This is consistent with experimental ^{1}H (Table 3.6) and ^{13}C evidence (41). The 3-methyl group in **24**, which is flanked by hydrogen atoms, has a relatively low barrier (0.32 kcal/mol) and a correspondingly low relaxation rate.

The highest relaxation rate in this series of compounds was observed for the C-12 methyl group in the benzanthracene derivative, **25**. This methyl group is subject to severe steric interference from the hydrogen atom in the 1-position. Computation predicts that this methyl group has by far the highest rotational barrier in the series (4.92 kcal/mol). A relatively high rotational barrier (0.61 kcal/mol) is also predicted for the fast relaxing C-7 methyl group of **25**. Modelling predicts that distortion of the molecule caused by the steric effects of the C-12 methyl group

reduces the symmetry of the interactions between the C-7 methyl group and its flanking peri hydrogen atoms. The resulting modified six-fold rotational symmetry contains some three-fold characteristics and the barrier is higher than that of 9-methylanthracene (0.16 kcal/mol) (Fig. 3.12).

With the apparent exception of the C-2 methyl group of **17**, where a small experimental R_1 difference from that of the C-5 methyl group is in the unexpected sense, and the possible exception of the C-1 and C-2 methyl groups of **16**, where the original tentative chemical shift assignments (8) should perhaps be reversed on the basis of this evidence, all of the ^1H R_1 values of this group of aromatic compounds show the predicted correlation with computed methyl group rotational barriers.

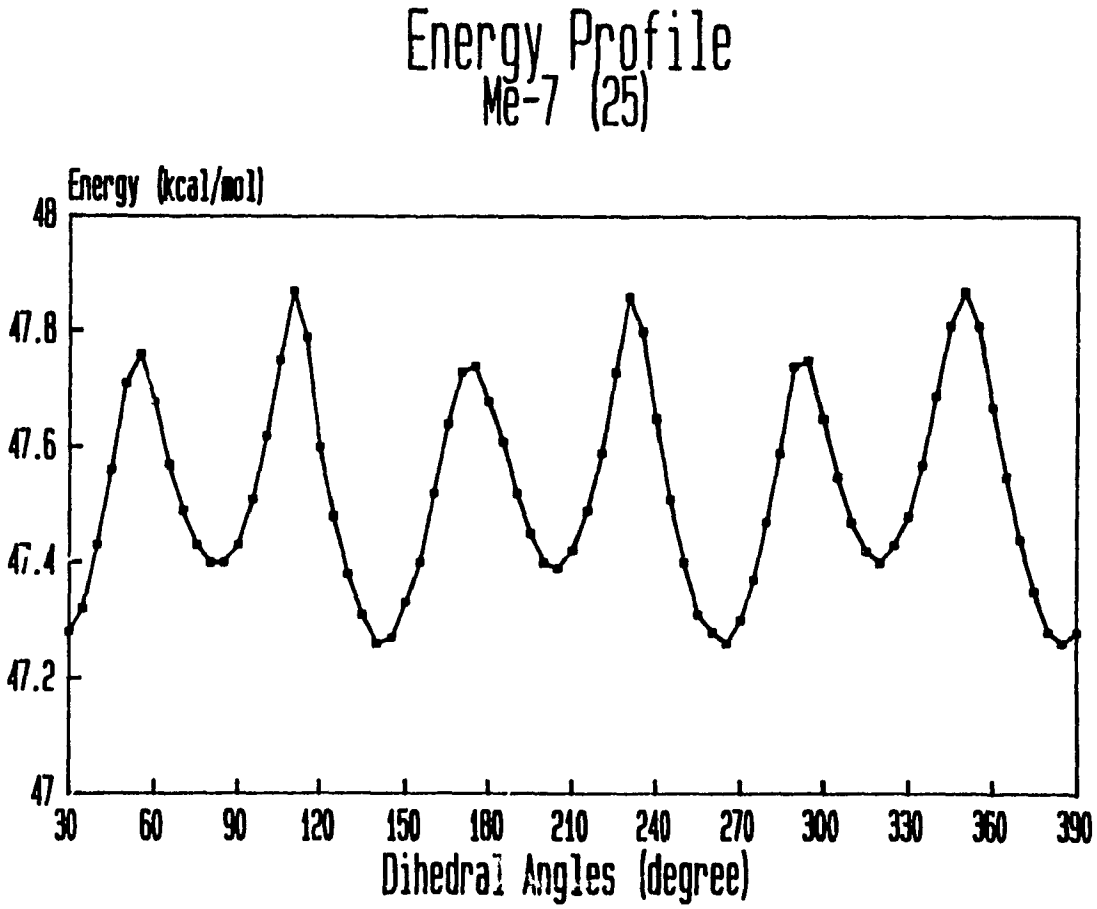

Fig. 3.12. Energy profile for C-7 methyl rotation (compound **25**).

Table 3.6. Methyl group ^1H-R_1 values and computed methyl rotational barriers of aromatic compounds[a]

Compound	Methyl group	^1H-R_1 value (s^{-1})	Rotational barrier (kcal/mol)
16	C-1	0.325[b]	0.69
	C-2	0.333[b]	0.50
	C-4	0.314	0.12
17[c]	C-1(3)	0.330	0.99
	C-2	0.300	0.38
	C-5	0.319	0.12
18	C-1(4)	0.304	1.41
	C-2(3)	0.242	0.55
19	C-2	0.318	1.95
	C-5	0.304	0.11
20	C-2	0.383	0.65
	C-5	0.322	0.09
21	C-2	0.383	0.78
	C-4	0.330	0.12
22	C-2	0.386	1.27
	C-4	0.338	0.13
23	C-1(5)	0.467	0.92
	C-4	0.378	0.10
24	C-1	0.422	1.32
	C-3	0.339	0.32
25	C-7	0.564	0.61
	C-12	1.580	4.92

[a] 400 MHz spectra, 0.1M in $CDCl_3$, except as noted. All experimental data are from ref. 8.

[b] Tentative assignments.

[c] C_6D_6 solution.

3.2.2.3 Terpenes

Dihedral driver calculations were carried out for some methyl groups for which experimental rotational barriers have been reported (46). For 2-methyl-2-butene, a model for some of the structural features of the terpenes, the calculated and experimental (in parentheses) methyl group rotational barriers were: C-1 (trans) 2.09 (1.9), C-2 (cis) 1.10 (1.4), C-4 0.90 (0.7) kcal/mol, i.e. in general agreement.

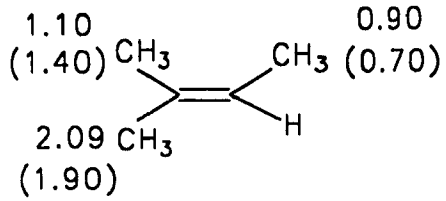

Internal comparisons of ^{1}H and ^{13}C methyl relaxation rates with calculated rotational barriers were made for a number of terpenoids (Fig. 3.6). A consistent correlation was found between ^{1}H and ^{13}C spin-lattice relaxation rates. In all cases, the ^{13}C relaxation rates were lower than those of the ^{1}H relaxation rates of the same methyl groups, measured under similar conditions of solvent and temperature.

Acyclic (geraniol, **26** in Table 3.7), monocyclic (carvone, **27**, and limonene, **28**), and bicyclic (α-pinene, **29**, and verbenone, **30**) monoterpenes, a monocyclic terpene-related compound (α-ionone, **31**), and a tricyclic diterpene (methyl O-methylpodocarpate, **32**) derivative, which provide a variety of methyl group

environments, were examined.

Geraniol, **26**: Geraniol is an open chain monoterpene which carries two isopropylidene (methyl-a and methyl-b) and one further allylic methyl group (methyl-c). Considerable conformational mobility is expected. The predicted rotational barrier of the terminal methyl group-a (trans to the C-6 proton) is lower than that of its geminal neighbour (cis to H-6) (1.26 vs 2.01 kcal/mol, respectively). The measured ^{1}H (0.23 vs 0.41 s^{-1}, respectively) and ^{13}C (0.10 vs 0.23 s^{-1}, respectively) R_1 values were consistent with this prediction.

However, the relaxation rates of the C-3 methyl group (methyl-c) were not consistent with prediction. Methyl-c has the lowest predicted rotational barrier, but has relaxation rates intermediate between those of methyl groups-a and -b. Examination of the ^{13}C relaxation rates reveals that C-2 relaxes faster than C-6, which has a similar molecular environment (0.20 vs 0.16 s^{-1}, respectively). This evidence suggests that motional freedom of the end of the molecule carrying the hydroxyl group is restricted, either through intermolecular association via hydrogen bonding, or through specific solvation of the oxygen atom. It appears likely that changes in molecular geometry associated with molecular association raise the rotational barrier of methyl-c. A standard molecular mechanics calculation does not take this possibility into account. Molecular mechanics calculations on a hydrogen bonded geraniol dimer suggested that changes in bond angles at the hydroxyl terminal of the molecule, which would be likely to affect the rotational barrier of methyl-c, are probable.

Carvone, **27**, and limonene, **28**: These six-membered ring monoterpenes have similar structures, and both contain allylic methyl groups at carbon-1 (methyl-a) and carbon-10 (methyl-b).

Molecular mechanics calculations predict that the a-methyl groups of both of these terpenes have higher rotational barriers than those of the b-methyl groups (e.g. 2.97 vs 2.11 kcal/mol for **27**). The experimental ^{1}H and ^{13}C R_1 values of the a-methyl groups are higher than those of the b-methyl groups in both compounds, consistent with this prediction (Table 3.7).

α-Pinene, **29**, and verbenone, **30**: α-Pinene and verbenone are bicyclic monoterpenes, both containing geminal dimethyl groups on saturated carbon atoms (methyl-a and methyl-b) and one allylic methyl group (methyl-c).

The computed methyl group rotational barriers of **30** increase in the order methyl-a, methyl-b, methyl-c. However, the experimental ^{1}H and ^{13}C R_1 values of **30** decrease in this order. Further, the experimental ^{1}H and the ^{13}C R_1 values of **29** are almost identical for all three methyl groups, whereas the computed rotational barriers have a significant dynamic range (Table 3.7). Clearly, computation completely fails to predict the relative relaxation rates of these two compounds. Allinger (31) has pointed out the limitations of the MM2 force field for strained bicyclic ring systems. The effects of errors in the predicted geometries of these molecules is evidently sufficient to render the calculation of relative methyl group rotational barriers invalid.

α-Ionone, **31**: This compound contains the greatest dynamic range of predicted rotational barriers in the terpenoid series, ranging from the relatively unhindered acetyl methyl group to a quite strongly hindered geminal methyl group. The range of rotational barriers is reflected in a large dynamic range of ^{1}H and ^{13}C relaxation rates, but two ^{13}C R_1 values are not reported because of overlap problems.

The measured relaxation rates correlate well with the predicted ^{1}H rotational barriers. Thus, the relatively unhindered acetyl methyl group (0.44 kcal/mol) has the lowest relaxation rate (0.49 s^{-1}), and the highly hindered a-methyl group (5.78 kcal/mol) the highest relaxation rate (1.62 s^{-1}). The allylic methyl group (c) is relatively unhindered (2.69 kcal/mol), and relaxes relatively slowly (0.67 s^{-1}). The second most hindered geminal methyl group (b) (4.26 kcal/mol) has the second highest relaxation rate (1.37 s^{-1}).

Methyl O-methylpodocarpate, **32**: The C-methyl (Me-18, Me-20) and O-methyl (Me-21, Me-22) groups of **32** are readily distinguishable through their ^{1}H relaxation rates, the O-methyl groups having low relaxation rates (0.54 - 0.59 s^{-1}) compared to the C-methyl groups (1.25 - 1.48 s^{-1}). Since methyl protons relax mainly to each other by the dipole-dipole mechanism, rather than to protons outside the group, this difference must result from differences in the rates of methyl group rotation (contributing to the τ_c term in Eq. [3.1]), the C-methyl groups being more hindered. The effects of differing steric influences on the rotational barriers of the O-methyl and the C-methyl groups is clearly demonstrated by the computed rotational barriers,

1.35 - 2.96 vs 3.87 - 3.91 kcal/mol, respectively, which are consistent with the experimental data. The significant difference between the ^1H relaxation rates of methyl-18 and methyl-20 (1.48 vs 1.25 s^{-1}, respectively) must result from greater steric hindrance to rotation of methyl-18 (3.91 vs 3.87 kcal/mol). Thus, the calculated rotational barriers correlate well with the experimental relaxation rates for **32** (Table 3.7).

Table 3.7. ^{1}H and ^{13}C spin-lattice relaxation rates[a] and calculated rotational barriers[b] of methyl groups of terpenoids

	^{1}H-R_1 (s^{-1})	^{13}C-R_1 (s^{-1})	Rotational barrier (kcal/mol)
Geraniol, **26**			
Me-a	0.23	0.10	1.26
Me-b	0.41	0.23	2.01
Me-c	0.31	0.11	0.74
Carvone, **27**			
Me-a	0.42	0.21	2.97
Me-b	0.35	0.18	2.11
Limonene, **28**[c]			
Me-a	0.24	0.19	2.09
Me-b	0.19	0.15	1.94
a-Pinene, **29**			
Me-a	0.22	0.15	2.64
Me-b	0.21	0.15	2.15
Me-c	0.21	0.15	2.33
Verbenone, **30**			
Me-a	0.47	0.24	2.09
Me-b	0.39	0.22	2.18
Me-c	0.38	0.21	2.36
a-Ionone, **31**			
Me-a	1.62	0.80	5.78
Me-b	1.37		4.26
Me-c	0.67	0.30	2.69
Me-d	0.49		0.44
Methyl O-methylpodocarpate, **32**			
Me-18	1.48		3.91
Me-20	1.25		3.87
Me-21	0.54		1.35
Me-22	0.59		2.96

[a] Determined at 400 MHz (^1H, 0.1 M in $CDCl_3$, degassed) or 20.1 MHz (^{13}C, 1 M in $CDCl_3$, non-degassed) using the inversion-recovery pulse sequence, and calculated by non-linear regression.

[b] Calculated using the dihedral driver option of MMX.

[c] C_6D_6 solution.

3.3 Conclusions

In the majority of compounds examined in this study, the computed methyl group rotational barriers correlate with the measured ^{1}H and ^{13}C spin-lattice relaxation rates, i.e. the relaxation rates show the responses to the steric influences on methyl group rotation which are predicted by molecular modelling. However, when a steroid is heavily substituted with polar groups, and when the measurement must be taken in a polar solvent, the correlation between ^{1}H and ^{13}C spin-lattice relaxation rates and the computed rotational barriers may break down. The discrepancy is most likely attributable to an inadequate model for the force field calculations, which are gas-phase, and do not take molecular interactions into account at the level at which the calculations were performed. There is evidence for preferential solvation effects, in which the methyl group adjacent to the polar substitutents is more affected than the remote methyl group. Thus, force field calculations of this type may work well, but they should be applied with caution in predicting properties of polar molecules measured in polar solvents.

In the series of aromatic compounds, one of the apparent exceptions (**16** in Table 3.6) perhaps indicates that tentative chemical shift assignments should be interchanged. The other case (**17**) arises where the predicted barrier in question is low, and the range of experimental R_1 values is small, possibly because of significant spin-rotation contributions.

Poor correlations in the terpene series arise in cases (**29** and **30** in Table 3.7) in which there are known deficiencies in the force fields for highly strained

molecules of this type (31), and in a case (geraniol) in which a gas phase calculation might be expected to be inadequate because it does not take into account molecular association or solvation. Reasonable correlations are obtained for the other terpenoids.

Chapter 4

DETERMINATION OF STRUCTURE AND STEREOCHEMISTRY BY NUCLEAR OVERHAUSER EFFECT DIFFERENCE MEASURFMENTS AND MOLECULAR MODELLING

A. 5,7-Diisopropyl--8,8-dimethyl-2-oxo-3-phenylimidino-[1,2-c]-tetrahydro-[1,3]-oxazine (DDPTO)

B. Terpenes

4.1 Introduction

The determination of the structure and stereochemistry of organic compounds, especially natural products, has always been a challenge to organic chemists. Introduction of pulse FT NMR spectrometers in the 1970's provided major advances in the tools available for structure determination. High magnetic field instruments and modern pulse sequences have made the assignment of ^{1}H spectra easier, directly leading to more reliable structure analysis.

In the first part of this Chapter, the structure determination of the newly synthesised compound, 5,7-diisopropyl-8,8-dimethyl-2-oxo-3-phenylimidino-[1,2-c]-tetrahydro-[1,3]-oxazine (DDPTO), is described using NOED measurements. The ^{1}H and ^{13}C NMR spectra were first assigned by various techniques (HD, NOED, CHORTLE, DEPT, etc.). Molecular mechanics calculations (MMP2) provided support for the NOED data and indicate the complete three-dimensional structure of DDPTO.

The second part of this Chapter shows high field (400 MHz) ^{1}H NMR assignments of terpenes which have not been investigated by high resolution NMR techniques since 1967. Misassignments in the ^{13}C spectrum of α-ionone (56) have been corrected by a 2D ^{13}C-^{1}H HETCOR experiment based on reliable ^{1}H assignment from NOED measurements.

4.2 Structure determination and stereochemistry of DDPTO (58)

DDPTO was synthesized in the laboratory of Dr. J. T. Edward, McGill University via Scheme 1. Compound **1** was reacted with boiling neat isobutyraldehyde, yielding a product which was believed to have either of two possible structure **2**, or **3**. The study described below was undertaken to identify the structure and stereochemistry of DDPTO.

This structural problem presents an interesting challenge, because both **2** and **3** contain four chiral centres. Since these chiral centres form isolated spin systems, scalar ^{1}H-^{1}H coupling information that might have related them is not available. Hence their relative stereochemistry was determined using dipolar (through space) coupling via ^{1}H nuclear Overhauser effect difference (NOED) spectroscopy (34, 59, 60).

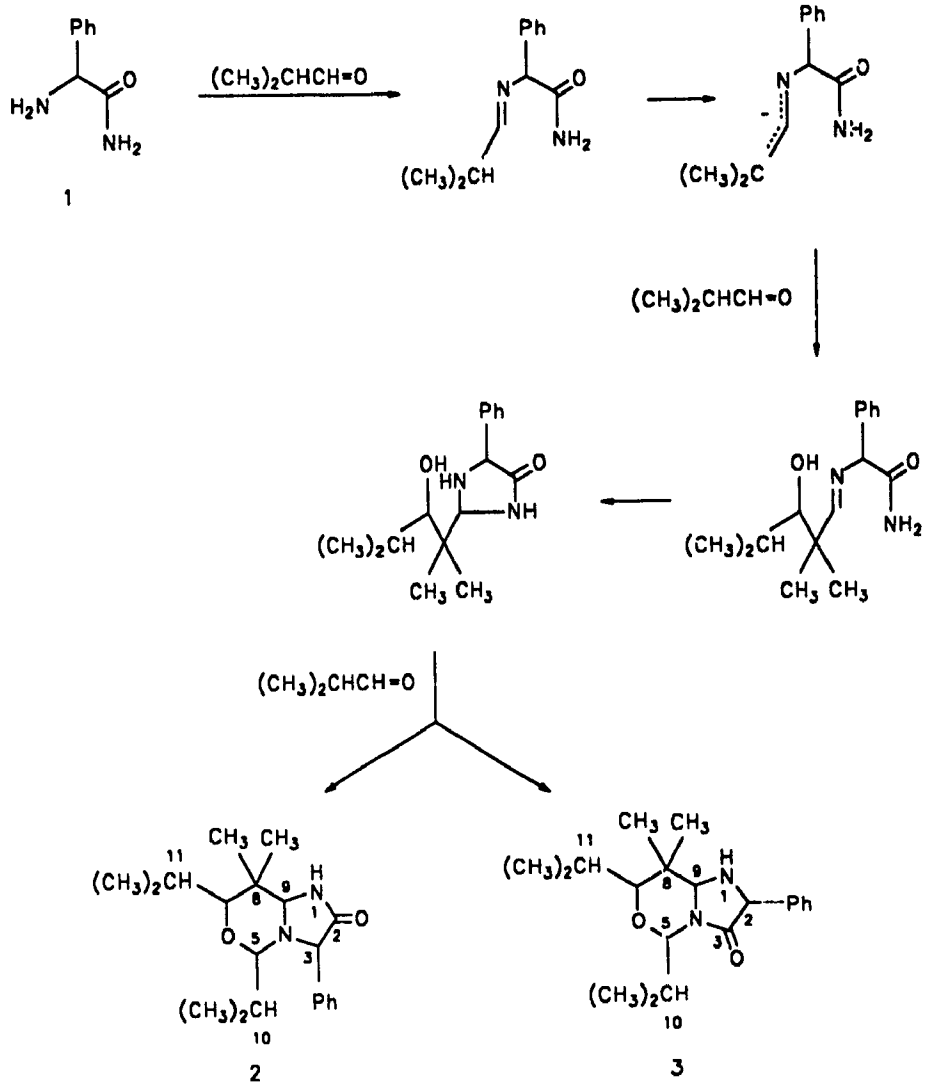

Fig. 4.1. Reaction scheme

4.2.1 ^{1}H spectral assignment

The 400 MHz (C_6D_6 solution) ^{1}H NMR spectrum (Fig. 4.2) showed well-resolved aromatic proton signals, which were assigned on the basis of their multiplicities and intensities (Table 4.1). The NH proton shows a broad singlet at δ8.47. The ring protons give rise to two singlets (H-3 and H-9), and two doublets due to spin coupling to the isopropyl groups (H-5 and H-7). The singlet at δ4.12 was broadened due to long-range coupling and so was assigned to the benzylic proton at C-3. The remaining (sharp) singlet (δ4.24) in this region must be H-9.

The geminal methyl groups at C-8 are diastereotopic since the molecule is chiral, and give rise to singlets at δ1.04 and δ0.82 (e and f).

Similarly, the isopropyl methyl groups are diastereotopic, and give rise to four doublets, those at δ0.85 (b) and δ0.88 (d) being incompletely resolved. Spin-decoupling experiments identified and established the spin connectivities of the complete isopropyl and associated ring proton spin systems (Fig. 4.3). Thus H-5 (δ3.94, J = 1.5 Hz), H-10 (δ1.44), the δ1.14 and δ0.88 methyl groups form one isolated spin system, while H-7 (δ3.14, J = 5.0 Hz), H-11 (δ1.70), the δ0.94 and δ0.85 methyl groups form the other.

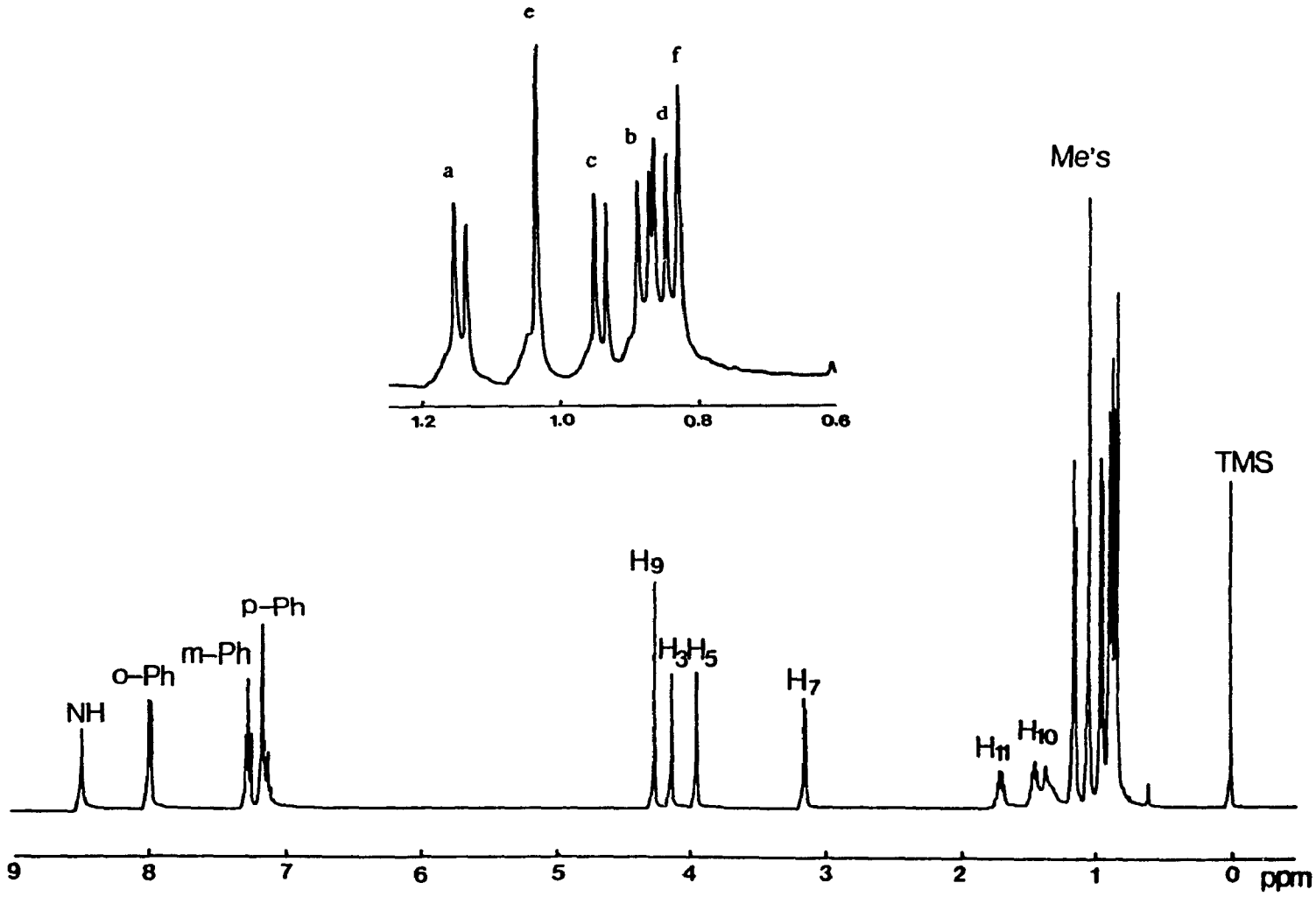

Fig. 4.2. ^1H spectrum of DDPTO at 400 MHz in a 0.1 M C_6D_6 solution.

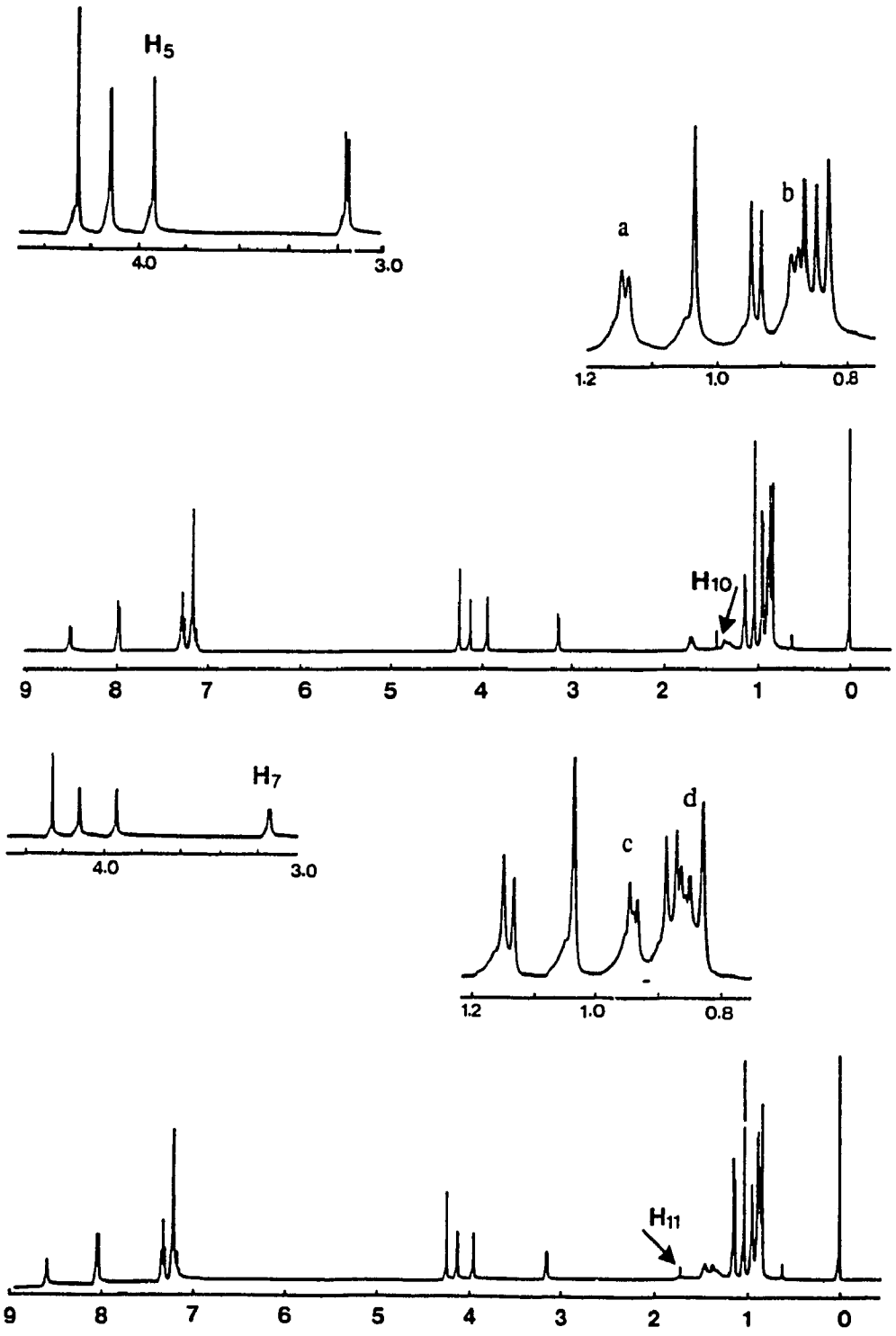

Fig. 4.3. ^{1}H-^{1}H homonuclear decoupling spectra of DDPTO at 400 MHz in a C_6D_6 solution.

4.2.2 Stereochemistry at chiral centres

The relative stereochemistry at the chiral centres was established by NOED experiments (Fig. 4.4a). Irradiation of the benzylic ring proton (H-3, Fig. 4.4a-ii) led to intensity enhancement of the signals from the ortho aromatic protons, H-5, H-10, but not for the NH proton signal. This demonstrates the close proximity of H-3 to H-5 and H-10, so that H-5 and H-3 must be on the same face of the ring system. The proximity of H-3 to H-5 and H-10 is consistent with structure **2**, but not **3**. Further, an NOE between the benzylic ring proton and the NH proton would have been expected for structure **3**, but not detectable.

Irradiation of H-9 (Fig. 4.4a-iii), which produces the other ring singlet, enhances the signals of the ortho aromatic protons, the NH proton, and the δ1.04 geminal methyl group (e), there is no detectable enhancement of signals from the other ring protons, indicating that H-9 is on the opposite side of the ring from H-3 and H-5. Detection of a relaxation pathway between H-9 and the ortho protons indicates that H-9 and the phenyl group are on the same face of the ring system.

Irradiation of H-5 (Fig. 4.4a-i) strongly enhances the signals of H-3, H-7. This indicates that H-5 and H-7 are in close proximity, i.e., on the same side of the molecule.

Irradiation of H-7 (Fig. 4.4a-v) strongly enhances the signal of H-5 (verifying the steric relationship of H-5 and H-7), and weakly enhances the signal of H-11, its vicinal neighbour.

It should be noted that irradiation of H-5 enhances the signals of both H-3 and H-7, but that the only ring proton affected by irradiation of H-3 and H-7 is H-

5. This suggests that H-5 is close to both H-7 and H-3, but that H-3 and H-7 are distant from each other. Examination of a molecular model of the assigned structure shows that H-3, H-5, and H-7 have an approximately linear relationship, such that a significant NOE pathway between H-3 and H-7 is not expected.

The NOE pathway between H-3 and H-10 (Fig. 4.4a-vi,ii) indicates that H-3 is close to the isopropyl group containing H-10, and that this group is in a conformation with H-10 close to H-3. A study of molecular models suggests that H-10 would be close to H-3 in the preferred conformation of the C-5 isopropyl group.

Irradiation of H-11 (Fig. 4.4a-vii) affects only the signal of its vicinal neighbour, H-7, and methyl groups, indicating that H-11 is remote from other ring protons.

Irradiation of the δ1.14 isopropyl methyl group (a, Fig. 4.4b-iv) enhances the signals of H-10 and the δ0.88 isopropyl methyl group (b), i.e., within the same isopropyl group, and also the ortho aromatic proton signals. Hence the δ1.14 isopropyl methyl group (a) is on the same face of the molecule as the phenyl group. Irradiation of the δ0.94 isopropyl methyl group (c, Fig. 4.4b-iii) enhances the signals of H-11 and H-7. Hence the δ0.94 isopropyl methyl group (c) is on the same face of the molecule as H-7.

The NOED experiments on the geminal methyl groups (Fig. 4.4b-i,ii) permit assignment of their signals. Thus irradiation of the δ1.04 methyl (e) produces an enhancement of the signal of its geminal neighbour, of H-11, and H-9. Irradiation of the δ0.82 methyl (f) produces enhancement of H-9, H-11, the δ1.04 geminal methyl (e), the NH, and the H-7 signals. It may be inferred that the geminal methyl groups

lie between C-7 (and C-11) and C-9, that the δ0.82 methyl (f) is on the same face of the molecule as H-7, and is close to NH, while the δ1.04 methyl group (e) is on the same face as H-9. The C-7 isopropyl group must have a low energy conformation with H-11 facing the gem-dimethyl groups.

Thus, the NOED data indicates that the structure of the molecule is **2** (plus its enantiomer). In the preferred conformations of the isopropyl groups, H-10 faces towards H-3, while H-11 faces the gem-dimethyl system. The major NOE (relaxation) pathways are indicated in Fig. 4.5.

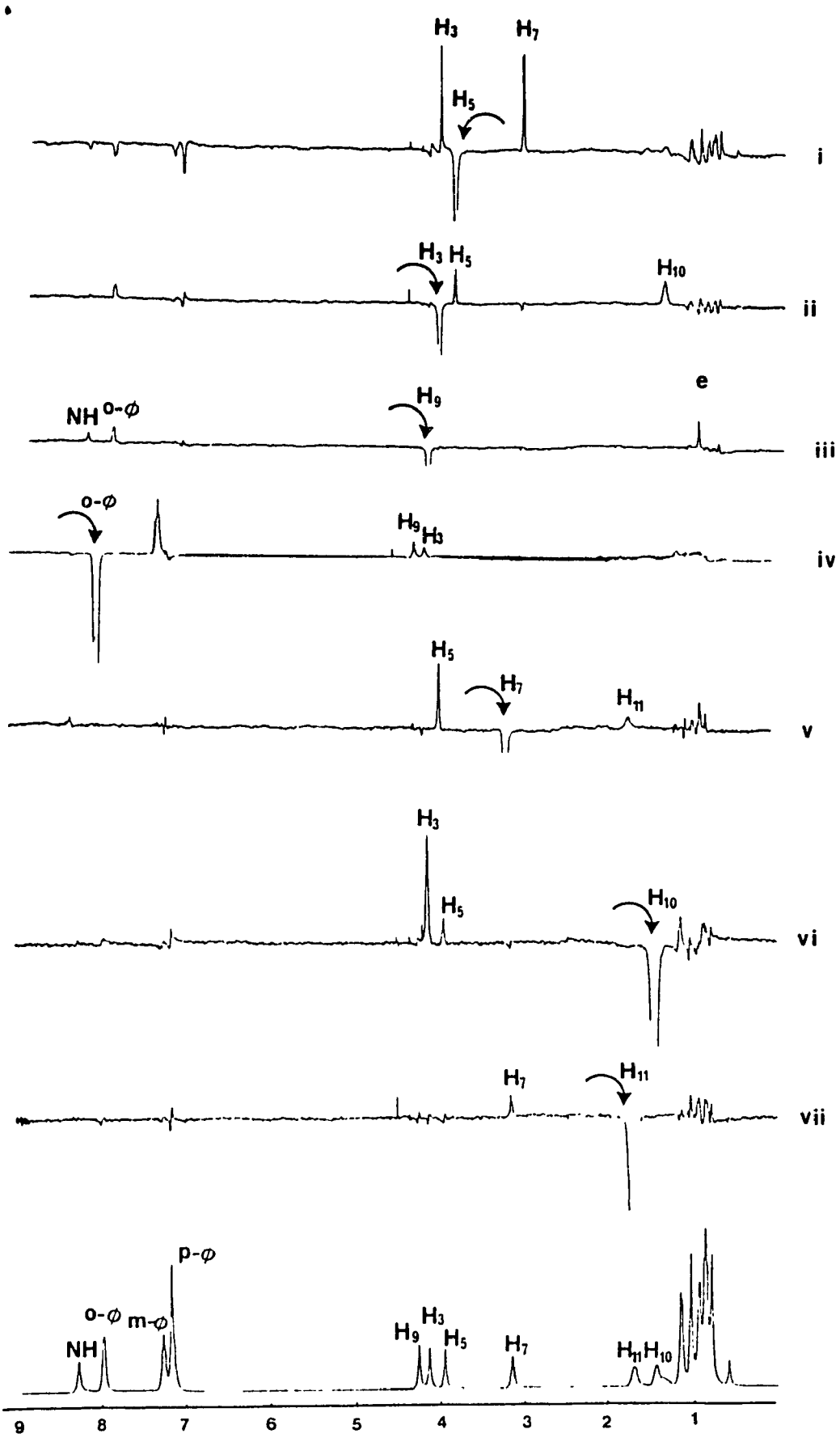

Fig. 4.4a. NOED spectra of DDPTO at 400 MHz in a 0.1 M C_6D_6 solution.

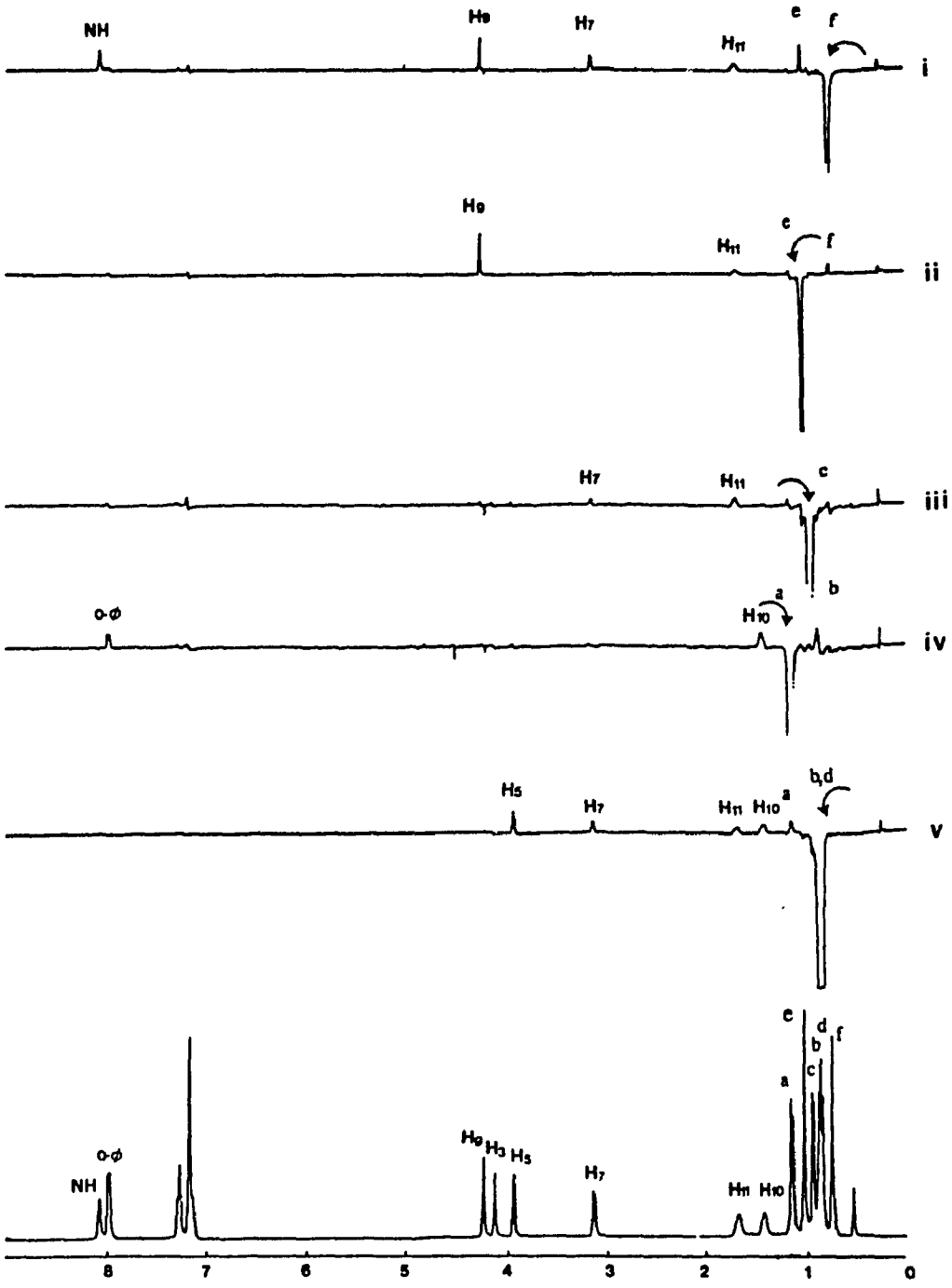

Fig. 4.4b. NOED spectra of DDPTO (methyl region) at 400 MHz in a C_6DC_6 solution.

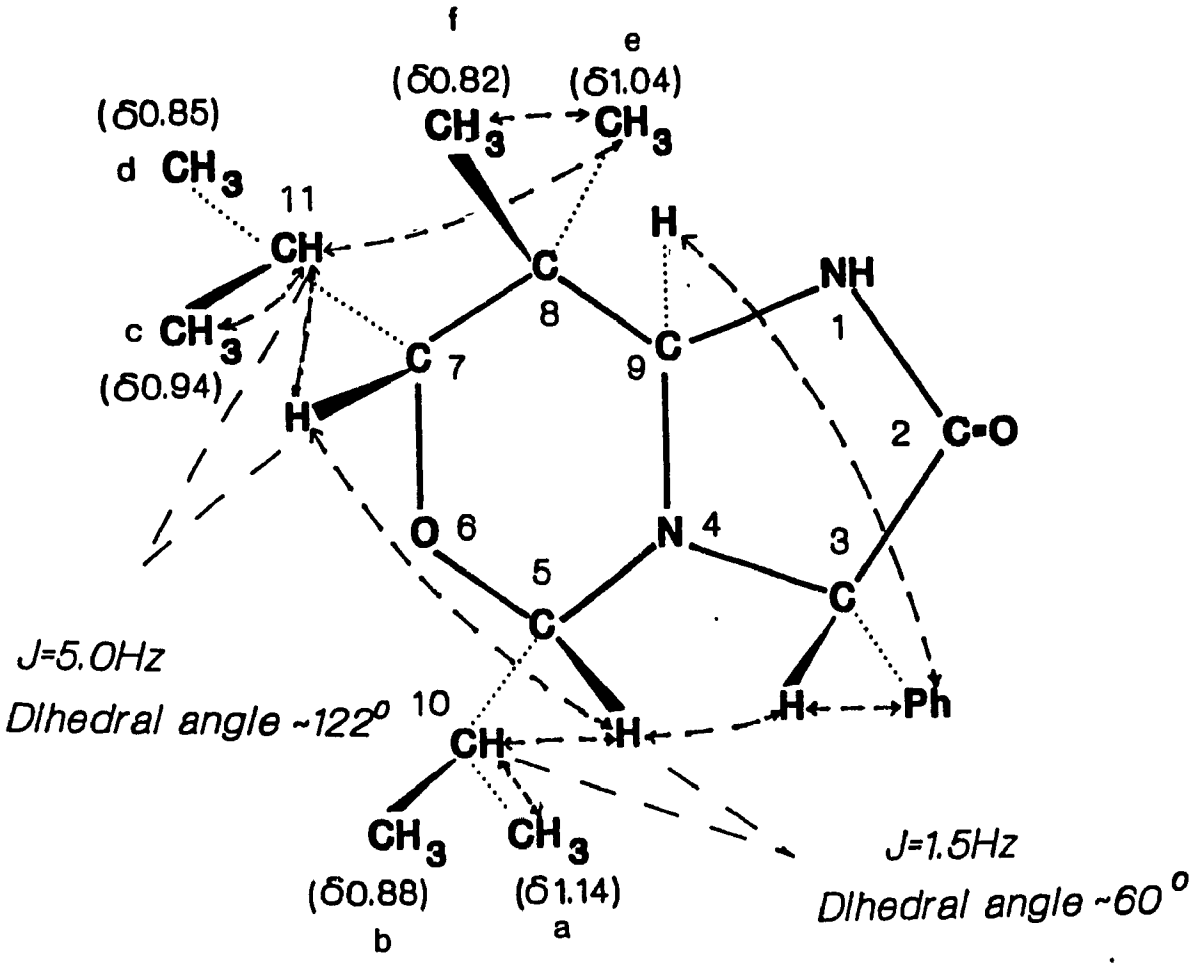

Fig. 4.5. NOE pathways of DDPTO.

4.2.3 ^{13}C spectrum assignments

The ^{13}C spectrum, which shows 18 resolved signals (Fig. 4.6) was assigned with the aid of the DEPT (34, Chap. 8) spectral editing sequence. Thus the six signals in the range 14-24 ppm were identified as methyl groups (all geminal methyl groups are diastereotopic), and nine signals (three of which were characterized by their chemical shifts as aromatic) were shown to arise from CH units. Correlation of the carbon signals with the chemical shifts of directly attached, previously assigned, protons was achieved using the CHORTLE method (53) (Fig. 4.7). Unequivocal assignment of all carbon signals except those at δ23.21, 22.98, and 18.97 was possible by this method. There is some uncertainty in the assignment of these three signals because of the small chemical shift differences of the attached protons.

The ^{1}H and ^{13}C chemical shift assignments are shown in the Table 4.1.

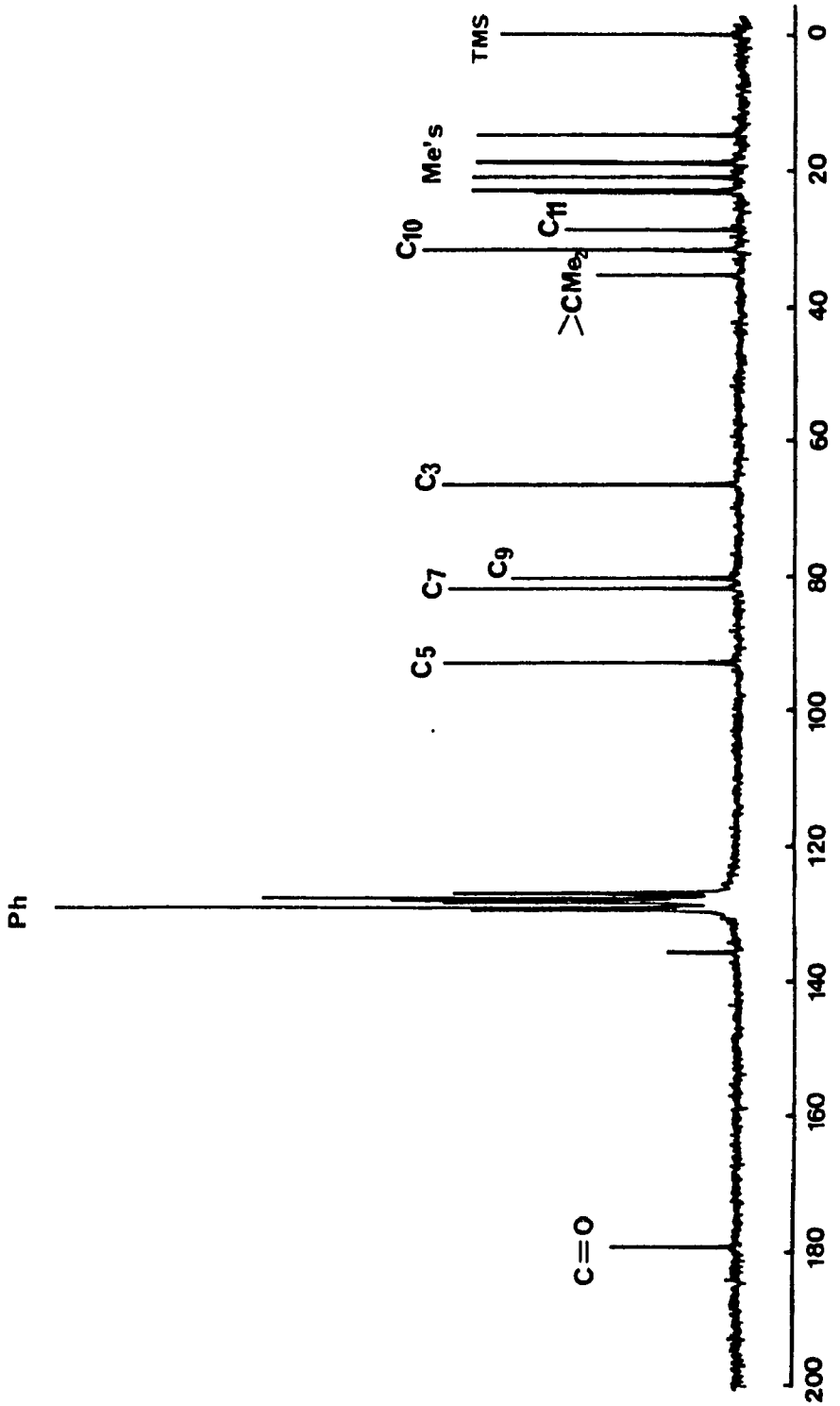

Fig. 4.6. ^{13}C spectrum of DDPTO at 20.13 MHz in a 1 M C_6D_6 solution.

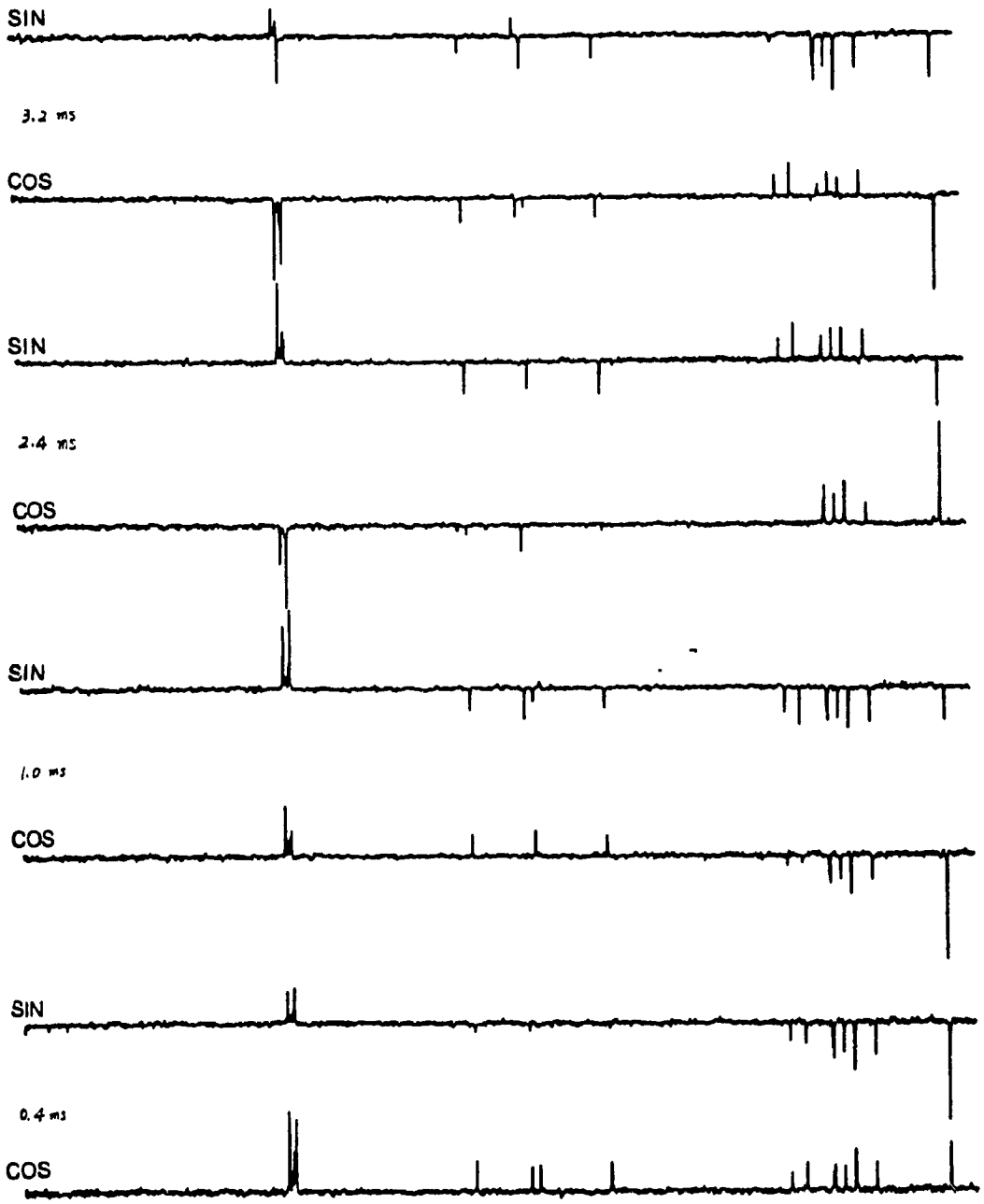

Fig. 4.7. CHORTLE (1D ^{13}C-^{1}H chemical shift correlation experiment) at 20.13 MHz in 0.1 M C_6D_6 solution. The data processing used the program CHFIT on an Olivetti M24, PC.

Table 4.1 ^{1}H and ^{13}C chemical shifts assignments of 2

Carbon atoms	$^{13}C^{a}$	$^{1}H^{b}$	$^{1}H^{c}$
(NH)		8.47	
C=O	179.01		
ϕ-1'	135.52		
m-ϕ	128.96	7.25	7.28
p-ϕ	127.93	7.13	7.17
o-ϕ	127.66	7.96	7.92
C-5	93.02	3.94 (J=1.5 Hz)	3.99
C-7	81.92	3.14 (J=5.0 Hz)	3.06
C-9	80.36	4.25	4.35
C-3	66.58	4.12	4.09
C-8	35.30		
C-10	31.65	1.44	1.50
C-11	28.66	1.70	1.68
Me-b	23.21[d]	0.88	0.90
Me-d	22.98[d]	0.85	0.89
Me-e	21.06	1.04	1.07
Me-c	19.04	0.94	0.93
Me-f	18.97[d]	0.82	0.85
Me-a	14.97	1.14	1.12

[a] Measured at 20.1 MHz, C_6D_6 solution.

[b] Measured at 400 MHz, C_6D_6 solution.

[c] Calculated from ^{13}C data using CHORTLE method (53).

[d] Assignment uncertain due to small ^1H chemical shift range.

4.2.4 Molecular mechanics

Further insight into the geometry of the molecule was obtained from molecular mechanics calculations, using an implementation of the Allinger MMP2 algorithm (24, 29) with provision for π-electrons. The lowest energy optimized structure, based on the configuration established by the NOED measurements, was predicted with the six-membered ring in a chair conformation, with both isopropyl groups equatorial, the N4--C3 bond pseudo-equatorial, and the C9--N1 bond pseudo-axial (Fig. 4.8). Molecular mechanics calculations in which rotation about the C5--C10 bond is driven indicated an overall energy minimum for the conformation with H-10 facing towards the phenyl group. The three-bond ^1H-^1H coupling constant calculated using the Karplus equation (61) for the predicted H5--C5--C10--H10 dihedral angle (about 60°) for this conformation is consistent with the observed value of 1.5 Hz.

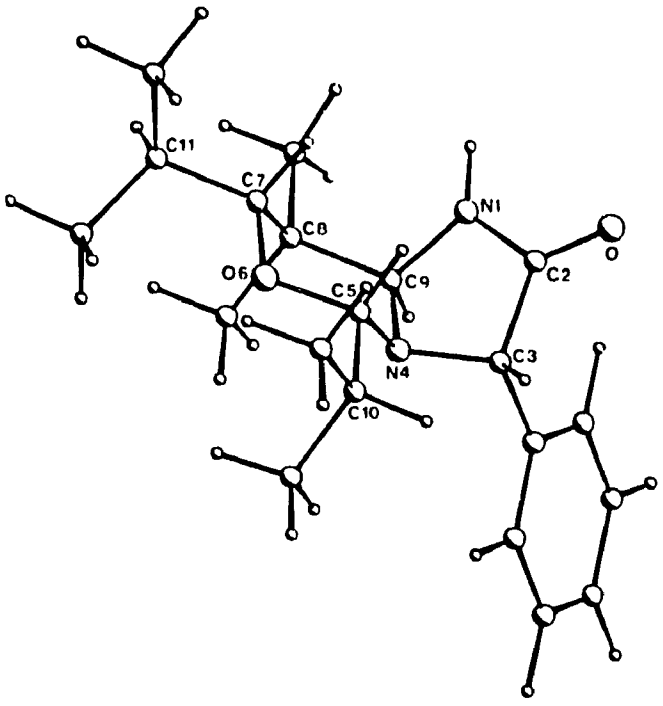

Fig. 4.8. Three-dimensional structure of DDPTO.

Similarly, energy calculations for rotation of the other isopropyl group about the C7--C11 bond indicated a broad low energy region centred on a H7--C7--C11--H11 dihedral angle of about 122°, with H-11 facing towards the gem-dimethyl group (Fig. 4.9). The calculated three-bond coupling constant for this angle is consistent with the observed 5.0 Hz coupling constant.

The H9--C9--N--H dihedral angle in the calculated minimum energy conformation is 87°, corresponding to a near minimum three-bond coupling constant predicted form a Karplus-type relationship. This is consistent with the absence of observable coupling in the H-9 and NH signals.

This molecular conformation, deduced from molecular mechanics calculations, is completely consistent with the NOED measurements.

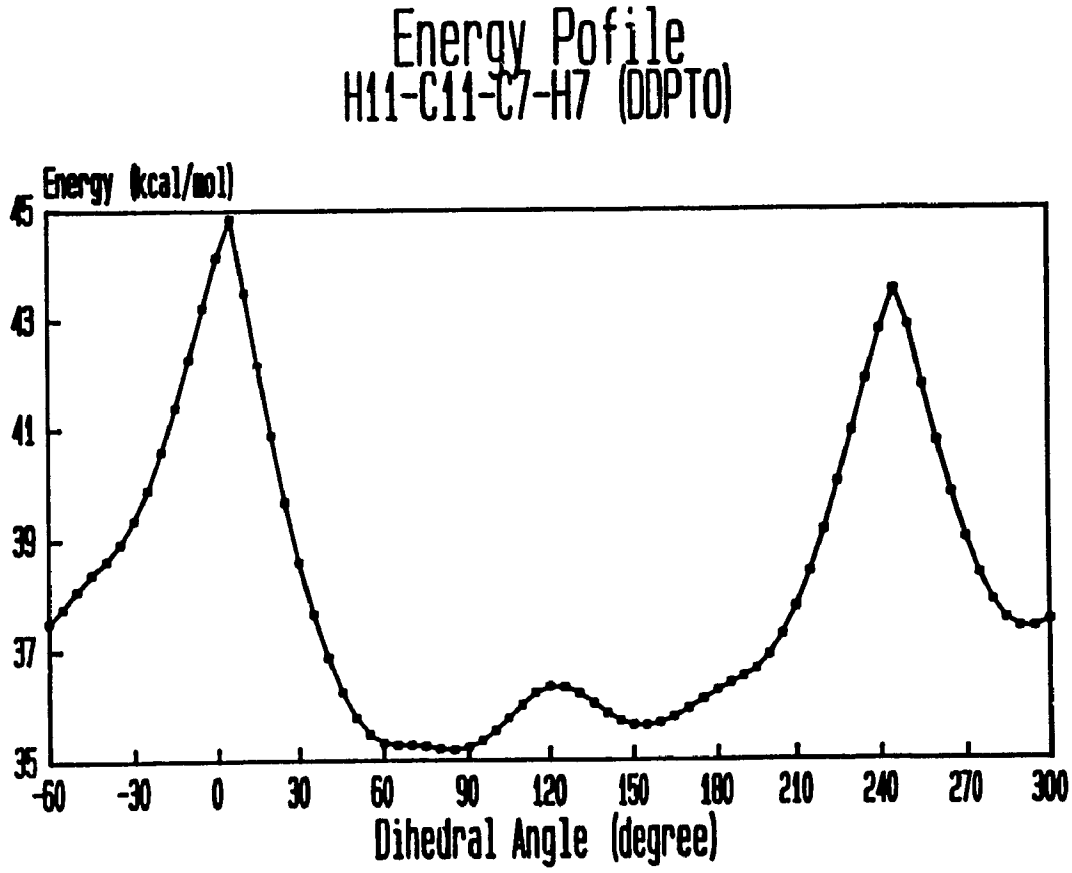

Fig. 4.9. Energy profile for C7--C11 bond rotation (DDPTO)

4.3 ^{1}H chemical shift assignments and stereochemistry of terpenes

Terpenes, compounds which occurs in great variety in plants, have been extensively studied. However, most NMR studies have concentrated on ^{13}C spectroscopy (41, 54, 63-65). ^{1}H spectra, especially the high field ^{1}H spectra of the terpenes in this study, have not been assigned since 1967.

In principle, ^{1}H NMR assignment could be obtained by the 2D ^{13}C-^{1}H HETCOR technique based on previously assigned ^{13}C spectra. However, such assignments are not always reliable, because some of the ^{13}C assignments are suspect and needed to be confirmed by other NMR techniques (63). The study described in this section has applied the NOED technique based on dipole-dipole interactions between nuclei to investigate the separation of protons in space, and to further assign the proton spectra of terpenes. 2D HETCOR and COSY techniques were used with caution when necessary.

The stereochemistry of terpenes has been studied using NOED data and molecular mechanics (MMX). The results from the calculations are in good agreement with the experimental data.

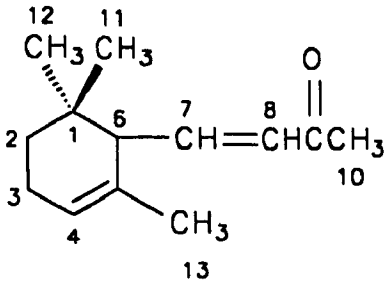

α-Ionone

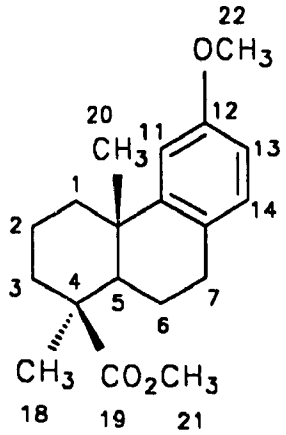

Methyl-O-methylpodocarpate

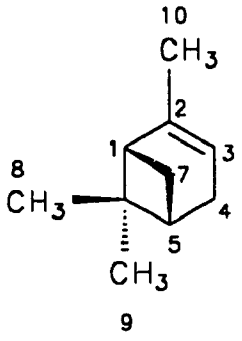

α-Pinene

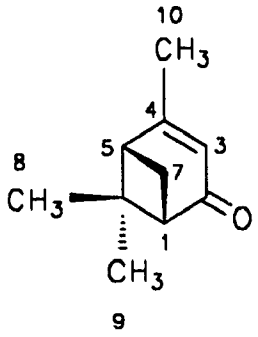

Verbenone

Fig. 4.10. Structures of terpenes.

4.3.1 α-ionone

a. ^1H spectrum assignments

α-Ionone contains one chiral centre (C-6). The stereo-chemical aspects of the following discussion apply to the enantiomer with H-6 on the upper face of the molecule.

The ^1H spectrum ($CDCl_3$, 400 MHz) (Fig. 4.11) consists of a doublet of doublets at δ6.62 (1H) which is assigned to H-7 based on its chemical shift and J coupling constant ($J_{7,8}$ = 15.8 Hz, $H_{6,7}$ = 9.7 Hz). Similarly, a doublet at δ6.05 (1H) is assigned to H-8 ($J_{7,8}$ = 15.8 Hz), and a broad, unresolved signal at δ5.5 (1H) is assigned to H-4. The magnitude of $J_{7,8}$ (15.8 Hz) indicates a trans double bond configuration.

The H-6 signal was identified as a partial obscured doublet at δ2.29 by a spin decoupling experiment in which irradiation at δ2.29 caused partial collapse of the δ6.62 (H-7) multiplet. The remaining ring proton signals consist of a broad singlet at δ2.05 (2H), and one proton multiplets at δ1.48 and δ1.23. The δ2.05 signal was assigned to the unresolved allylic H-3 protons on the basis of chemical shift and NOED evidence.

The acetyl methyl-10 signal was identified from its chemical shift and line width as a sharp singlet at δ2.24, overlapping the H-6 signal. The allylic methyl-13 signal was assigned to the singlet at δ1.57, broadened by long range coupling.

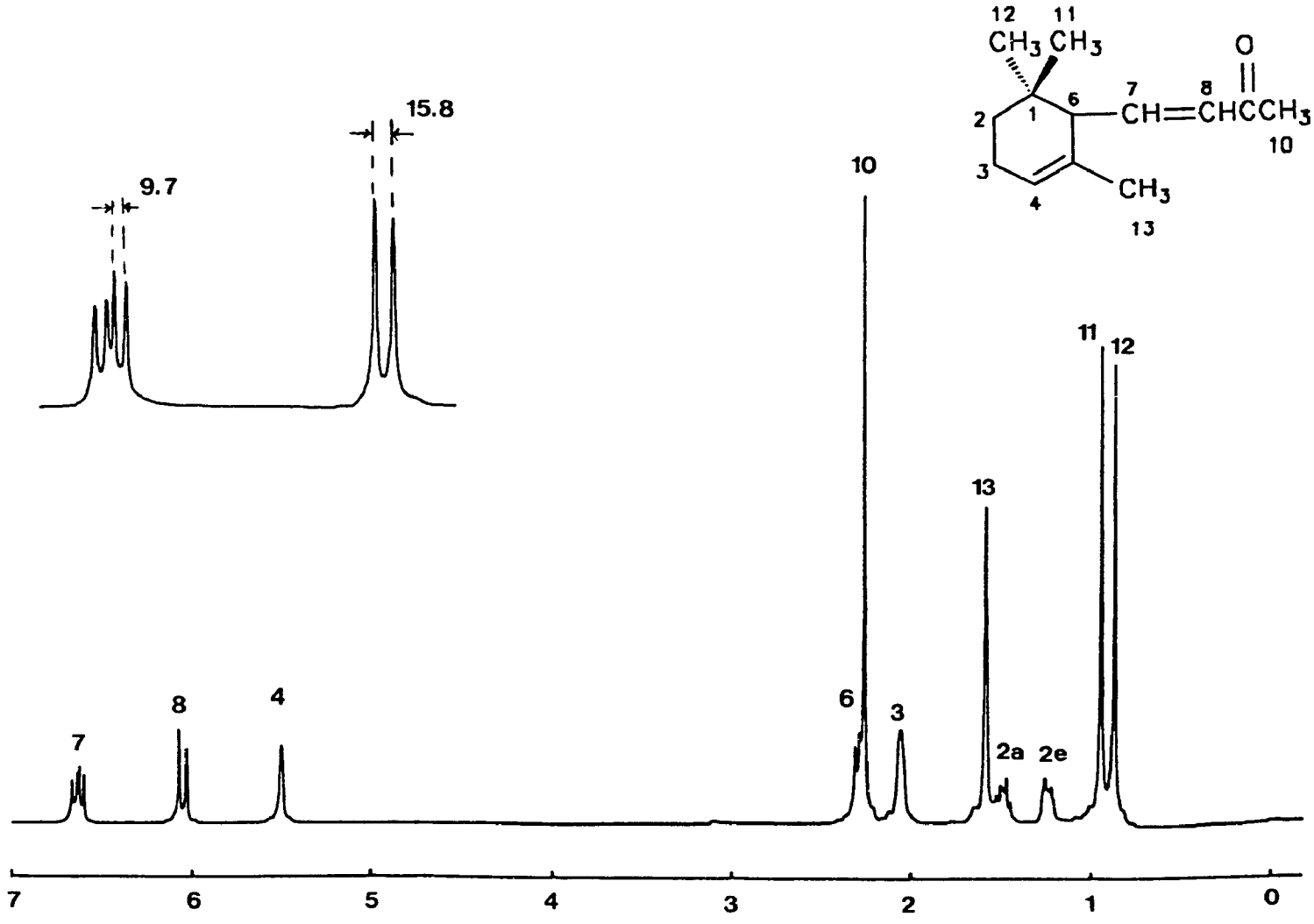

Fig. 4.11. ^1H spectrum of α-ionone at 400 MHz in a 0.1 M $CDCl_3$ solution.

The remaining methyl signals, at δ0.86 and δ0.93, were assigned to the diastereotopic geminal methyl groups (methyl-12 and methyl-11) through NOED experiments, which also aided assignment of some of the ring proton signals.

Irradiation of the δ0.86 methyl-12 transitions (Fig. 4.12-i) produced enhancement of the intensities of the H-7 and H-6 signals, with weak enhancement of the δ1.23, 1.48 H-2 signals. This signal was, therefore, assigned to methyl-12, which is on the same face (lower face) as H-7. Irradiation of the δ0.93 methyl-11 transitions (Fig. 4.12-ii) produced no H-7 enhancement, but fairly strong enhancement on the H-6 signal, which indicated that this methyl-11 must be in the same face (upper face) as H-6. There was weak enhancement of the H-3 and the δ1.23 H-2 signal.

Irradiation of the H-7 (lower face) transitions (Fig. 4.12-iii) caused enhancement of the δ1.48 H-2 signal, which was, therefore, assigned to H-2a (axial, on the lower face). Irradiation of the δ1.48 transitions (H-2a, Fig. 4.12-iv) confirmed the C-2 geminal proton assignments by producing a large enhancement of the δ1.23 (H-2e, equatorial) signal. Irradiation of the H-4 transitions (δ5.50, Fig. 4.12-v) caused enhancement of the signal previously assigned to the C-3 protons, and allylic methyl-13 group, consistent with the assignment.

Irradiation of the H-6 (δ2.29, upper face) transitions (Fig. 4.12-vi) caused strong enhancement of H-8 (δ6.05) and weak enhancement of H-7 (δ6.62) and methyl-13, which indicated that H-6 is <u>trans</u> to H-7, and <u>cis</u> to H-8. Irradiating H-8 caused the same enhancement on H-6 (Fig. 4.12-vii).

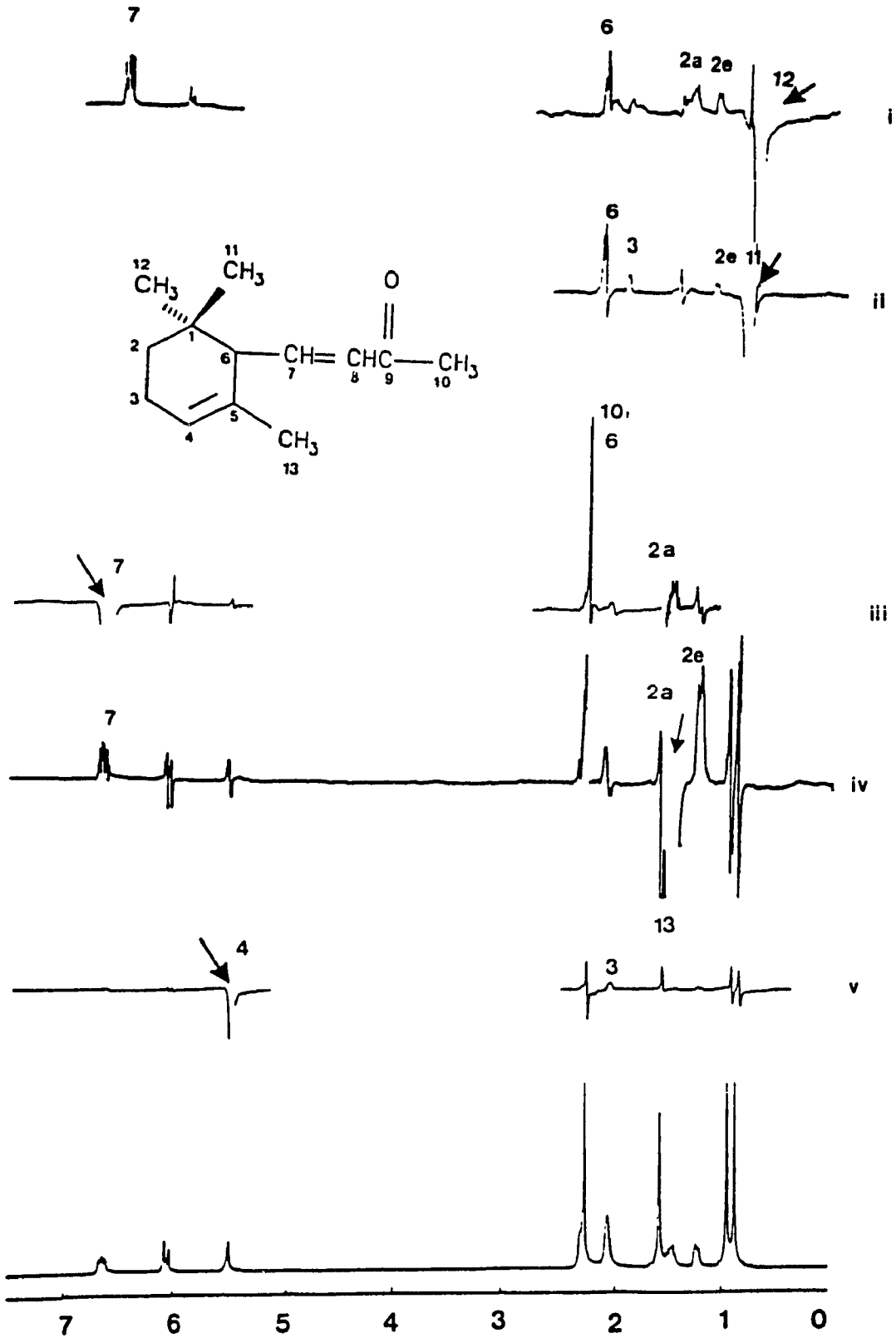

Fig. 4.12. NOED spectra of α-ionone at 400 MHz in a 0.1 M $CDCl_3$ solution.

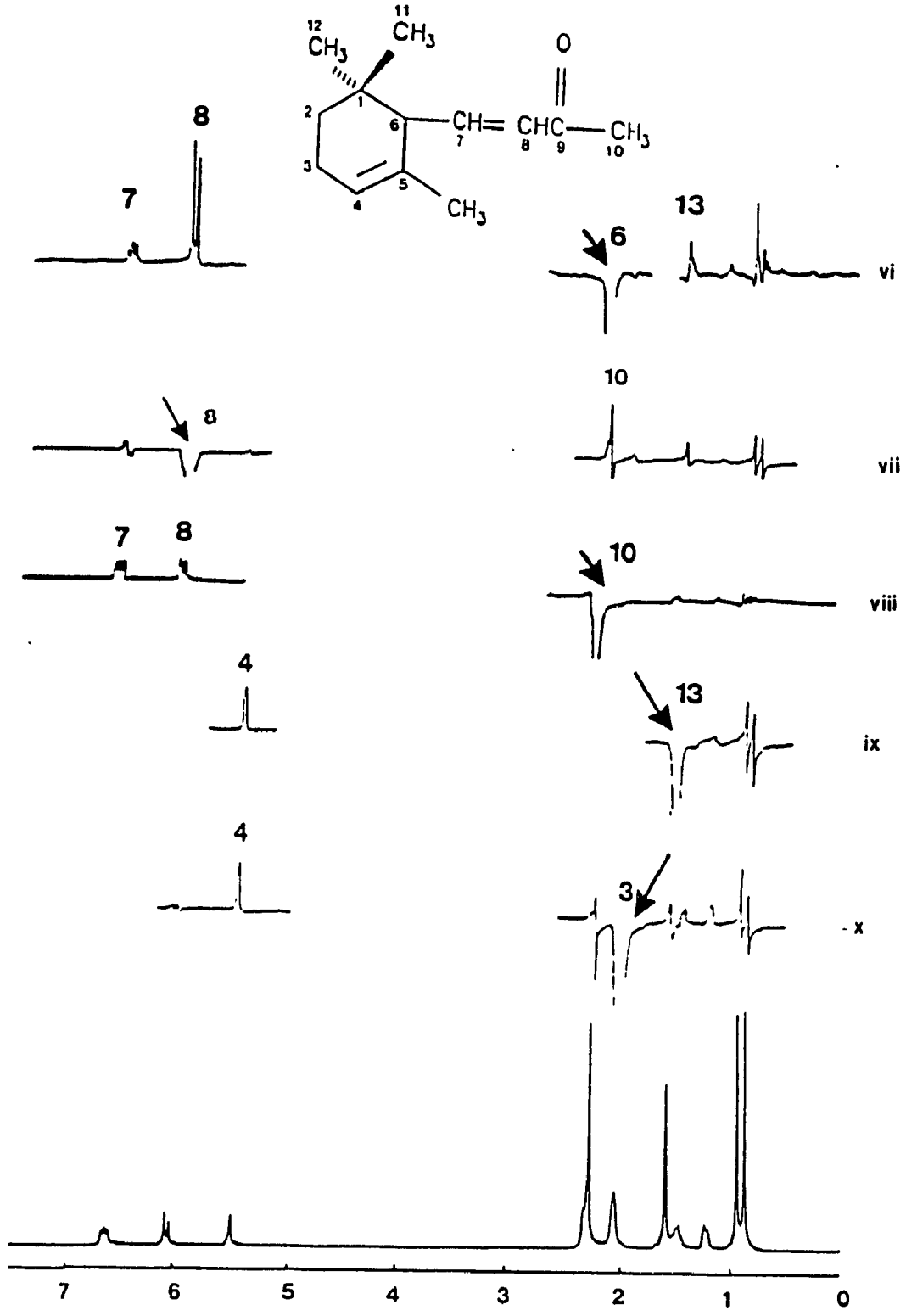

Fig. 4.12 NOED spectra of αionone (continued).

Methyl-10 (acetyl methyl group) presented a strong enhancement when H-7 was irradiated (Fig. 4.12 ix) and a weak enhancement when H-8 was irradiated (Fig. 4.12-viii), so that the conformation of methyl-10 can be assumed to be mostly trans to H-8, and sometimes cis to H-8 considering the single bond (C8--C9) rotation. Conversely, irradiation of methyl-10 (Fig. 4.12-i) caused enhancements of both H-7 and H-8, confirming the single bond rotation. Molecular modelling which will be discussed later also demonstrated that the lowest energy is when the acetyl methyl-10 and H-8 are trans, consistent with the NOED data.

The stereo-conformation and NOE pathways are given in Fig. 4.13.

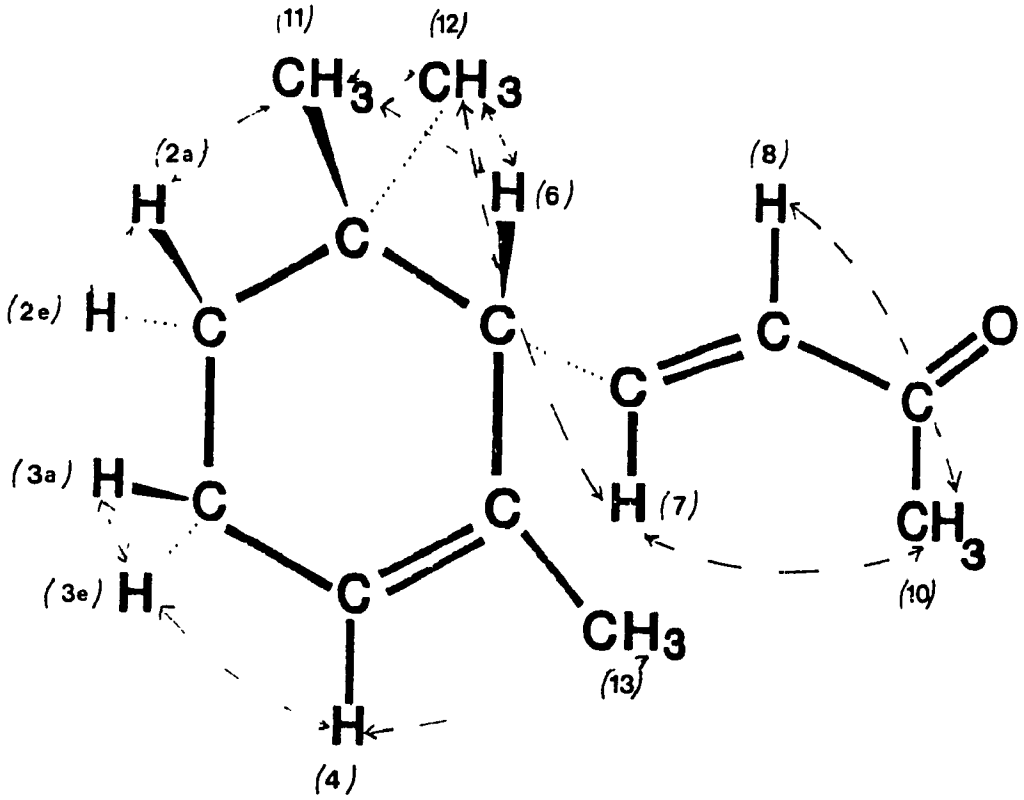

Fig. 4.13. Stereochemistry and NOE pathways of α-ionone.

b. ^{13}C Spectrum assignment

^{13}C spectral assignment was performed previously by the partial decoupling method (57). The 2D-heteronuclear chemical shift correlation experiment (HETCOR, in $CDCl_3$ solution, 100.03 MHz) shows that methyl groups were misassigned in the previous study. There are only twelve signals appearing in the spectrum (from thirteen carbons), therefore it is assumed that there are two ^{13}C signals overlapped in the spectrum. The 2D ^{13}C-^{1}H HETCOR spectrum indicates that the signals from methyl-10 and methyl-11 overlap at δ26.91, rather than methyl-11 and methyl-12 (assigned previously). The correlated ^{1}H and ^{13}C chemical shift assignments are shown in Table 4.2.

Table 4.2 ^{1}H and ^{13}C chemical shift assignments of α-ionone

^{1}H	ppm[a]	^{13}C	ppm[b]
2a	1.48	2	31.34
2b	1.23		
3a,3e	2.05	3	23.07
4	5.50	4	122.77
6	2.29	6	54.40
7	6.62	7	148.94
8	6.05	8	132.50
Me-10	2.24	Me-10[c]	26.91
Me-11	0.93	Me-11[c]	26.91
Me-12	0.86	Me-12	27.79
Me-13	1.57	Me-13	22.79

[a] Measured in 0.1 M $CDCl_3$ solution at 400 MHz using a Bruker WH-400 spectrometer at ambient temperature (degassed by the freeze-pump-thaw technique).

[b] Measured in 1M $CDCl_3$ solution at 20.13 MHz using a Bruker WP-80SY spectrometer at ambient temperature with the broadband decoupler on.

[c] These two signals overlapped in the spectrum.

c. Molecular mechanics

The lc :est energy conformation was identified through molecular mechanics calculations (MMX) as having the butenone side chain and the upper face geminal methyl-11 pseudo-axial, the other geminal methyl-12 being pseudo-equatorial (Fig. 4.14). The butenone side chain in the model adopts a minimum energy conformation with H-6 and H-7 approximately anti (dihedral angle of H6--C6--C7--H7 = 169°). The calculated (PCMODEL) $J_{6,7}$ coupling constant (11.3 Hz) is in reasonable agreement with the observed value (9.7 Hz), supporting this conformational assignment. A 360° rotation of the C8--C9 bond in a dihedral driver calculation showed two local minima (Fig. 4.15) for the methyl-10 orientations. In the preferred conformation (0.25 kcal/mol lower), methyl-10 and H-8 are trans, as mentioned above.

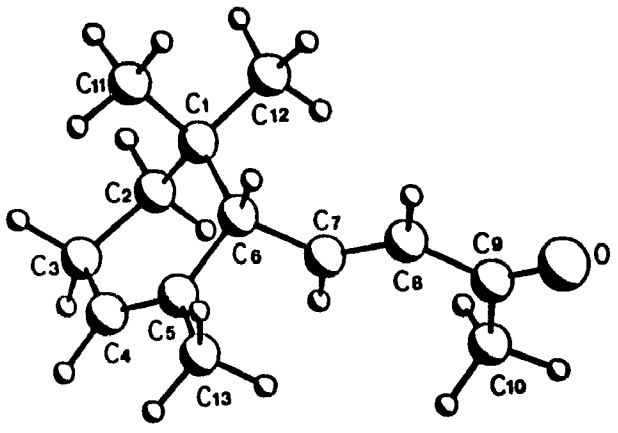

Fig. 4.14. Three-dimensional structure of α-ionone.

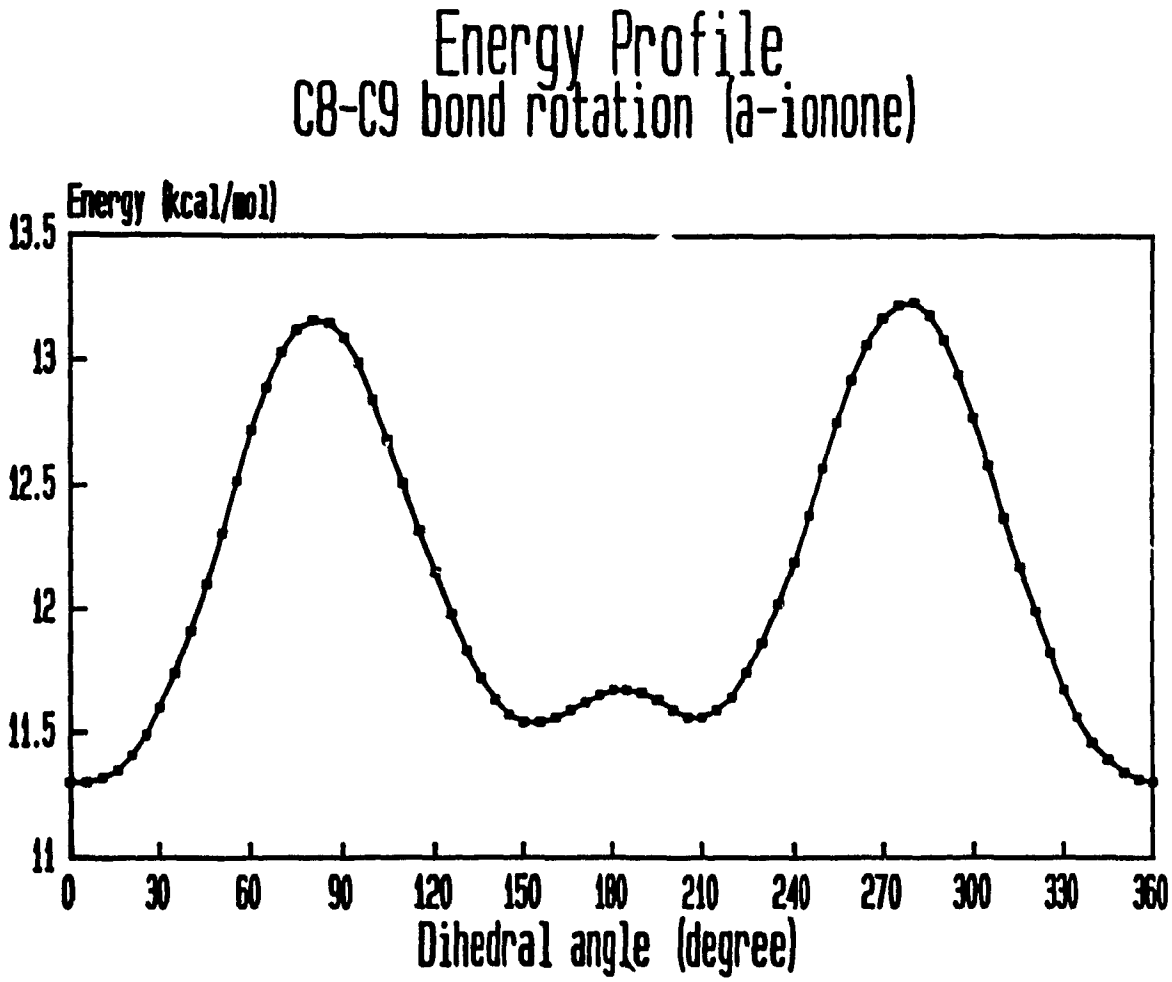

Fig. 4.15. Rotational energy profile for C8--C9 bond rotation (α-ionone).

4.3.2 Methyl-O-methylpodocarpate (66)

a. ^1H chemical shift assignment

The 400 MHz spectrum (0.1 M $CDCl_3$) (Fig. 4.16) of the diterpene derivative methyl-O-methylpodocarpate (MMP) consists of four methyl singlets, three aromatic proton signals and two heavily overlapping methylene regions (1.8-2.1 ppm, and 2.1-2.3 ppm) which are difficult to assign. A combination of 1D- and 2D-NMR techniques was successfully applied to assign the spectrum, while the stereochemistry was investigated using molecular modelling, NOED and R_1 techniques.

The aromatic signals at δ6.95, 6.79, 6.65 were assigned based on their chemical shifts and J coupling constants. The δ6.95 doublet is assigned to H-14 due to its single J coupling with H-13 ($J_{14,13}$ = 8.38 Hz). The doublet of doublets at δ6.65 possesses the same J coupling constant as H-13 (8.38 Hz) and a smaller (long range) coupling (2.68 Hz). Thus this signal is assigned to H-13 with long range coupling due to H-11. The other aromatic proton signal at δ6.79 must be H-11, which has only long rage coupling from H-13 (2.68 Hz).

Two intense singlets at δ3.64 and δ3.75 are assigned, on the basis of their chemical shifts and intensities, to the methoxyl groups 21 and 22. Methyl groups 18 and 20 give rise to singlets at δ1.26 and δ1.02. The remaining peaks are from ring protons which are assigned from NOED (Fig. 4.17) and 2D experiments.

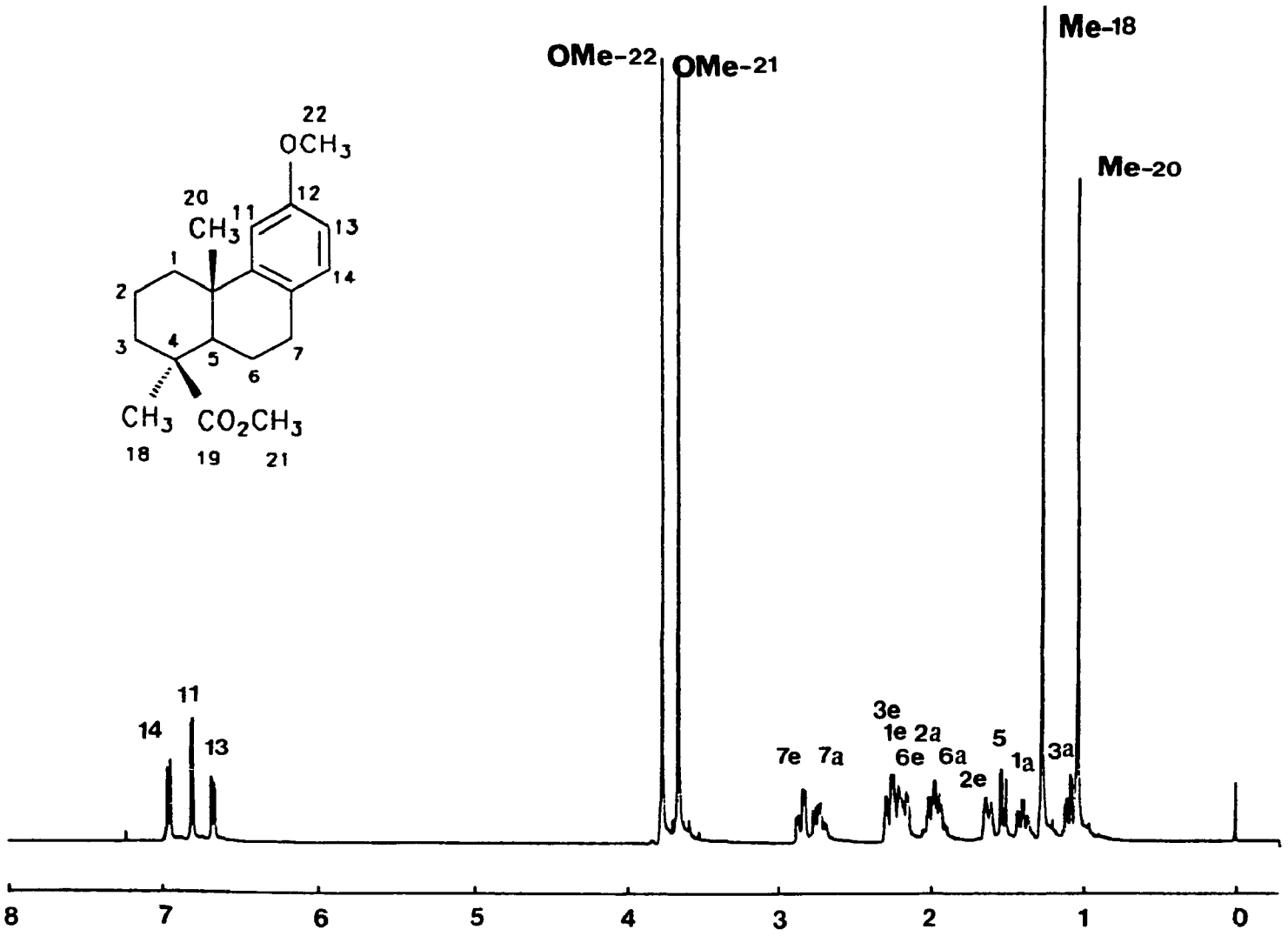

Fig. 4.16. ^1H spectrum of MMP at 400 MHz in a 0.1 M $CDCl_3$ solution.

Irradiation of the singlet at δ3.75 (a methoxy group, Fig. 4.17-iii) caused the same level of enhancement of aromatic protons H-13 and H-11, indicating that this singlet is aryl methoxyl-22. Therefore, the other singlet at δ3.64 must be the ester methoxyl-21, which did not cause any enhancement of other proton signals when it was irradiated (Fig. 4.17-iv).

Irradiating the higher field C-methyl peak at δ1.02 (Fig. 4.17-ii) produced a strong enhancement at aromatic proton-11 (δ6.79). demonstrating that this methyl group is near the aromatic ring , i.e. methyl-20. consequently, the lower field methyl signal at δ1.26 was assigned to methyl-18, which is on the chiral centre, C-4. Irradiation of the methyl-18 singlet (Fig. 4.17-i) caused a clear enhancement of a doublet at δ1.51 signal, and a weak enhancement of a multiplet at δ1.07. Hence, the δ1.51 signal was assigned to H-5, which is on the lower face of ring A (axial position) and which shows a lower multiplicity. The multiplet at δ1.07 could be the axial proton at C-3 (H-3a) which is also on the lower face of ring A.

Irradiation of the peak at δ1.51 (H-5, Fig. 4.17-v) strongly enhanced the methyl-18 signal, confirming the previous assignment, and created distinct enhancements at δ1.07 and δ1.37. Since the δ1.07 multiplets were assigned to H-3a (axial), the δ1.37 signal could be due to either H-1a or H-6e (equatorial). Irradiation of the methylene multiplet at δ2.83 (Fig. 4.17-vii) generated an intense enhancement of aromatic proton H-14 (δ6.95) and its geminal neighbour (δ2.72), indicating that the transition at δ2.83 arises from one of the H-7 protons, which is close to H-14 (molecular mechanics shows that it can only be H-7e). Its geminal neighbour must

cause the signal at δ2.72. There was also obvious enhancement at δ1.51 (H-5) when the signal at δ2.72 was irradiated (Fig. 4.17-viii), demonstrating that this proton and H-5 are on the same face (lower face) of ring B. This should, therefore, be H-7a (axial), and the signal at δ2.83 must be H-7e. The other enhancement at δ2.15 from irradiating H-7a showed that this signal belongs to H-6e, according to their orientations. Hence, the doubtful δ1.37 signal must be H-1a rather than H-6e.

Irradiating the H-3a signal at δ1.07 (Fig. 4.17-vi) created strong enhancements at δ2.25, which is in the heavily overlapping region (δ2.1-2.3) and at H-5, the axial proton; irradiating H-1a, at δ1.37 (Fig. 4.17-x), caused enhancements at δ2.24 and also of the H-5 signal. Thus the overlapped transitions at δ2.25 and δ2.24 are assigned to H-3e and H-1e, respectively. The enhancement of H-5 when H-1a and H-3a were irradiated shows that H-5, H-3a and H-1a are all axial protons on the lower face of ring A. However, the assignments of H-1a and H-3a are still not certain since the NOE enhancements were too weak. There was no enhancement of H-5 when methyl-20 was irradiated (Fig. 4.17-ii), so that methyl-20 and H-5 are assumed to be on opposite faces. In other words, the AB ring junction is in a trans configuration.

Very weak enhancement at δ1.61 when H-1a was irradiated (Fig. 4.17-x) suggested that the signal may be assigned to H-2e (equatorial). Irradiation of the multiplet at δ1.61 (Fig. 4.17-ix) strongly enhanced a multiplet at δ1.99 in the other overlapping region (δ1.8-2.1) and weakly enhanced the H-1a, H-1e, H-3a and H-3e signals. This indicated that the δ1.61 and δ1.99 signals arise from geminal protons, most likely on C-2. However, the assignment of the two protons was still uncertain.

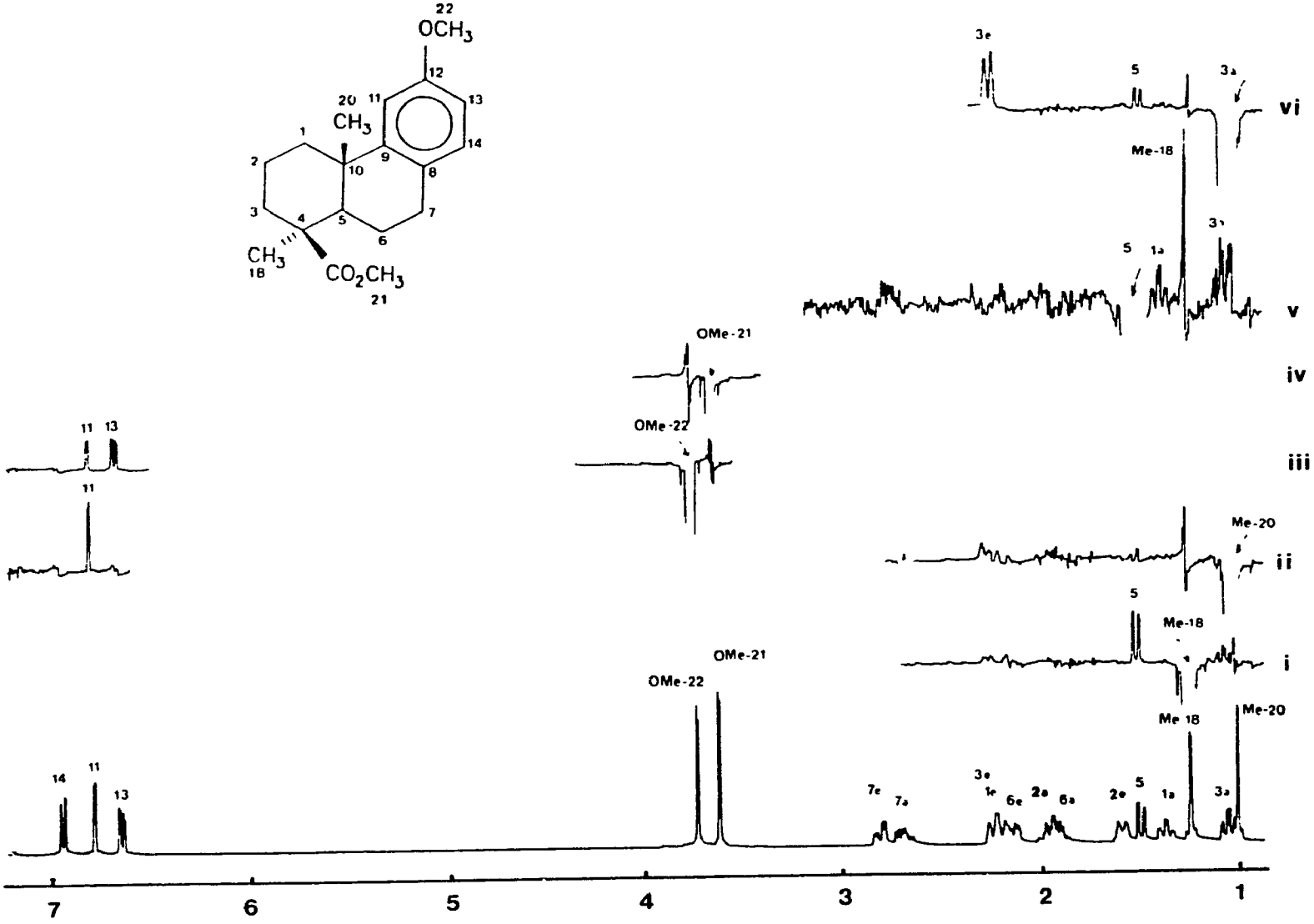

Fig. 4.17. NOED spectra of MMP at 400 MHz in a 0.1 M $CDCl_3$ solution.

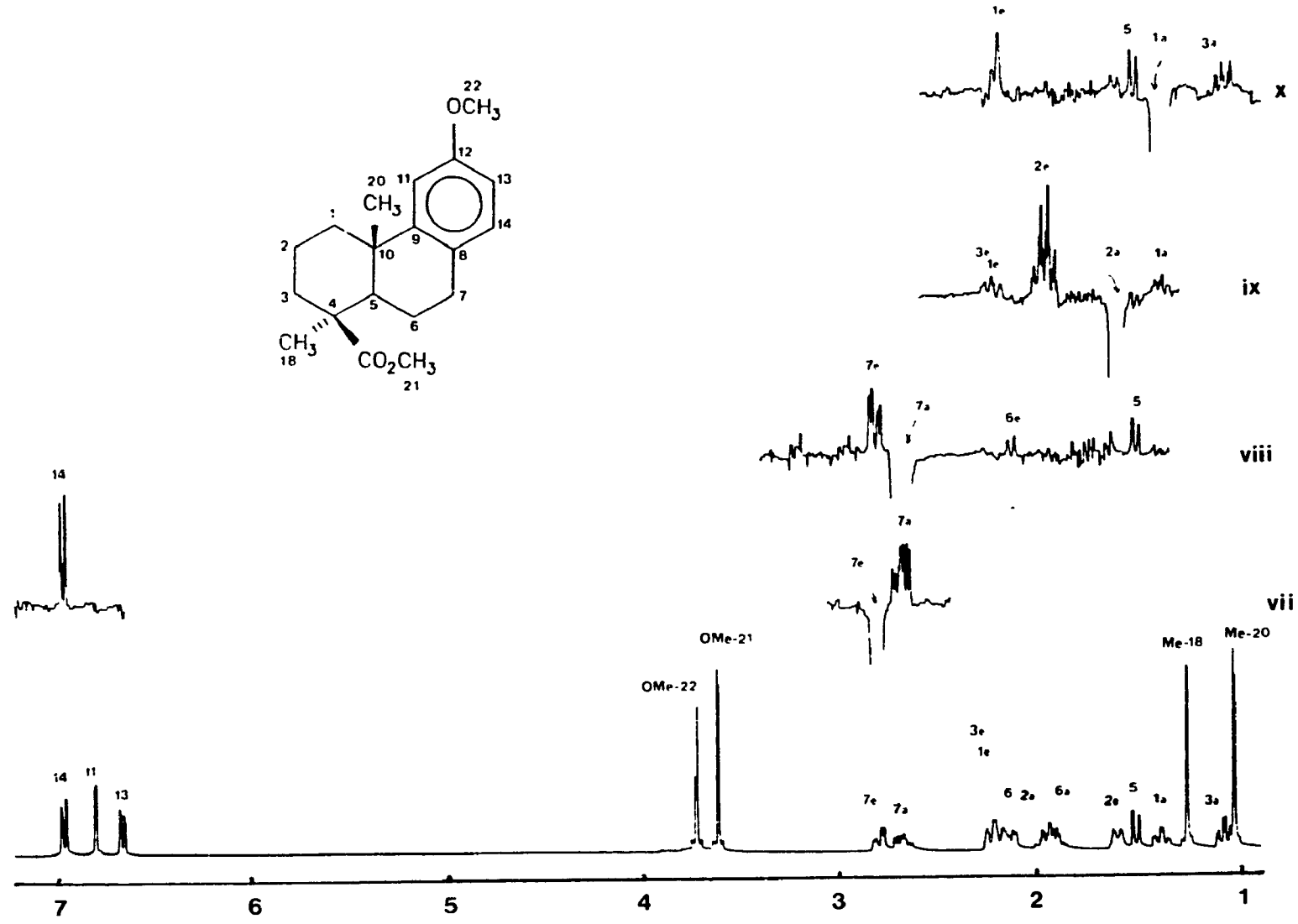

Fig. 4.17 NOED spectra of MMP (continued).

Integration showed that the multiplet region at δ1.8-2.1 consists of 2 protons: one was assigned to H-2a or H-2e (δ1.99), thus the other is likely to be H-6a. However, the chemical shift assignment of H-6a was not obvious from 1D NMR experiment.

To clarify some of the ^{1}H 1D assignments, 2D ^{1}H-^{1}H COSY and ^{13}C-^{1}H HETCOR spectra were required. The COSY was used to confirm some of the scalar couplings and the HETCOR was used to make some of the ^{1}H assignments based on the 1D NMR ^{13}C literature assignments (54) which were considered to be reliable.

From the NOE data it was difficult to distinguish H-3a and H-1a due to the similar enhancement (usually very weak) which always appeared at both resonances. C-3 shows a peak at δ37.6 in the $^{13}C\{^{1}H\}$ spectrum which correlates with the signals at δ2.25 and δ1.07 in the F1 (^{1}H) domain in the HETCOR spectrum. For H-1, the ^{13}C-1 at δ39.4 (from literature) is correlated to multiplets at δ2.24 and δ1.37 in the proton domain (Fig. 4.18). Therefore, the signal was assigned to H-1a. The assignments for H-6 and H-2 were also confirmed using the F1 trace from the HETCOR. The ^{13}C resonance at δ19.9 (C-2) showed a correlation to δ1.99 and δ1.61 in the ^{1}H domain. The C-6 signal at δ21.1 was correlated to protons at δ2.15 and δ1.98.

The COSY experiment confirmed the methylene ^{1}H assignments from the NOED experiments showing scalar coupling between the geminal protons.

400 MHz ^{1}H spectrum assignments of MMP are shown in Table 4.3. The NOE enhancements are shown in Table 4.4.

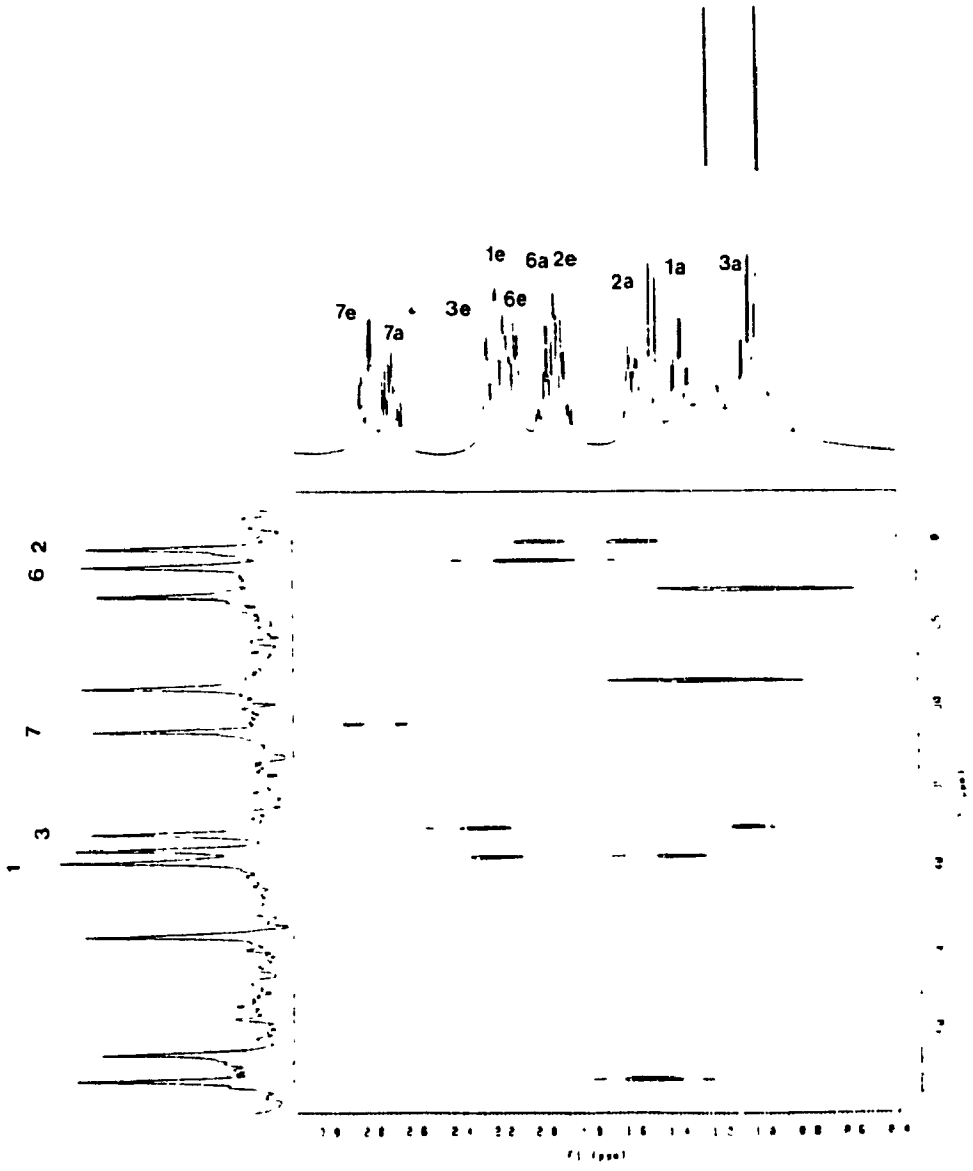

Fig. 4.18. 2D-HETCOR spectrum of MMP in a 1 M $CDCl_3$ solution.

Table 4.3 ^{1}H chemical shift assignments and experimental R_1 values of MMP

H	ppm	R_1	H	ppm	R_1
1a	1.37	1.38	7a	2.70	1.39[c]
1e	2.23		7e	2.84	1.37[c]
2a	1.61[a]	1.27[b]	11	6.79	0.72
2e	1.99[a]		13	6.65	0.33
3a	1.07	1.74	14	6.95	0.43
3e	2.25		Me-18	1.26	1.48
5	1.51	0.77[c]	Me-20	1.02	1.25
6a	1.94		OMe-21	3.64	0.54
6e	2.16		OMe-22	3.75	0.59

[a] Uncertain assignment, might be reversed.

[b] The rate may belong to H-2e due to the uncertain assignment.

[c] By null point method (39).

Table 4.4 NOE enhancements of MMP

{^{1}H}	Enhancement
1a	1e, 5
2a/2e	2e/2a (s)
3a	3e (s), 5
5	Me-18 (s), 7a (w), 6e (w), 1a, 3a
7a	7e (s), 6e, 5
7e	7a (s), 14 (s)
Me-18	5, 3a (w)
Me-20	11 (s), 6a, 1e
OMe-21	None
OMe-22	11, 14

s = strong; w = weak

b. Molecular mechanics

Molecular mechanics calculations on the configuration with the AB ring junction trans identify the lowest energy conformation with ring A as a chair and ring B as a twisted chair (Fig. 4.19). The stereochemistry at C-4 shows methyl-18 equatorial and the ester methoxyl group as facing away from any ring protons, which is consistent with the NOE data. Theoretical energy barriers of the C4-C19 bond rotation are 5.59 kcal/mol and 13.67 kcal/mol, containing two energy minima. In the preferred conformation, the carbonyl group faces away from C-3 with a O16--C19--C4--C3 dihedral angle of 179°.

The aromatic methoxyl group-22 can have two conformations, facing either H-11 or H-13 and approximately co-planar with the aryl ring (Fig. 4.19). The NOE results showed the same possibility for the two conformations (same intensity of enhancements when OMe-22 was irradiated). The very low rotational barrier of the C12--O17 bond rotation (1.21 kcal/mol) indicates that the aryl methoxyl group rotates almost freely in solution. The equilibrium constant of the two conformations is calculated to be near unity, in agreement with the NOE result.

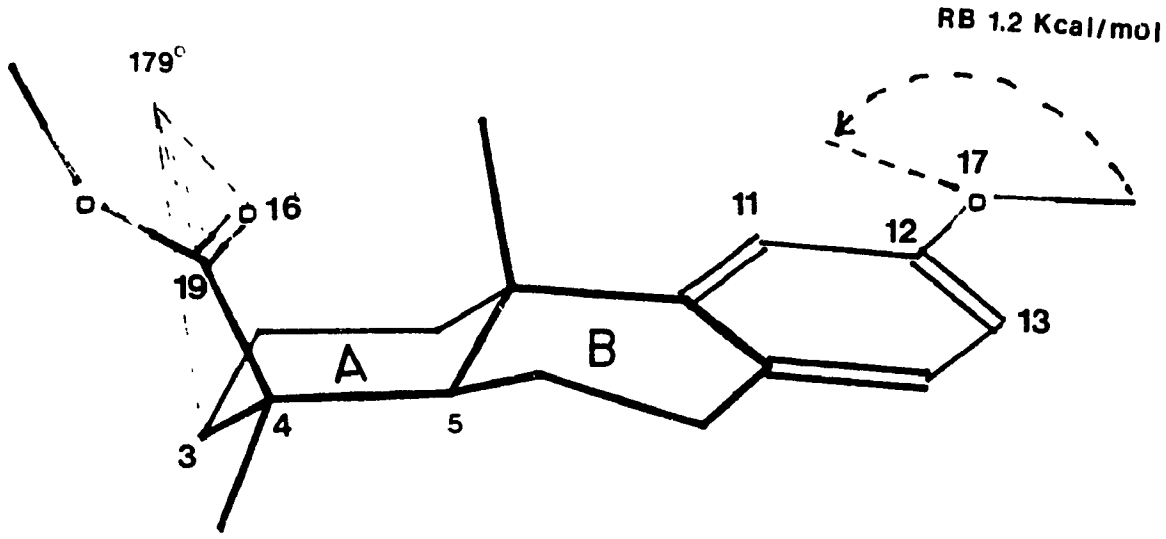

Fig. 4.19. Three-dimensional structure of MMP (hydrogens are omitted).

4.3.3 α-Pinene and verbenone

α-Pinene and verbenone have similar structures. Each of them contains one allylic methyl group (Me-10) and two geminal methyl groups (Me-8 and Me-9). The four membered ring imposes a rigid geometry on the molecule.

a. ^1H chemical shift assignments by NOED measurements

The high field ^1H spectra (400 MHz, 0.1 M in $CDCl_3$ solution) were assigned successfully by NOED measurements (Table 4.5). The NOED pathways and three-dimensional structures of these two terpenes are shown in Fig. 4.19. 2D-heteronuclear chemical shift correlation spectra give good agreement with previously assigned ^{13}C spectra (41).

b. Molecular mechanics

The minimum energies of α-pinene and verbenone are 38.76 and 40.02 kcal/mol, respectively, calculated by molecular mechanics (MMX). The $J_{7,5}$ coupling constant in α-pinene was calculated to be 7.57 Hz (for dihedral angle of 33^0), which is in reasonable range with the experimental data (5.53 Hz).

Table 4.5 ^1H chemical shift assignments of α-pinene and verbenone

^1H[a]	α-pinene	Verbenone
1	1.93	2.44
3	5.18	5.72
4	2.17	
5	2.07	2.64
7a	1.15	2.81
7e	2.33	2.07
Me-8	1.26	1.50
Me-9	0.84	1.01
Me-10	1.65	2.02

[a] Measured at 400 MHz in a 0.1 M $CDCl_3$ solution. Samples were degassed.

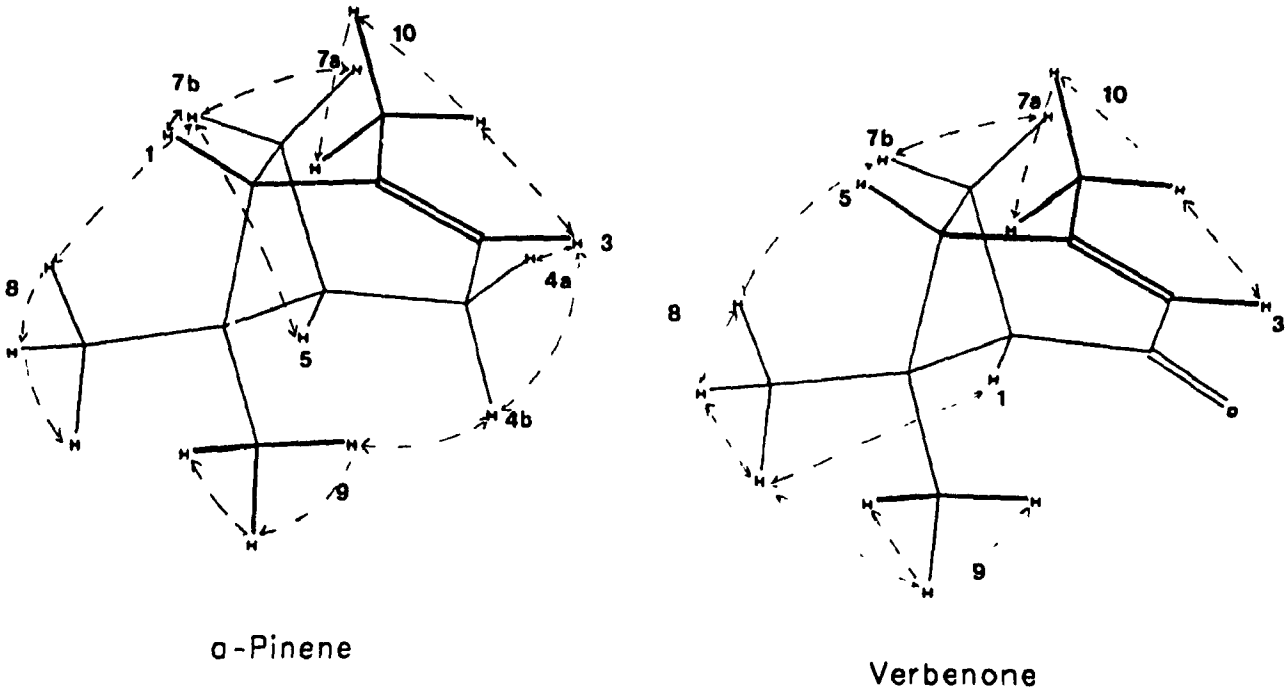

Fig. 4.20. NOE pathways and three-dimensional structures of α-pinene and verbenone.

4.3.4 Conclusions

The 400 MHz ^{1}H spectra of a newly synthesized compound, DDPTO, and four terpenes were successively assigned using NOED and some 2D NMR techniques. CHORTLE and ^{13}C-^{1}H HETCOR experiments were used to assign ^{13}C spectra or to check the previous ^{13}C assignments. Molecular mechanics calculations show a very good correlation with the experimental NOED data, which greatly assists the analysis of the stereochemistry of these organic compounds.

Chapter 5

AN INVESTIGATION OF DYNAMICS, STEREOCHEMISTRY AND CHEMICAL SHIFT ASSIGNMENTS OF ORGANIC COMPOUNDS USING COMPUTED AND EXPERIMENTAL R_1 CORRELATION AND MOLECULAR MODELLING

5.1 Introduction

Intramolecular motion and chemical exchange, such as dissociation of labile protons in OH or NH groups, ring interconversion, single bond rotation, and H-D exchange in deuterium oxide solution occur commonly during NMR measurements. These conformational or exchange processes can usually be "seen" easily from line broadening in the spectrum or can be detected by varying the temperature of the measurement (67). In this Chapter, a new method, experimental and computed R_1 correlation, has been used to monitor the dynamic motion of some molecules in solution at ambient temperature and, at the same time, the predictive ability of molecular mechanics associated with R_1 calculation has also been examined.

It is known that conformational exchange may significantly affect the spin-lattice relaxation rates of nearby protons (34). When the exchange rate, k_{ex}, is slow on the chemical shift time scale, but R_1 is much greater than k_{ex}, individual spins in the two sites of exchange will, on average, relax back to equilibrium before experiencing any change in shift. The result is that each line will relax at its own rate, R_1. This is slow exchange on the R_1 time scale. If k_{ex} is much faster than R_1 for each site, but still slow on the chemical shift time scale, then the magnetization vectors will visit each chemical shift, and relax at the appropriate rate for that shift, many times during the course of relaxation. The observed relaxation rate will now

be the weighted average of the two contributing relaxation rates. This is fast exchange on the R_1 time scale but slow exchange on the chemical shift time scale. When k_{ex} is much faster than both the R_1 and chemical shift time scales, the spectra from the two sites of exchange will collapse to a single resonance. The chemical shift and R_1 of this signal will not belong to either one of the two sites, but exist as a weighted average.

Relative R_1 values may be calculated from inter-proton distances predicted by molecular mechanics calculations, since internuclear distances are fixed in the molecular mechanics model. This represents an extreme situation in which no dynamic process is taken into account. In this study, the spin-lattice relaxation rates derived from this ideal model were compared with the experimental data to investigate dynamic motion and flexibility of the molecules in solution.

Poor correlations for protons undergoing exchange were expected, in contrast to non-exchanging protons in rigid molecules. Most of the molecules studied in this Chapter contain moieties which experience relatively fast exchange or internal motion on the chemical shift time scale, the exception being nefopam. However, all the motions are faster than the R_1 time scale, so that any proton undergoing exchange or internal motion will have a "false" R_1 value which can be monitored by the R_1 correlation method.

Four natural products, gibberellic acid, gelsemine, brucine, and methyl O-methylpodocarpate, and one synthetic compound, nefopam, were selected as the models in this study.

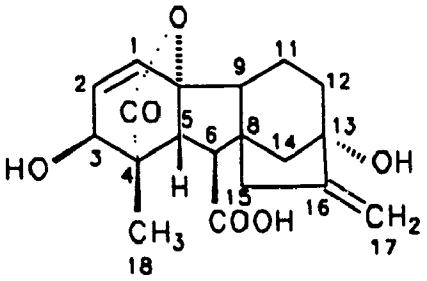

Gibberellic acid

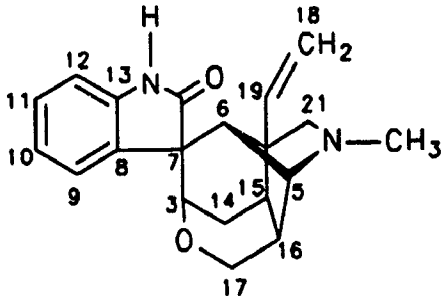

Gelsemine

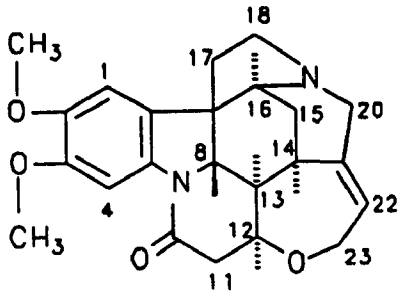

Brucine

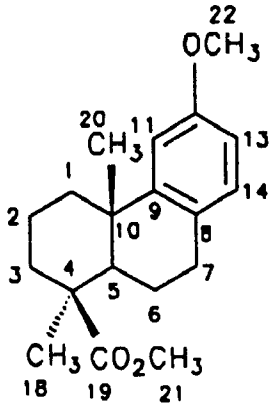

Methyl O-methylpodocarpate

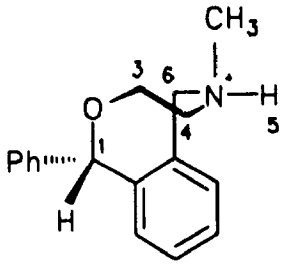

Nefopam

Fig. 5.1. Structures.

5.2 Results and discussion

5.2.1 Gibberellic acid

Gibberellins are an important group of phytohormones which regulate, together with other plant hormones and inhibitors, the growth and development of higher plants (68). Gibberellic acid was the first compound isolated in the group and its structure and properties have been studied for many years (69). The ^{1}H and ^{13}C NMR spectra of gibberellic acid have been assigned completely by Preiss and Bernstein (69, 70) at 200 MHz and 300 MHz in mixed solution using NOED and 2D techniques.

Using the assigned ^{1}H and ^{13}C spectra, the spin-lattice relaxation rates of protons and carbons were investigated. The ^{1}H R_1 values were compared with the computed relative R_1 values determined by molecular modelling.

a. Chemical shift assignments and R_1 determination

The ^{1}H 400 MHz spectrum was determined on a Bruker WH-400 spectrometer in a 0.1 M mixed solution of C_6D_6:Pyr-d_5:CD_2Cl_2 (43:6:4, the same solvent mixture was used as in ref. 70.) (Fig. 5.2). The chemical shifts of the protons were consistent with the previous assignment (70). The ^{13}C spectrum was recorded on a Bruker WP-80SY spectrometer at 20.13 MHz in a 1M DMSO-d_6 solution. DEPT and 2D-HETCOR techniques were used to assign the ^{13}C spectrum, and the result agrees with Preiss's work (69).

The spin-lattice relaxation rates of all the methine protons range from 0.49 s^{-1} for H-5, which has only one near neighbour proton (H-6), to 1.32 s^{-1} for H-9, which has relatively efficient relaxation pathways with several nearby protons. The most efficient relaxation occurs between geminal protons due to their short inter-proton distances. All the methylene protons in gibberellic acid relax two to three times faster (2.22 to 2.79 s^{-1}) than the methine protons. The vinylic protons, H-17, H-17', and the methyl protons relax at an intermediate rate, as expected.

The carbon R_1 values of gibberellic acid included an unusually low rate for methyl group 18, possibly arising from fast methyl rotation in solution (shorter τ_c, see Chapter 3 for a discussion of this factor), causing a significantly reduced efficiency of the dipole-dipole relaxation.

The chemical shifts and R_1 values of ^1H and ^{13}C spectra are presented in Table 5.1.

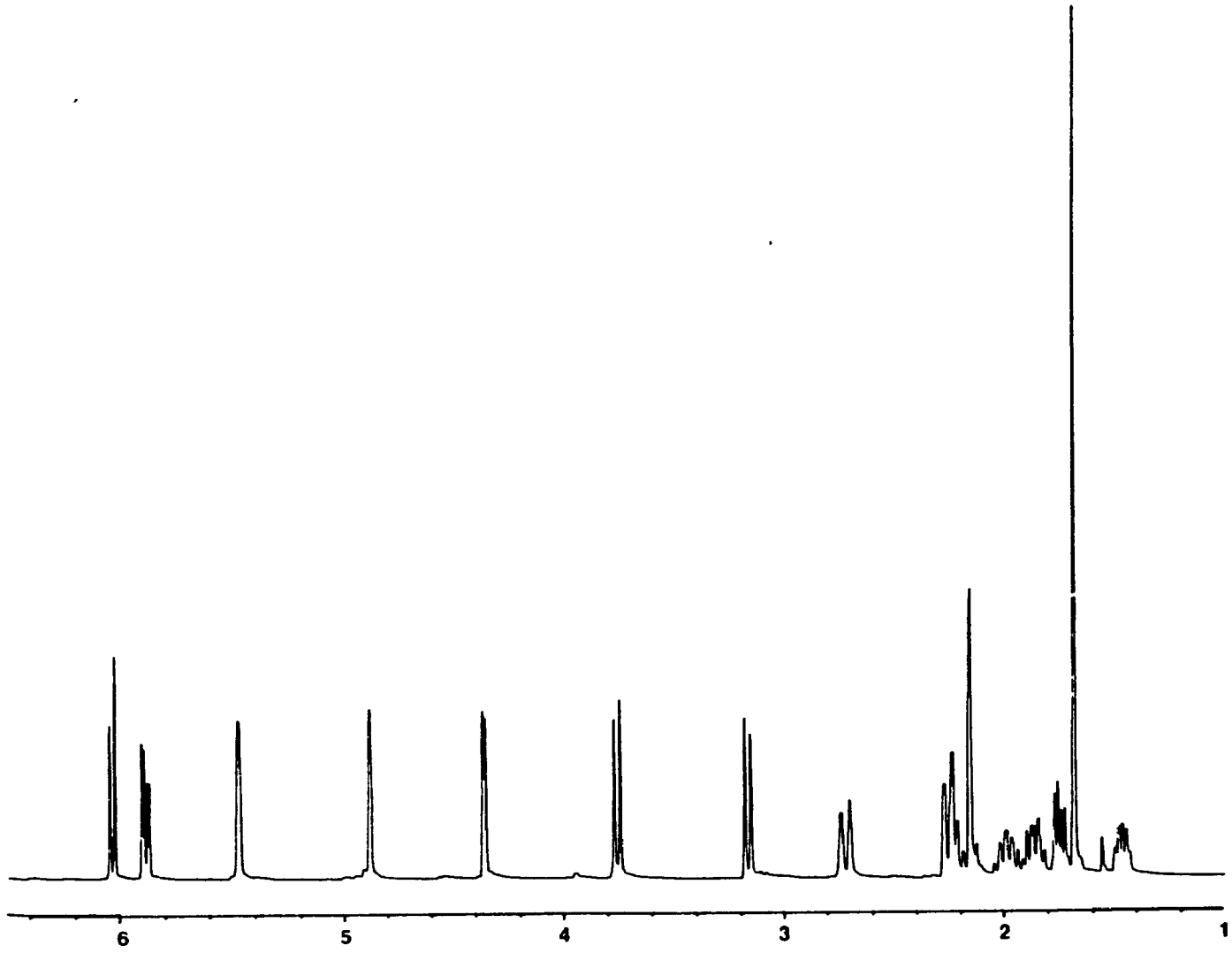

Fig. 5.2. ^1H spectrum of gibberellic acid at 400 MHz in a 0.1 M mixed (C_6D_6:Pyr-d_5:CD_2Cl_2 43:6:4) solution.

Table 5.1 Chemical shift assignments and R_1 values of gibberellic acid

^1H[a]	ppm	$R_1(s^{-1})$	^{13}C[b]	ppm	$R_1(s^{-1})$
1	6.02	0.61	1	131.28	3.48[c]
2	5.88	0.70[c]	2	133.18	3.87[c]
3	4.35	0.71	3	68.41	3.48[c]
5	3.75	0.49	4	52.95	e
6	3.16	0.67	5	52.11	3.71
9	1.74	1.32	6	50.78	3.74
11a	1.96	2.55[c]	7	172.91	e
11b	1.45	2.79[c]	8	49.35	e
12a	2.17		9	50.33	3.13
12b	1.85	2.32[c]	10	90.39	e
14a	2.15[d]	2.54	11	16.43	4.64[c]
14b	2.15[d]	2.54	12	38.66	4.13
15a	2.71	2.22	13	76.48	e
15b	2.17		14	44.38	6.33[c]
17	4.87	1.67	15	42.65	5.13
17'	5.46	1.66	16	157.49	e
CH_3	1.67	1.57	17	105.95	5.20
			CH_3	14.20	1.64
			19	178.48	e

[a] Measured at 400 MHz in 0.1 M C_6D_6:Pyr-d_5:CD_2Cl_2, 43:6:4. The sample was degassed for R_1 determination.

[b] Measured at 20.13 MHz in 1 M DMSO-d_6 solution.

[c] By null point method (39).

[d] Overlapped with other peaks.

[e] Relaxation was too slow to be measured under the conditions of the experiment.

b. Molecular Modelling and R_1 Correlation

Molecular mechanics calculations were carried out for the known configuration of gibberellic acid at ring junctions and sites of substitution (69). The lowest energy structure of gibberellic acid is predicted by molecular mechanics calculations as having ring A in a twisted chair with the AB ring junction trans, ring C in a boat form with the BC ring junction cis. Methyl group 18 and the carboxyl group are pseudo-equatorial in ring A and B (Fig. 5.3).

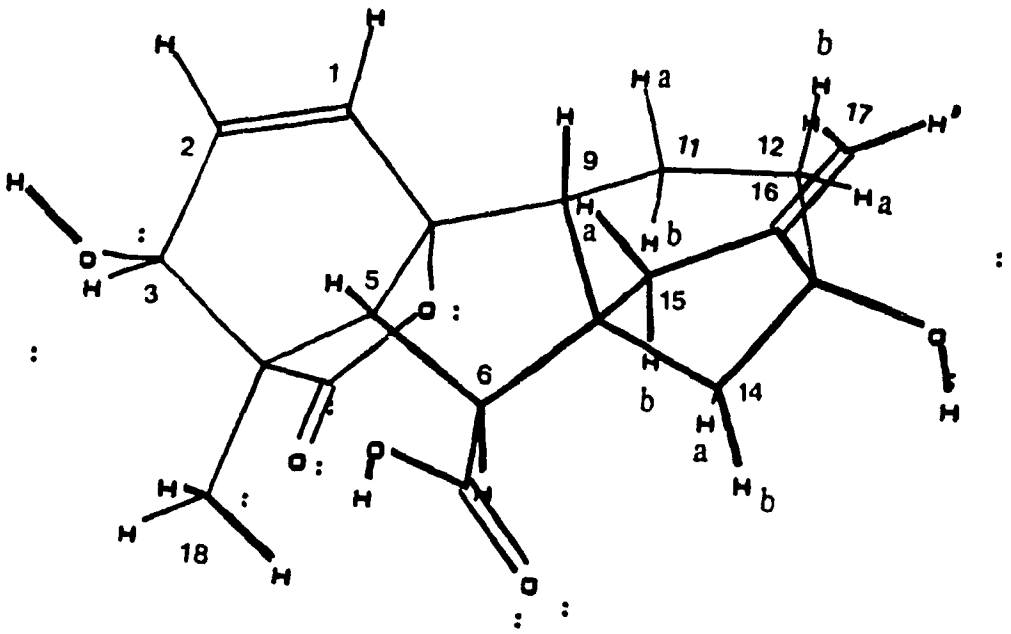

Fig. 5.3. Three-dimensional structure of gibberellic acid.

A correlation of relative relaxation rates from molecular modelling with normalized experimental R_1 values was performed. If a model is exactly the same as the molecule in solution, all points in the correlation chart will be, theoretically, on the diagonal. Dynamic processes (e.g. ax-eq exchange, bond rotation, and ring interconversion) will be indicated when certain points are far from the diagonal. Since the structure of the molecule is quite rigid, the computed relative proton R_1 values (normalized to H-9) are, therefore, expected to be well correlated with the experimental data. The correlation chart (Fig. 5.4) shows all points lying along the diagonal, and this excellent agreement between experimental and calculated values indicates that molecular modelling is successful, and that no significant dynamic motions are taking place in solution. Since proton spin-lattice relaxation rates are extremely sensitive to interproton distances, a successful correlation such as was obtained for gibberellic acid provides excellent evidence that a) the chemical shift assignments are correct, and b) the stereochemistry is correctly assigned. Thus, gibberellic acid is an appropriate control sample which verifies the validity of this approach.

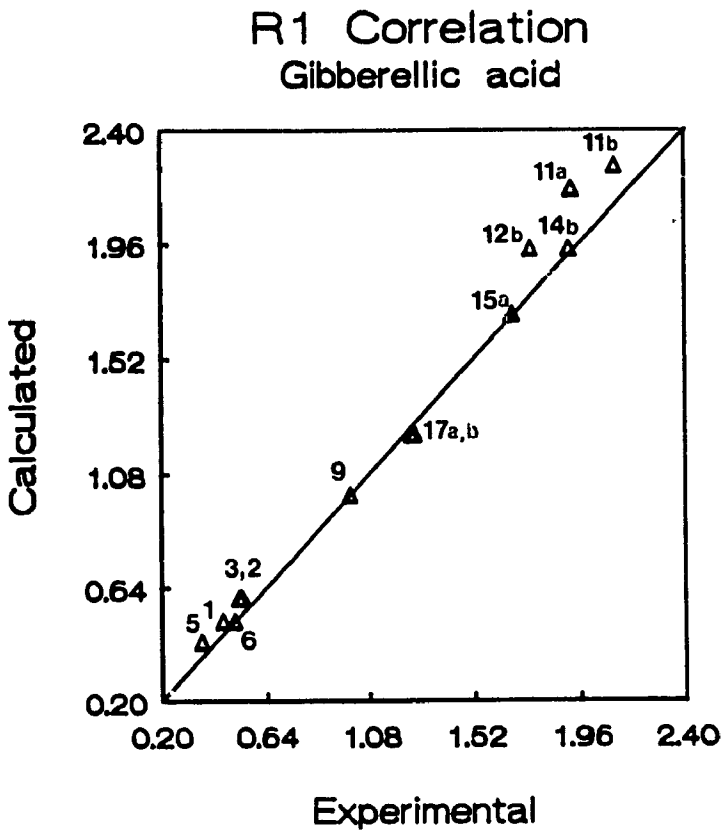

Fig. 5.4. R1 correlation chart of gibberellic acid.

5.2.2 Gelsemine

The structure of gelsemine was established through X-ray crystallographic analysis (71). The ^{13}C NMR spectrum was assigned earlier at 55.51 MHz (72). More recently, the ^{1}H and ^{13}C NMR spectral assignments at 360 MHz and 90.84 MHz, respectively, were reported by Schun and Cordell (73).

a. Chemical shift assignments and R_1 determination

The ^{1}H spectrum was first assigned from a 2D ^{13}C-^{1}H HETCOR experiment, which was based on the previously assigned ^{13}C spectrum (72). However, the calculated and experimental R_1 values of gelsemine based on its ^{1}H chemical shift assignments showed unreasonably bad correlations (Fig. 5.5), indicating that the ^{1}H chemical shift assignments must be checked out. NOED measurements combined with 2D-HETCOR experiments were used to reassign the ^{1}H and ^{13}C spectra at 400 MHz and 100 MHz, respectively, (Bruker WH-400); the misassigned C-12, C-9, C-6 and CH_3 carbon resonances have been corrected.

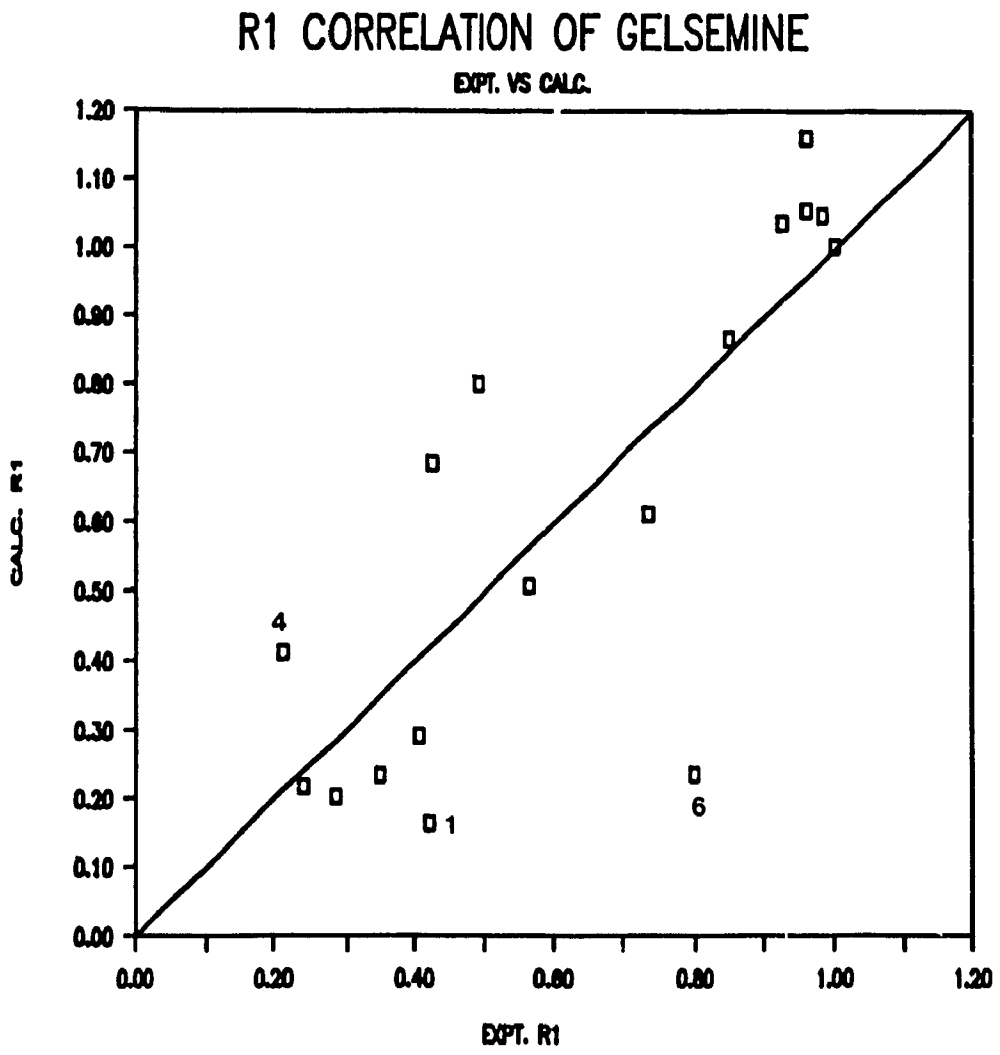

Fig. 5.5. R_1 correlation chart of gelsemine (with wrong chemical shift assignments).

Very good resolution is shown in the 400 MHz ^1H spectrum (Fig. 5.6). The aromatic protons (H-9, H-10, H-11, H-12) have absorptions in the δ6.7 to δ7.4 region, as expected. A broadened singlet at δ8.67 is assigned to the NH proton from its chemical shift. The sharp singlet peak at δ2.25 arises from the N-CH_3 protons. The remaining protons on the rings were identified from NOED and 2D-HETCOR experiments. The NOED measurements and data analysis were carried out using the same method as that which has been described in detail in Chapter 4, and the NOE enhancements are shown in Table 5.2. The NOE results and complete assignments of ^1H and ^{13}C spectra at 400 MHz and 100 MHz (Table 5.3) are in excellent agreement with the previous assignments of Schun and Cordell (9).

The ^1H R_1 values (Table 5.3) vary from the slowly relaxing aromatic protons and methine protons (0.62 - 0.7 s^{-1}) to the fast relaxing geminal methylene protons (2.40 - 2.70 s^{-1}). The vinylic protons (H-18_{cis}, H-18_{trans}) and some methine protons (H-5, H-6, H-15, H-16) which have more efficient relaxation pathways produce intermediate R_1 values (1.10 - 1.70 s^{-1}). The N-CH_3 protons relax mainly within the methyl group. The intermediate relaxation rate of the methyl group (1.88 s^{-1}) indicates that the methyl and lone pair inversion and methyl rotation about the C-N bond may occur in solution. All methine carbons relax at a rate of ca. 1 s^{-1}, except C-19 (R_1 = 0.5 s^{-1}), which is in the vinylic side chain. Since C19--C20 bond rotation in solution is expected, it is not surprising that the R_1 value of H-19 is reduced significantly. The R_1 values of the methylene carbons (C-14, C-17, C-21) range from 1.60 to 1.90 s^{-1}, as expected. The greatly reduced R_1 of the methyl carbon (0.76 s^{-1}) again illustrates methyl rotation in solution.

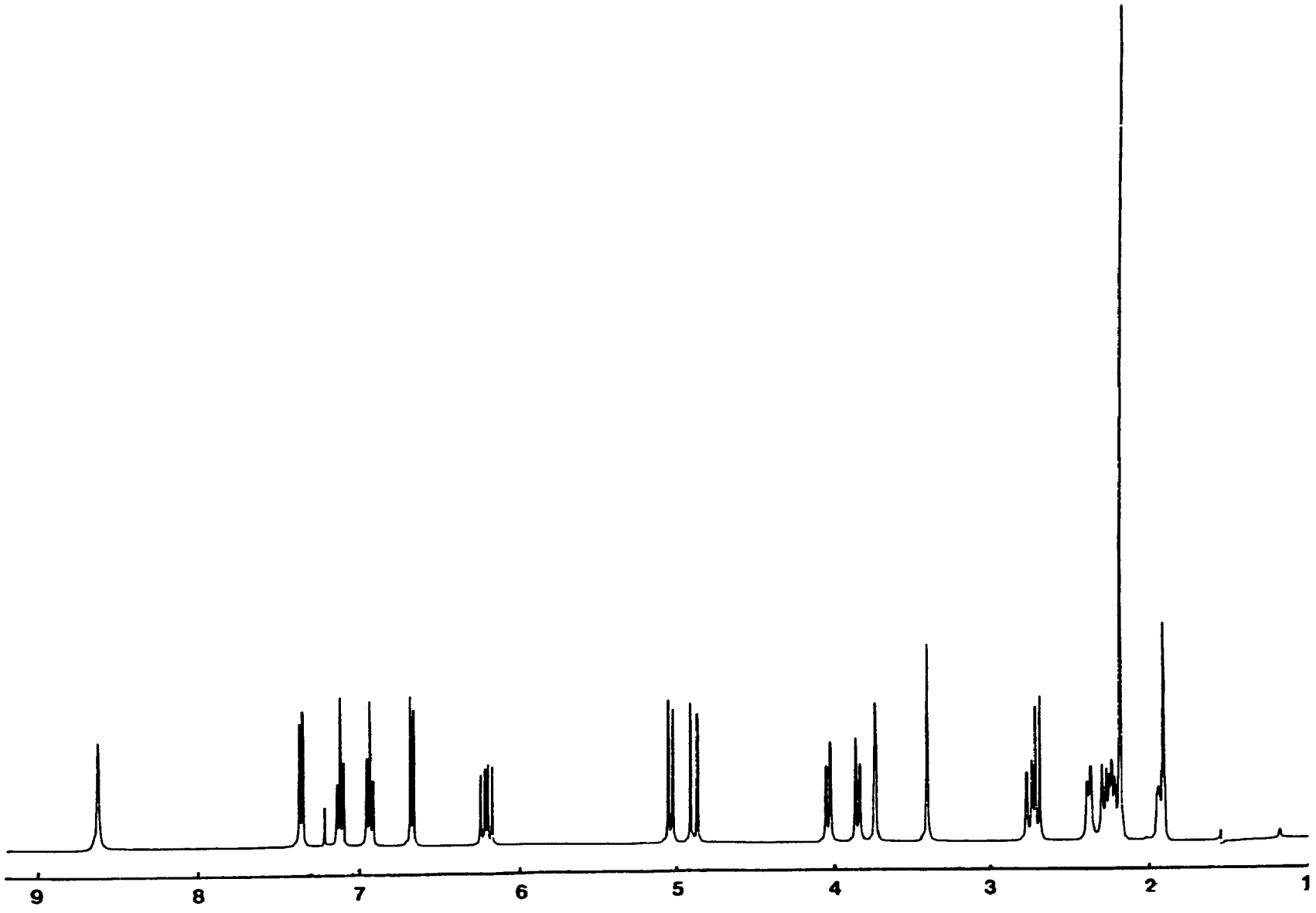

Fig. 5.6. ^1H spectrum of gelsemine at 400 MHz in 0.1 M $CDCl_3$ solution.

Table 5.2 NOE enhancements of gelsemine

{^{1}H}	Enhancement
3	14a, 14e
5	15, 9(s), 12(w), 6/14e*
6	19(s), 3(s), 5(s), 14a(s), 21_{endo}, 17e(w)
14e	14a(s), 3, 17e(w)
14a	14e, 3, 17a(w), 19(w)
16	5(s), 17a, 17e, 15(s)
17a	17e(s), 9, 5, 16
17e	17a(s), 16(w)
19	18c(s), 6(s)
21_{exo}	21_{endo}(s), 19(w)
CH_3	5(s), 6(s), 21en(w), 16(w)

s: strong; w: weak; *: overlapped region

Table 5.3 ^{1}H and ^{13}C chemical shift assignments and R_1 values of gelsemine

$^{1}H^{a}$	ppm	$R_1(s^{-1})$	$^{13}C^{b}$	ppm	$R_1(s^{-1})$
3	3.79	0.69	2	179.6	c
5	3.46	1.45	3	69.3	0.97
6	1.97	1.10	5	71.9	0.97
9	7.39	1.14	6	50.4	0.91
10	6.97	0.70	7	54.3	c
11	7.15	0.70	8	132.1	c
12	6.71	0.62	9	128.0	1.09
14a	2.81	2.68	10	121.5	1.01
14e	2.00	2.60[d]	11	127.8	1.00
15	2.30	1.70[d]	12	108.9	0.95
16	2.44	1.69	13	140.9	c
17a	3.90	2.52	14	22.6	1.89
17e	4.08	2.54	15	35.6	1.00
18c	4.93	1.18	16	38.0	1.10
18t	5.08	1.33	17	61.3	1.67
21_{exo}	2.76	2.41	18	112.1	1.31
21_{endo}	2.34	2.63[d]	19	138.4	0.5
CH_3	2.25	1.88	20	54.0	c
NH	8.67	1.17	21	65.8	1.65
			CH_3	40.4	0.76

[a] Measured at 400 MHz (Bruker WH-400) in 0.1 M $CDCl_3$ solution at ambient temperature. The sample for R_1 determination was degassed by the freeze-pump-thaw method.

[b] Measured at 20.13 MHz (Bruker WP-80SY) in ca. 1 M Cl^- solution at ambient temperature.

[c] Relaxation was too slow for accurate measurement under the experimental conditions.

[d] Uncertain data due to overlap.

b. Molecular Modelling

Molecular mechanics calculations identify the lowest energy structure of gelsemine (Fig. 5.7) with rings A and B co-planar (conjugated π-system), ring C chair, ring D boat, ring E and ring F half chair, back to back. The vinylic side chain is in the pseudo-equatorial position with H-19 towards H-6, consistent with the NOED data. The rigid five membered ring structure predicted by molecular mechanics agrees well with the X-ray structure, except for the conformation of the N-CH_3 group. It has been suggested from the NOESY (73) and NOED data above that the lone pair and the methyl group bonded to the N atom may invert with ease in solution. Molecular mechanics shows almost identical energies (CH_3 axial: 64.91 kcal/mol; eq: 65.04 kcal/mol) for both conformers, which is consistent with the results from NOED experiments, where irradiation of the CH_3 transitions enhanced both axial and equatorial protons (H-6 and H-21exo). Two sets of correlations were carried out, corresponding to the two conformations of the N-CH_3 group (Fig. 5.8).

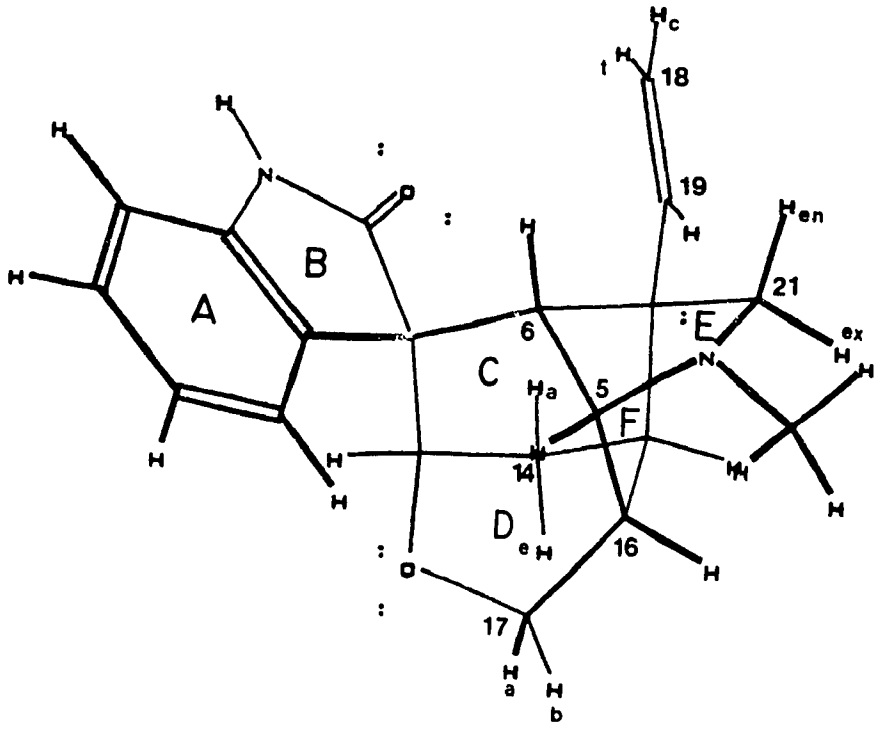

Fig. 5.7. Three-dimensional structure of gelsemine.

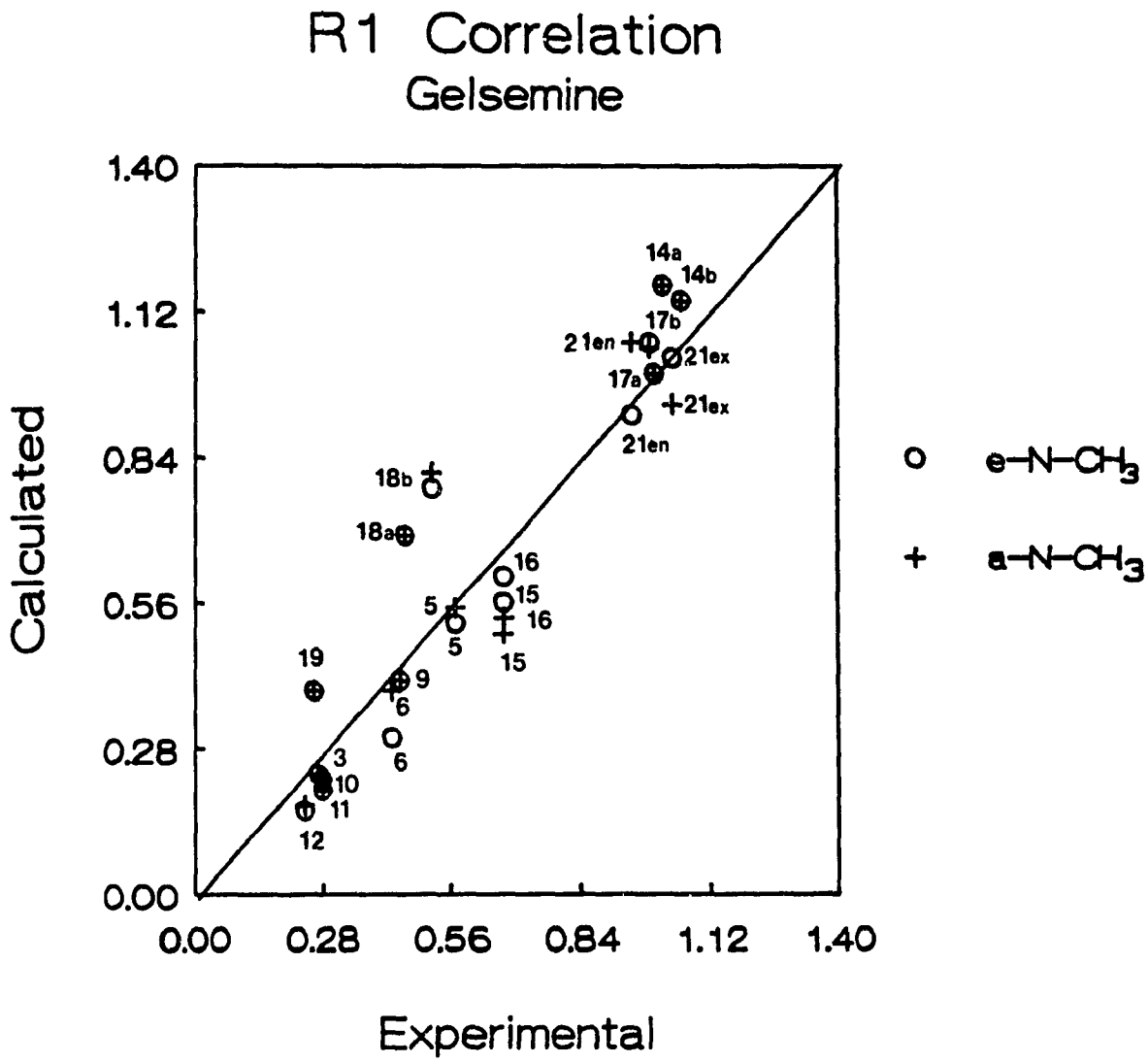

Fig. 5.8. R_1 correlation chart of gelsemine.

The big differences in the two conformers are predicted for H-6, H-21_{endo} and H-21_{exo}. When the methyl group is axial, a good correlation is obtained for H-6 (axial proton), which has 1,3 non-bonded interactions with the axial methyl group, but a poor correlation is obtained for H-21_{endo} and H-21_{exo}. When the methyl group is equatorial, there is a bad correlation for H-6 but good correlations for both H-21_{endo} and H-21_{exo}. The contributions of relaxation pathways predicted by molecular modelling indicate that the relaxation rates of these three protons are partly dependent on the position of the methyl group, e.g. when the CH_3 is equatorial, the relaxation contributions from the CH_3 to H-6, H-21_{endo} and H-21_{exo} are 1.08%, 1.60% and 3.49%, respectively; whereas when the CH_3 is axial, they are 6.68%, 4.45% and 1.10%, respectively. This result is consistent with the NOE evidence that the axial and equatorial inversion of the methyl group occurs on the R_1 time scale, and the experimental R_1 values for these three protons are the weighted average of the contributions of the two conformers.

The effects of side chain rotation, the common intramolecular motion in solution, can be observed from the points for H-18_{cis}, H-18_{trans}, and H-19 - these are isolated from the diagonal. The barriers for C20--C19 bond rotation are calculated to be 5.96 kcal/mol and 13.75 kcal/mol (Fig. 5.9), corresponding with two local minima with H-19 towards either H-6 or H-21_{endo}. (In the preferred conformation, H-19 is towards H-6.) This rotation of the side chain introduces a shorter τ_c term in equation 3.1, which reduces the R_1 values of protons in the side chain (refer to Chapter 3). Since molecular modelling does not take any dynamic procedures into

account, the three protons (H-19, H-18_{cis} and H-18_{trans}) in the vinyl side chain show higher rates from calculation than from experiment, as expected. This is a very good example of using R_1 correlation chart to study the dynamic processes of molecules in solution.

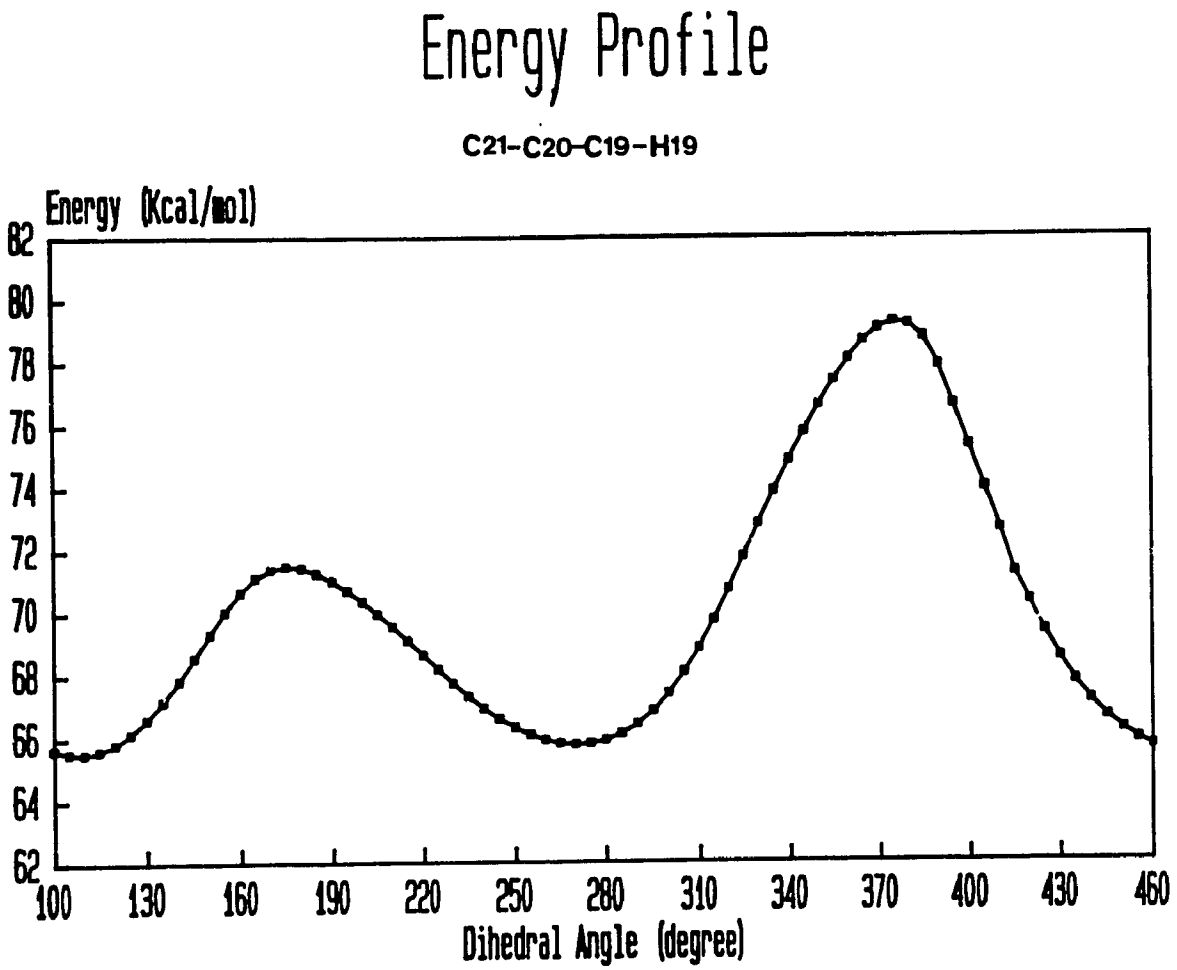

Fig. 5.9. Energy barrier profile of C20-C19 bond rotation.

5.2.3 Brucine

The well-known alkaloid brucine, which is very similar to strychnine, has been investigated extensively (74). The ^{1}H NMR spectrum at 400 MHz was assigned by comparison with the strychnine assignment (75) and by NOED, as well as by several 2D experiments (76). The three-dimensional structure of brucine was also obtained through NOED experiments (76). The fully assigned ^{1}H NMR spectrum has been used in the R_1 correlation study.

^{1}H spin-lattice relaxation rates of brucine (dihydrate form and dried form) were measured at 400 MHz (Bruker WH-400) in 0.1 M $CDCl_3$ solution. The R_1 values in Table 5.4 show that all the methylene protons have the most efficient relaxation rate (1.50 - 3.09 s^{-1}), as expected. However, the protons which are in rigid ring systems show faster relaxation rates than those in relatively flexible rings (assumed from a physical model) e.g., H-15a, H-15b, H-17a, H-17b, H-18a and H-18b present higher R_1 values than H-11a, H-11b, H-23a and H-23b. Methine protons relax at an intermediate rate (about 1.5 s^{-1}) and vinylic protons have R_1 values of about 1 s^{-1} or less. A ^{13}C R_1 determination was carried out at 20 MHz (Bruker WP-80SY).

Molecular mechanics calculations indicate the lowest energy structure (Fig. 5.10), with ring D chair, ring E boat, ring F chair-like with the oxygen atom pointing up; and ring C boat-like with N-9, C-10, C-11, C-12 approximately co-planar (dihedral angle: 5^0). Molecular mechanics calculations showed excellent consistency with the NOE studies from Bernstein and Hall (76), and supported the

conclusion of these authors that the three-dimensional structures existing in solution and the crystalline state are identical. R_1 correlations were used to detect molecular flexibility and intramolecular motion in solution. The R_1 values of brucine from molecular modelling and experiment showed a generally good correlation (Fig. 5.11). However, there are some points which are some distance from the diagonal to be interpreted. The R_1 values of protons which are near to N-19, such as H-18a, H-18b, and H-20b, may be affected by the coordination of water molecules on N-19, and the dipole-dipole interactions through space between the coordinated water molecules and protons on C-17 and on C-15 may affect R_1 values of these protons. Hence their experimental R_1 values are not correctly predicted. The R_1 values of H-23a and H-23b may be influenced indirectly by the adjacent oxygen, which may also coordinate with water molecules. When the sample has some water coordinated, the experimental relaxation rates of H-15a, H-15b, H-23a and H-23b were different from those of the anhydrous sample (Table 5.4). In Table 5.4, normalization (with respect to H-11b) was performed so that the differences of relative R_1 values of hydrated and dehydrated samples can be compared.

Table 5.4 ^{1}H and ^{13}C R_1 values of brucine

H	$R_1(s^{-1})^a$	$R_1(s^{-1})^b$	C	$R_1(s^{-1})^c$
1	1.03 (0.57)[e]	1.03 (0.59)	1	1.70
4	0.58[d](0.32)	0.40 (0.23)	4	1.79
8	1.13 (0.62)	1.23 (0.71)	8	1.51
11a	1.89 (1.04)	1.69 (0.97)	11	2.56[e]
11b	1.81 (1.00)	1.74[d](1.00)	12	1.14
12	1.50[d](0.83)	1.47 (0.84)	13	1.54
13	1.44 (0.80)	1.36 (0.78)	14	1.37
14	1.59 (0.88)	1.39[d](0.80)	15	2.49[d]
15a	3.03[d](1.67)	3.33 (1.91)	16	1.55[d]
15b	3.09(1.71)	3.33 (1.91)	17	2.56[e]
17a,b	2.58[d](1.43)	2.59 (1.49)	18	2.79[d]
18a	2.32[d](1.28)	2.34 (1.34)	20	2.56
18b	2.90[d](1.60)	3.03[d](1.74)	22	1.27[d]
20a	2.35 (1.30)	2.48 (1.43)	23	2.18[d]
20b	2.43 (1.34)	2.36 (1.36)	2-OCH_3	0.84
22	0.77[d](0.43)	0.78 (0.45)	3-OCH_3	0.73
23a	1.93 (1.07)	2.68 (1.54)		
23b	1.50 (0.83)	1.91 (1.10)		
2-OCH_3	1.01 (0.56)	1.03 (0.59)		
3-OCH_3	1.17 (0.65)	1.19 (0.68)		

[a] Measured at 400 MHz in 0.1M $CDCl_3$ solution. Sample was treated by molecular sieves to remove water.

[b] Same as above but without removing water.

[c] Measured at 20 MHz in ca. 0.5M $CDCl_3$ solution.

[d] Measured by null point method (39).

[e] Shifts are overlapped.

* Normalized values are in parentheses.

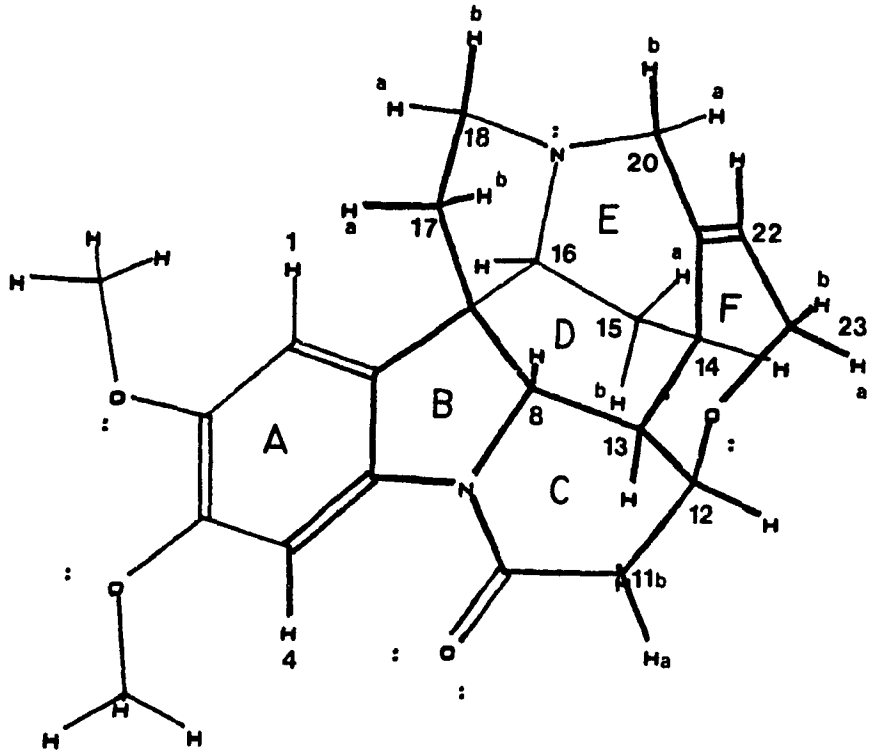

Fig. 5.10. Three-dimensional structure of brucine.

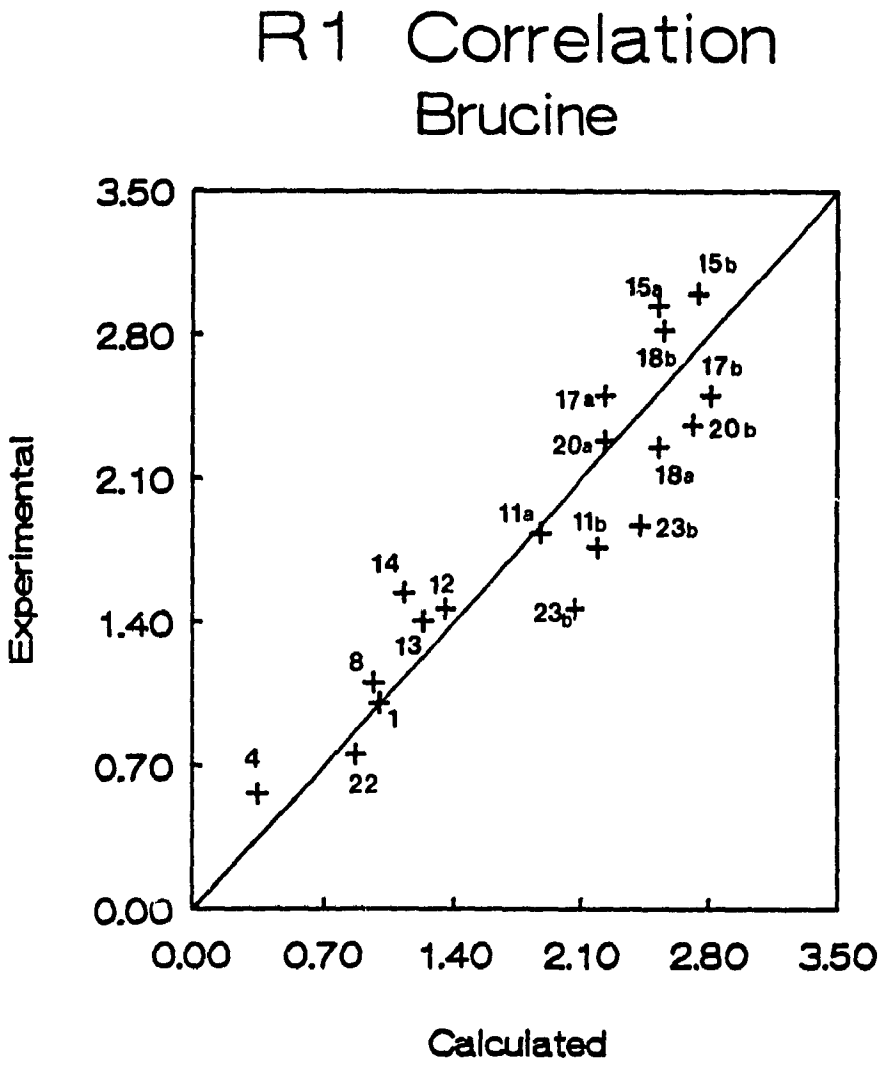

Fig. 5.11. R_1 correlation chart of brucine.

5.2.4 Methyl-O-methylpodocarpate

The complete 400 MHz ^1H spectrum (0.1 M in $CDCl_3$) of the diterpene derivative methyl O-methylpodocarpate has been assigned by NOED and 2D HETCOR techniques (see Chapter 4). ^1H spin-lattice relaxation rates were measured when the signals were reasonably free of overlap (Table 5.5). They reflect the number and distance of near proton neighbours, and range from those of the slowly relaxing aromatic protons (0.33 - 0.73 s^{-1}), which have inefficient relaxation pathways, to those of the geminal methylene protons (1.27 - 1.39 s^{-1}). The single aliphatic methine proton, H-5, has an intermediate R_1 value, 0.77 s^{-1}. The C-methyl and O-methyl groups are readily distinguishable through their relaxation rates, the O-methyl groups having low relaxation rates (0.54 - 0.59 s^{-1}) compared to the C-methyl groups (1.25 - 1.48 s^{-1}). Since methyl protons relax mainly to each other by the dipole-dipole mechanism, rather than to protons outside the group, this difference must result from differences in the rates of methyl group rotation, the C-methyl groups being more hindered. The significant difference between the relaxation rates of methyl-18 (1.48 s^{-1}) and methyl-20 (1.25 s^{-1}) must result from greater steric hindrance to rotation of methyl-18.

Methyl O-methylpodocarpate has an AB-trans ring junction. Molecular mechanics calculations established the lowest energy geometry of the molecule (Fig. 5.12), with rings A and B in chair and twisted chair conformations, respectively. At C-4, the methyl group is equatorial, and the ester function axial.

Table 5.5 ^1H chemical shifts and R_1 values of MMP

H	Chemical shift (ppm[a])	R_1[b](s^{-1})
1a	1.37	1.38
1e	2.24	
2a	1.61[c]	1.27[d]
2e	1.99[c]	
3a	1.07	1.74
3e	2.25	
5	1.51	0.77[e]
6a	1.98	
6e	2.15	
7a	2.72	1.39
7e	2.83	1.37
11	6.79	0.72
13	6.65	0.33
14	6.95	0.43
Me-18	1.26	1.48
Me-20	1.02	1.25
OMe-21	3.64	0.54
OMe-22	3.75	0.59

[a] Measured in 0.1 M $CDCl_3$ solution at ambient temperature at 400 MHz.

[b] Measured by non-linear regression unless otherwise noted.

[c] Uncertain assignment.

[d] May be due to H-2e because of uncertain assignment.

[e] Measured by null point method (39).

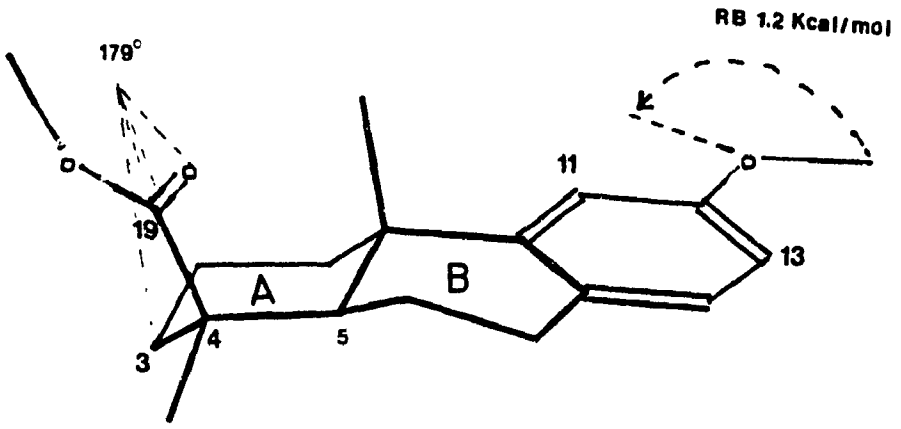

Fig. 5.12. Three-dimensional structure of MMP.

Calculation of a rotational energy profile (Fig. 5.13) for the C4-C19 bond revealed two maxima, with a lower rotational barrier of 5.1 kcal/mol. In the preferred conformation, the carbonyl oxygen atom faces away from C-3, with a C3-C4-C19-O22 dihedral angle of 179°. The ester methoxyl group is predicted to be

twisted away from any ring protons, consistent with the NOE data.

The aryl methoxyl group may adopt two low energy conformations, with the methyl group approximately co-planar with the aromatic ring and facing either H-11 or H-13. Molecular mechanics calculations indicated no significant preference for either conformation (Fig. 5.14), consistent with NOE data, which showed similar enhancements of H-11 and H-13 when the methoxyl transition were irradiated. The low calculated rotational barrier of 1.2 kcal/mol indicates that this methoxyl group rotates freely.

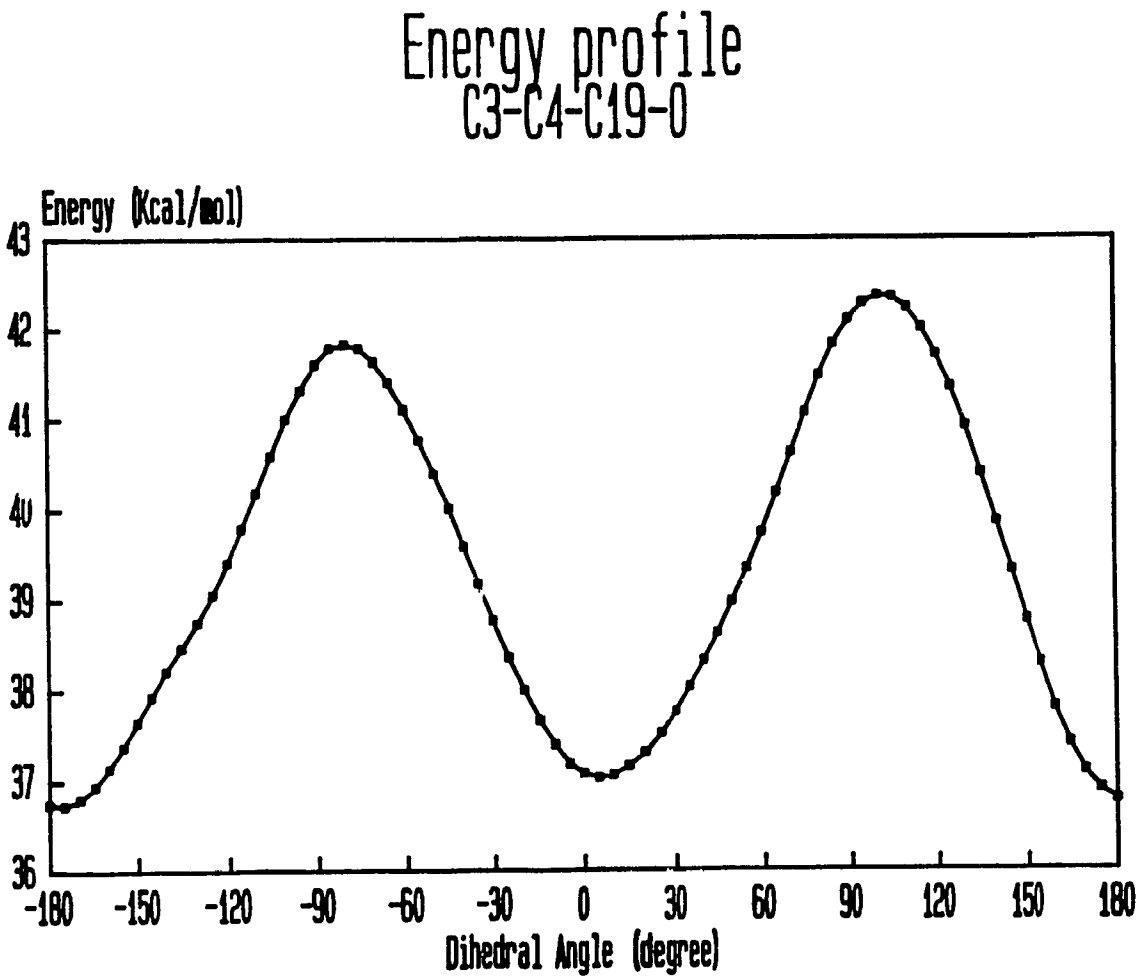

Fig. 5.13. Energy barrier profile for C4-C9 bond rotation.

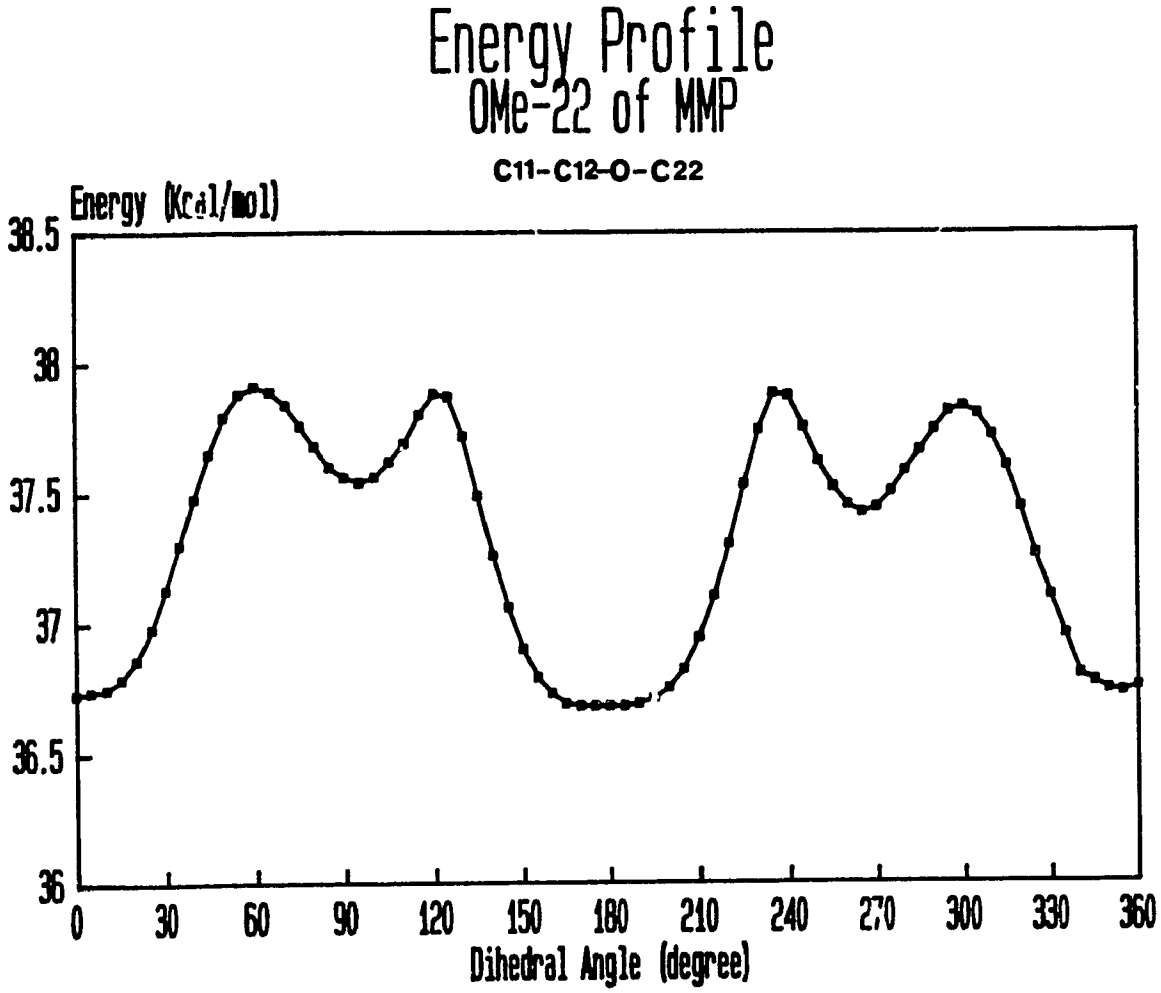

Fig. 5.14. Energy barrier profile for C12-O bond rotation.

Correlation of relative relaxation rates, calculated from inter-proton distances derived from the molecular mechanics computations, with normalized (with respect to H-7e) experimental R_1 values showed general consistency (Fig. 5.15). Two sets of correlations were carried out, corresponding to the two conformations of the aryl methoxyl group. As expected, when the methoxyl group faces H-11, the computed relaxation rate of H-13 is too low; when it faces H-13, the computed relaxation rate of H-11 is too low, compared with the experimental values. Thus, the model is consistent with the experimental R_1 and NOE data, which predict rapid interchange between two almost equally populated conformations.

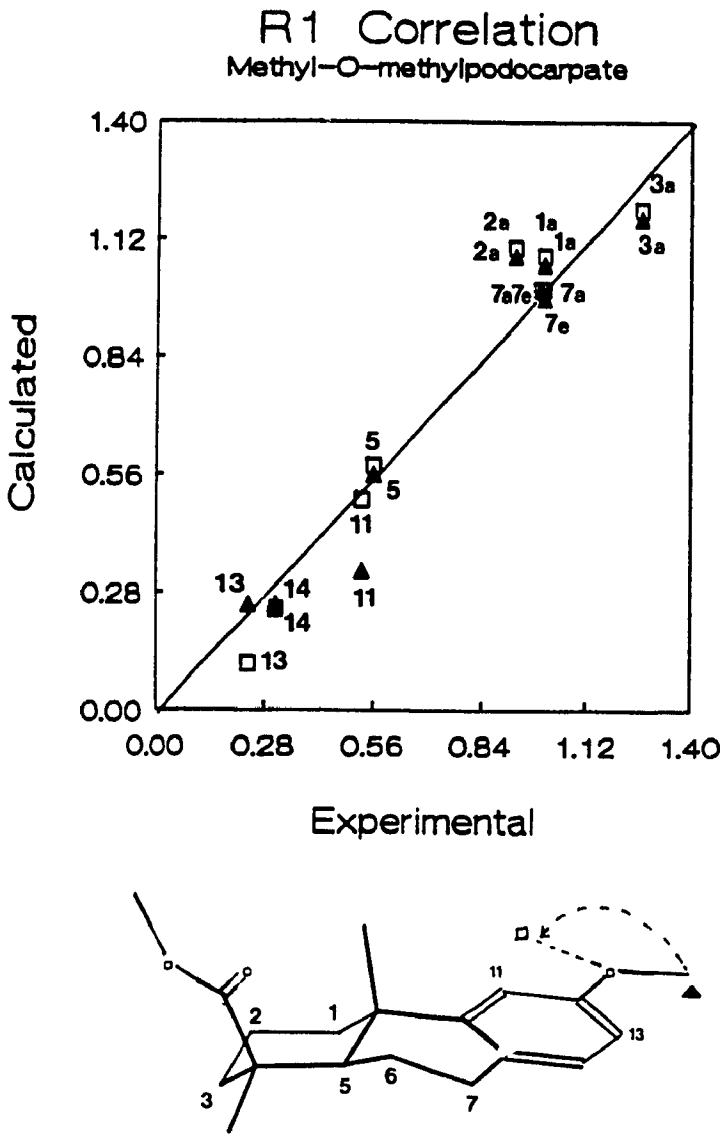

Fig. 5.15. R_1 correlation of MMP.

5.2.5 Nefopam

Racemic nefopam hydrochloride [(±)-3,4,5,6-tetrahydro-5-methyl-1H-2,5-benzoxazocine hydrochloride (±)-1] is an established, potent analgesic antiinflammatory drug.

The stereochemistry of nefopam.HCl in the solid state and in solution has been studied using single crystal X-ray diffraction and NMR spectroscopy (77, 78). The NMR data have revealed the presence of two distinct, major and minor N-protonated species in CD_2Cl_2 solution differing in the stereochemistry of the N-methyl group as follows:

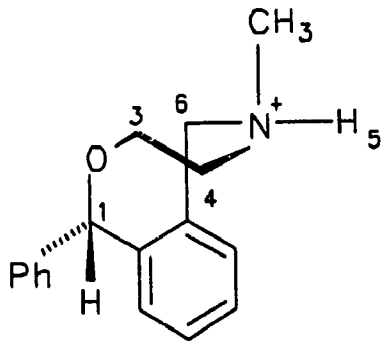

Major

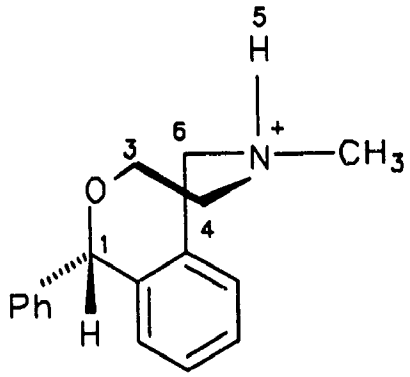

Minor

The eight-membered ring has a modified boat-chair conformation with the 1-phenyl ring equatorial and the N-methyl group either axial (major) or equatorial (minor). These two species in the NMR spectrum have been assigned previously at 200 MHz in the ratio of ca. 3:2. In this study, the ^1H spectrum (Fig. 5.16) was carried out at 400 MHz (Bruker WH-400) and the ^1H spin-lattice relaxation rates in CD_2Cl_2 solution at ambient temperature were determined. The results are shown in Table 5.6. and Table 5.7.

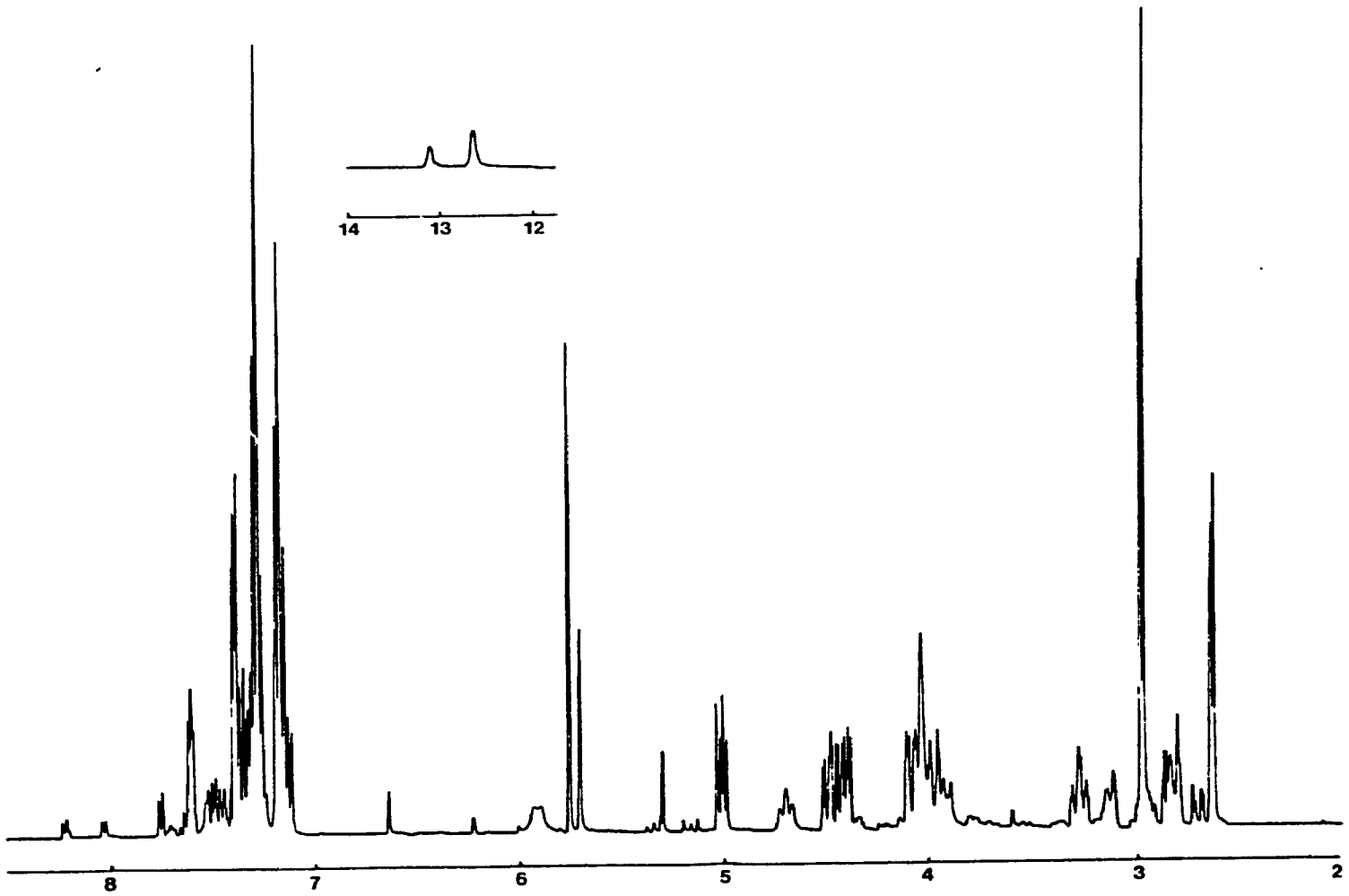

Fig. 5.16. ^1H spectrum of nefopam at 400 MHz in a CD_2CL_2 solution.

Table 5.6 Aliphatic ^1H chemical shifts of nefopam major and minor species (14)

^1H	Major	Minor
1	5.78	5.73
5	13.08	13.55
3a	4.49	4.73
3e	4.10	3.98
4a	3.29	2.96
4e	2.81	3.13
6a	5.00	5.92
6e	4.41	3.91
CH_3	2.97	2.64

Table 5.7 Experimental[a] and computed[b] R_1 values of aliphatic protons of nefopam

	Major(s^{-1})				Minor(s^{-1})			
^1H	Exp.	Nor.	Cal.	Nor.	Exp.	Nor.	Cal.	Nor.
1	0.46	0.43	0.31	0.45	0.53	0.51	0.30	0.45
5	1.23	1.14	0.51	0.74	1.54	1.50	0.50	0.75
3a	1.04	0.96	0.62	0.90	1.30	1.26	0.62	0.93
3e	1.08	1.00	0.69	1.00	1.03	1.00	0.67	1.00
4a	1.31	1.21	0.74	1.07	1.20	1.17	0.67	1.00
4e	1.36	1.26	0.79	1.14	1.47	1.43	0.76	1.13
6a	1.20	1.11	0.78	1.13	1.19	1.16	0.83	1.24
6e	1.10	1.02	0.81	1.17	1.28	1.24	0.82	1.22
CH_3	1.04	0.96			1.31	1.27		

[a] Measured at 400 MHz in CD_2Cl_2 solution (Bruker WH-400).

[b] Carried out on an Olivetti M24 PC.

Molecular mechanics shows that both major and minor species have identical energy (37.57 kcal/mol). The small difference of populations between major and minor species (3:2) in NMR measurement may be arised from solvent effect. The methyl rotational barriers of the two species are very similar (major: 1.08 kcal/mol; minor: 1.15 kcal/mol), indicating that steric factors in the eight-membered ring for both species are similar. The calculated ^1H R_1 values (Table 5.7. normalized to H-3e, equatorial) for both species are almost identical except for H-6a (pseudo axial) and H-6e (pseudo equatorial). These two protons show higher R_1 values in the minor than in the major species. The dynamic range of R_1 values from modelling is much smaller than that from experiment. The R_1 correlations of the major and minor species (Fig. 5.17) demonstrate that the worst correlation is for H-5, the most labile proton. It is not only the interconversion with the methyl group on nitrogen, but exchange from the solvent, that causes the experimental R_1 value of H-5 to be much higher than predicted (since the exchange will accelerate relaxation). Exchange of H-5 also affects the relaxation of H-3a, H-4a, H-4e and H-6e. Therefore, it is not surprising that the correlation points of these protons do not lie on the diagonal. Although the exchange and interconversion of the molecule are slow on the chemical shift time scale (we can "see" two species from the ^1H spectrum), they are fast on the R_1 time scale. Hence, any R_1 value determined from experiment should be considered as the weighted average rate from the two species.

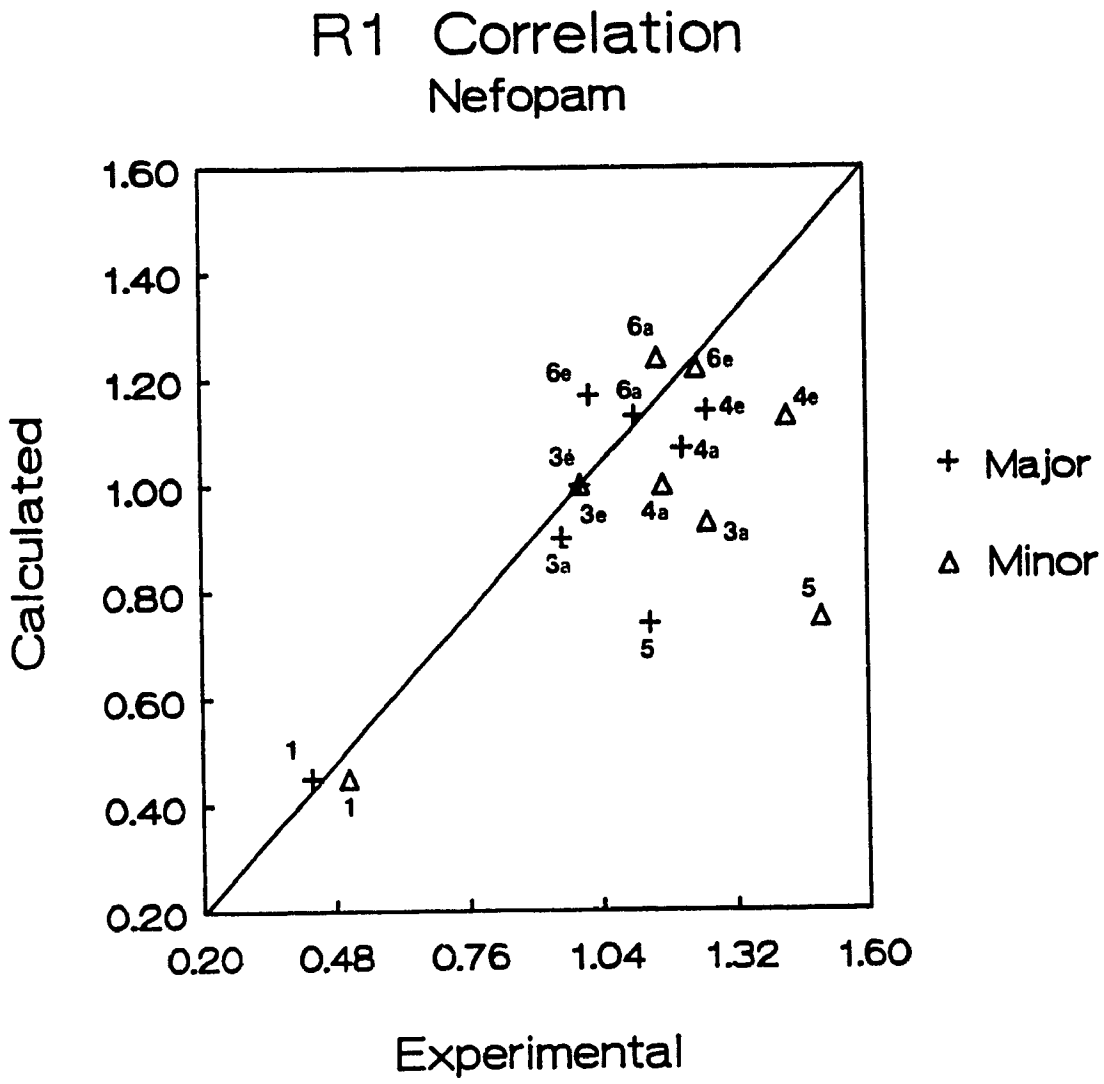

Fig. 5.17. R_1 correlation of nefopam.

5.3 Conclusions

For molecules undergoing exchange or dynamic motion in solution, R_1 correlation is a useful tool to evaluate the flexibility of the molecule and to identify the locations of the atoms affected by these motions. As shown in this Chapter, the most rigid molecule, gibberellic acid, shows the best correlation, whereas the worst correlation is found for nefopam, the most flexible compound. For relatively rigid molecules which have some internal motion (e.g. single bond rotation), the R_1 correlation method indicates the location of the local motion. Usually, an exchanging proton will show a higher experimental than calculated R_1 value, as can be seen for H-5 of nefopam. On the other hand, protons undergoing single bond rotation will have lower experimental than calculated R_1 values, as in gelsemine. However, there are still some things unclear, e.g. it is expected that correlation points of H-11 and H-13 of methyl-O-methylpodocarpate stay in both sites of the diagonal, due to the rotation of OMe-22, but the points in the correlation chart (Fig. 5.15) presented systematically lower positions than expected. We note here that the R_1 correlation method for probing internal dynamics is so far not very precise, since limitations in the modelling process, the flexibility of the molecule, and many external influences such as exchange with the solution will alter the R_1 determination. Even the very rigid compound, gibberellic acid, does not show perfect correlation.

R_1 correlation can also be applied as a powerful method to check the reliability of chemical shift assignments and molecular modelling. If the assignment of a proton is not correct, the correlation chart will contain unreasonable points which are far from the diagonal, as in the gelsemine study.

Chapter 6

EXPERIMENTAL

6.1 Materials

The compounds used for the studies described in this thesis were obtained from Aldrich and Sigma Chemical Companies or as gifts from collaborators. Deuterated solvents were purchased from MSD Isotopes.

6.2 NMR measurements

^{1}H NMR spectra were determined (0.1 M in $CDCl_3$, CD_2Cl_2, C_6D_6 or DMSO-D_6 solutions) at 400 MHz using a Bruker WH-400 spectrometer located at the Montreal Regional High Field NMR Laboratory. ^{13}C spectra were determined at 20.1 MHz (1 M in $CDCl_3$ or DMSO-d_6 solutions) using a Bruker WP-80SY spectrometer fitted with a 10 mm broadband probe. ^{1}H-R_1 values and ^{1}H NOED spectra were usually measured on degassed samples, using the freeze-pump-thaw method, since paramagnetic contributions from dissolved oxygen influence the overall relaxation rates. Samples for ^{13}C measurements were not degassed. The DEPT spectral editing sequence (34) and 1D-CHORTLE (53) experiments were used as an aid to ^{13}C spectral assignments.

6.2.1 ^{1}H and ^{13}C Spin-lattice relaxation Rates

R_1 values were measured using the standard inversion-recovery two pulse sequence (79), followed by non-linear regression analysis (performed on an Olivetti M24 microcomputer) of data down-loaded from the Bruker Aspect 2000 spectrometer computer. Data analysis was confined to the initial slope region (5), defined by a single exponential. In a typical ^{1}H-R_1 experiment, 8 or 16 scans from a sample were acquired into 16k data blocks. For ^{13}C relaxation measurements, 200 scans were aquired. A pre-equilibration period of 5 * T_1 of the slowest relaxing nuclei in the molecule was allowed before the acquisition of each scan. A minimum of fifteen experiments with different delays were carried out to ensure that enough points below the null-point could be obtained. Typical regression errors are ± 0.01 s^{-1}.

Normalization was performed for the internal comparison of methyl ^{1}H relaxation rates (Chapter 3) and R_1 correlation charts (Chapter 5). This procedure accounts for changes in operating conditions, and differences in tumbling rates caused by the differences of molecular size and shape.

6.2.2 ^{1}H and ^{13}C NOE experiments

^{1}H NOED experiments used the technique involving multiple irradiation of the components of multiplets (61). The saturation period for each proton resonance was set to 1-5 times its T_1 value. A control spectrum was acquired by setting the irradiation frequency far from all resonances in the spectrum. The decoupler power was usually adjusted to 41 L - 45 L, depending on the intensity and resolution of

the resonance to be irradiated. The entire process was supercycled until sufficient S/N had been reached. Generally, it requires 80 - 200 scans for each experiment. The difference spectra were obtained by subtracting the control FID from the FID containing NOE information.

^{13}C-{^{1}H} NOE enhancements were measured by the standard gated decoupling method (80) with some refinements (3). A relaxation delay of 5 * T_1 of the slowest relaxing carbon period was applied before any new scans. The NOE and control spectra were alternately acquired until S/N ratio was satisfactory (usually 200 - 400 scans).

6.2.3 2D NMR experiments

2D ^{1}H-^{1}H COSY and ^{13}C-^{1}H HETCOR spectra were carried out at 9.4 Tesla on a Varian VXR400S spectrometer or a Bruker WH-400 spectrometer. The COSY spectrum of compound **32** was processed using a 512 * 1024 data matrix, with 6.25 Hz digital resolution in the f_1 and f_2 domains, sine bell weighting, and averaging of 16 FIDs. The ^{13}C-^{1}H HETCOR data set for **32** was processed using a 512 * 1024 matrix, with digital resolution in the ^{13}C and ^{1}H domains of 8.9 and 13.4 Hz, respectively, with sine bell weighting and averaging of 320 FIDs per increment.

6.3 Molecular mechanics calculations

Molecular mechanics calculations were carried out with an Olivetti M24 microcomputer (with 640k memory, co-processor, hard disk and Microsoft mouse) and on a Personal IRIS 4D/25G workstation (Silicon Graphics, Inc.), using the

programs MMX and PCMODEL (Serena Software, Bloomington, Indiana, U.S.A.). MMX, a batch program lacking graphics output, is an implementation of the Allinger MMP2 algorithm (19). It includes π-calculations and the dihedral driver option. The earlier version of PCMODEL has graphics output but does not include π-calculations and dihedral driver (with optimization). The structures of compounds were initially input by mouse and optimized using PCMODEL, followed by π-calculation and dihedral driver calculation using MMX. A recent version of PCMODEL, 3.0 (PC and IRIS versions), allows π-calculations and dihedral driver optimization to be performed, making calculations more convenient. Rotational energy profiles and barriers were calculated using the dihedral driver with 360^0 rotation in 5^0 steps.

Relative spin-lattice relaxation rates were calculated on a micro-computer from the proton co-ordinates obtained from PCMODEL or MMX for the minimum energy structures. The software for this calculation was written by L. D. Colebrook in this laboratory using TURBO-PASCAL. The inter-proton distances from molecular mechanics calculations are recognized by the software, and the relative R_1 values are calculated according to equation [3.1]. In addition, relaxation pathways are evaluated in this program. The centroid approximation (81-83) was used for the relaxation contributions of methyl groups. Calculated relative relaxation rates were normalized to the experimental R_1 value of a suitable fast relaxing proton (7)

Chapter 7

SUMMARY

Molecular mechanics calculations, including energy minimization and the dihedral driver procedure, predict the lowest energy conformation of a molecule and useful structural parameters, such as bond lengths, bond angles, dihedral angles with J-coupling constants, intra-molecular hydrogen bonds, etc. This information greatly helps prediction of molecular structures and experimental data analysis.

A combination of spin-lattice relaxation, nuclear Overhauser enhancement and molecular mechanics calculations has been demonstrated to be a powerful tool for the determination of structure and stereochemistry of organic molecules. Unlike the individual experimental methods, or purely theoretical calculations, this combined technique can be used as a two-way method for evaluating the accuracy of force field calculations and interpreting NMR spectroscopy. For example, methyl group rotation in solution has been investigated through both ^{1}H and ^{13}C spin-lattice relaxation rates and molecular mechanics. A general consistency between experimental data and calculation has been observed for most molecules studied in this thesis, when the modelling was valid. Situations in which the modelling was invalid because of its limitations when solvation or molecular association is present have been evaluated.

Intra-molecular motions or local conformational exchanges have been evaluated from correlation of computed and experimental R_1 data. A relationship between molecular mobility and the quality of the correlations of ^{1}H-R_1 values has

been qualitatively established.

The limitations of the MM2 and MMX force field have been discussed in this thesis. The computed models for strained molecules containing four-membered rings have failed to correlate with the experimental data, indicating an inadequate force field for this system. This inadequacy of MM2 has been noted by Allinger and addressed in the development of the MM3 force field.

It is shown that ^1H chemical shift assignments of molecules may be checked by correlation of computed and experimental R_1 data.

Further research is suggested using the MM2 and MMX or MM3 force fields (when MM3 becomes available for Silicon Graphics computers) and spin-lattice relaxation measurements to investigate structural problems and dynamic motions of larger molecules, such as peptides and small proteins. In addition, molecular orbital calculations are also suggested, in comparison with molecular mechanics calculations, for the same kinds of molecules.

REFERENCES

1. I. Solomon, Phys. Rev., **99**, 559 (1955)

2. N. Bloembergen, E. M. Purcell, and R. V. Pound, Nature, **160**, 475 (1947)

3. W. J. Chazin, Ph. D. thesis, Concordia University (1983)

4. R. L. Vold, J. S. Waugh, M. P. Klein, and D. E. Phelps, J. Chem. Phys., **48**, 3831 (1968)

5. R. Freeman, S. Wittekoek, and R. R. Ernst, J. Chem. Phys., **52**, 1529 (1970)

6. L. D. Hall, Chem. Soc. Rev., **4**, 401 (1975)

7. L. D. Colebrook and L. D. Hall, Org. Magn. Reson., **21**, 532 (1983)

8. W. Chazin and L. D. Colebrook, Magn. Reson. Chem., **23**, 597 (1985)

9. J. W. ApSimon, H. Beierbeck, and J. K. Saunders, Can. J. Chem., **53**, 338 (1975)

10. J. W. Blount and J. B. Slothers, J. Mag. Reson., **27**, 515 (1977)

11. J. Bastard, J. M. Bernassau, Do Khac Dui, M. Fetizon and E. Lesueur, J. Phys. Chem., **90**, 3936 (1986)

12. J. I. Kaplan and G. Fraenkel, NMR of Chemical Exchanging Systems, Academic Press, New York (1980)

13. D. E. Woessner, B. S. Snowden Jr, and G. H. Meyer, J. Chem. Phys., **50**, 719 (1969)

14. D. E. Woessner and B. S. Snowden Jr., Adv. Mol. Relaxation Processes, **3**, 181 (1972)

15. C. Deverell, R. E. Morgan and J. H. Strange, Mol. Phys., **18**, 553 (1970)

16. J. D. Cutnell and J. A. Glasel, J. Am. Chem. Soc., **98**, 264 (1976)

17. L. Werbelow, J. Magn. Reson., **34**, 439 (1979)

18. E. Hashinger and R. M. Lynden-Bell, J. Magn. Reson., **31**, 33 (1978)

19. U. Burkert and N. L. Allinger, Molecular mechanics, ACS Monograph, 177 (1982)

20. D. H. Andrews, Phys. Rev., **36**, 544 (1930)

21. T. L. Hill, J. Chem. Phys., **36**, 544 (1946)

22. I. Dostrovsky, E.D. Hughes, and C.K. Ingold, J. Chem. Soc., **173** (1946)

23. P. de la Mare, L. Fowden, E. D. Hughes, C. K. Ingold, and J. Mackie, J. Chem. Soc., 3200 (1955)

24. F. H. Westheimer, Steric Effects in Organic Chemistry, Ed. by M. S. Newman, John Wiley & Sons, New York (1956); F. H. Westheimer and J. E. Mayer, J. Chem. Phys., **14**, 733 (1946)

25. N. L. Allinger and J. T. Sprague, J. Am. Chem. Soc., **95**, 3893 (1973)

26. E. M. Engler, J. D. Andose, and P. V. R. Schleyer, J. Am. Chem. Soc., **95**, 8005 (1973)

27. N. L. Allinger, J. Am. Chem. Soc., **99**, 8127 (1977)

28. N. L. Allinger, Adv. Phys. Org. Chem., **13**, 1 (1976)

29. T. Clark, A Handbook of Computational Chemistry, John Wiley & Sons (1985)

30. J. Kao and N. L. Allinger, J. Am. Chem. Soc., **99**, 975 (1977)

31. N. L. Allinger, H. Y. Young and Jenn-Hui Lii, J. Am. Chem. Soc., **111**, 8551 (1989)

32. Jenn-Hui Lii and N. L. Allinger, J. Am. Chem. Soc.,**111**, 8566 (1989)

33. Jenn-Hui Lii and N. L. Allinger, J. Am. Chem. Soc., **111**, 8576 (1989)

34. J. K. M. Sanders and B. Hunter, Modern NMR Spectroscopy, A Guide for Chemists, Oxford University Press, Oxford (1987)

35. R. Freeman, A Handbook of Nuclear Magnetic Resonance, Longmans (1987)

36. J. W.Akett, NMR and Chemistry, An Introduction to the Fourier Transform-multinuclear Era 2nd Ed. Chapman and Hall (1983)

37. D. Neuman and M. P. Williamson, The Nuclear Overhauser Effect in Structural and Conformational Analysis, VCH, New York (1989)

38. T. K. Leipert, D. W. Marquardt, J. Magn. Reson., **24**, 181 (1976)

39. R. Freeman and M. L. Levitt, J. Magn. Reson., **33**, 473, (1979)

40. M. S. Caceci and W. P. Cacheris, BYTE, **9**, 340 (1984)

41. E. Breitmaier and W. Voelter, C-13 NMR Spectroscopy, High Resolution Methods and Applications in Organic Chemistry and Biochemistry, 3rd Edition, VCH, New York, 327-337 (1986)

42. A. W. Overhauser, Phys. Rev., **92**, 411, 1955

43. G. D. Fasman (Ed.), Prediction of Protein Structure and the Principle of Protein Conformation, Plenum Press, New York (1989)

44. **ibid.** p317.

45. J. B. Lambert, R. J. Nienhaus, and J. W. Keepers, Angew. Chem., Int. Ed. Engl., **20**, 487 (1981)

46. R. Rowan, P. Mazzocchi, C. Kanagy, and M. Regan, J. Magn. Reson., **39**, 27 (1980)

47. R. K. Harris, Nuclear Magnetic Resonance Spectroscopy. A Physicochemical View. Pitman Publishing Inc., Marshfield, 89-90 (1983)

48. J. I. Seenman, H. V. Secor, P. J. Breen, V. H. Grassian, and E. R. Bernstein, J. Am. Chem. Soc., **111**, 3140 (1989)

49. M. L. Martin, G. J. Martin, and J. J. Delpuech, Practical NMR Spectroscopy, Heyden, London, 169-170 (1980)

50. J. K. M. Sanders and J. Mersh, Prog. n.m.r. spectrosc., **15**, 353 (1982)

51. L. D. Hall and J. K. M. Sanders, J. Am. Chem. Soc., **102**, 5703 (1980)

52. O. Yamamoto, K. Hayamizu, K. Sekine, and S. Funahira, Analyt. Chem., **44**, 1796 (1972); N. K. Wilson and J. B. Stothers, J. Magn. Reson., **15**, 31 (1974)

53. G. A. Pearson, J. Magn. Reson., **64**, 487 (1985)

54. T. Nishida, I. Wahlberg and C. R. Enzell, Org. Magn. Reson., **9**, 203 (1977)

55. Q. Ning and L. D. Colebrook, to be published

56. A. Allerhand, D. Doddrell, and R. Komoroski, J. Chem. Phys., **55**, 189 (1971)

57. W. Offermann, Org. Magn. Reson., **20**, 203 (1982)

58. Q. Ning and L. D. Colebrook, Can. J. Chem., **67**, 1560 (1989)

59. W. J. Chazin, L. D. Colebrook, B. R. Davis, I. R. N. McCormick, and J. Johnson, Can. J. Chem., **63**, 2332 (1985)

60. W. J. Chazin and L. D. Colebrook, J. Org. Chem., **51**, 1243 (1984)

61. M. Kinns and J. K. M. Sanders, J. Magn. Reson., **56**, 518 (1984)

62. M. Karplus, J. Chem. Phys., **30**, 11 (1959); J. Am. Chem. Soc., **85**, 2870 (1963)

63. M. Coxon, G. J. Hydes, and P. J. Steel, J. Chem. Soc., Perkin Trans II, 1351 (1984)

64. H. Beierbeck, J. W. Easton, and J. K. Saunders, Can. J. Chem., **60**, 1173 (1982)

65. E. Wenkert, B. L. Buckwalter, I. R. Burfitt, M. J. Gasic, H. E. Gottlieb, E. W. Hagaman, F. M. Schell, P. M. Wovkulich and A. Zheleva, Topics in Carbon-13 NMR Spectroscopy. ed. by G. C. Levy, **1**, 87-105, Wiley-Interscience, New York (1976)

66. Q. Ning and L. D. Colebrook, and F. Commodari, Magn. Reson. Chem., (1991) in press.

67. B. Lindman, Dynamic NMR Spectroscopy, Academic Press, New York (1982)

68. A. Crozier, The Biochemistry and Physiology of Giberellins, Praeger Publisher, New York (1983)

69. A. Preiss and G. Adam, Magn. Reson. Chem. **25**, 239 (1987)

70. M. Bernstein, personal communication.

71. W. H. Orgell, *Lloydia*, **26**, 36 (1963)

72. E. Wenkert, C. J. Chang, A. O. Clouse, and D. W. Cochran, Chem. Commun., **961**, (1970)

73. Y. Schun and G. A. Cordell, J. Nat. Prod., **48**, 969 (1985)

74. Ref. 3

75. W. J. Chazin, J. T. Edward, and L. D. Colebrook, Can. J. Chem., **61**, 1749 (1983)

76. M. Bernstein and L.D. Hall, Can. J. Chem., **63**, 483 (1985).

77. L. K. Hansen, A. Hordvik, and A. J. Aasen, Acta Chem. Scand., **38**, 327 (1984)

78. R. Glaser, S. Cohen, D. Donnel, and I. Agranat, J. Pharm. Sci., **75**, 772 (1986)

79. R. L. Vold, J. S. Waugh, M. P. Klein, and D. E. Phelps, J. Chem. Phys., **48**, 3831 (1968)

80. R. Freeman, H. D. W. Hill, and R. Kapstein, J. Magn. Reson., **7**, 327 (1972)

81. B. Honig, B. Hudson, B. D. Sykes and M. Karplus, Proc. Natl. Acad. Sci. US. **68**, 1289 (1971)

82. R. Rowan, L. A. McCammon and B. D. Sykes, J. Am. Chem. Soc., **96**, 4773 (1974)

83. R. Rowan, A. Warshel, B. D. Sykes and M. Karplus, Biochem., **13**, 970 (1974)